

Complexation Reactions of Some Poly-n-topic Ligands – Towards Large $[n \times n]$ Square
Grids ($n = 2-4$).

By

© Andrew Elliott

A dissertation submitted to the
Department of Chemistry and the
School of Graduate Studies

in partial fulfillment of the requirements for the degree of

Master of Science

In

Chemistry

Faculty of Science

Memorial University of Newfoundland

St. John's

Newfoundland

Abstract:

The coordination chemistry of a series of poly-n-topic pyrimidine, pyridazine, benzothiazole and triazole based ligands was studied. The ligands were designed with donor pocket arrangements which have the potential to form self-assembled multimetallic $[n \times n]$ grids. Such assemblies can exhibit interesting magnetic and redox properties, and have potential application in data storage at the molecular level. Ligand synthetic strategies and synthetic methods will be discussed and typical grid complexes described. Reactions with Mn(II), Ni(II), Co(II), and Cu(II) were attempted and the products characterized by X-ray and variable temperature magnetism. Antiferromagnetism typically dominates the magnetic behaviour in such systems, but in the cases of some $[2 \times 2]$ Cu(II)₄ square grids ferromagnetic behaviour was observed, which was attributed to the strict magnetic orbital orthogonality, resulting from the orientation of the Jahn-Teller axes in the grid.

Acknowledgements:

This project, which consisted of both laboratory research and literature research resulted in the writing of this dissertation. This was the result of years of hard work, which would not have been possible without the help and support of numerous people. I would like to thank my supervisor, Dr. Laurence K. Thompson for his advice, guidance, and patience over the course of this program. Without the guidance of Dr. Thompson and other members of the Thompson research group this would not have been possible, and I am truly grateful. I would like to thank in particular Dr. Konstantin Shuvaev and Dr. Muhammed Usman Anwar for the support and assistance throughout this project. Special thanks go out to Dr. Louise Dawe, for her guidance and assistance with this project in the lab, collecting and analyzing crystallographic data, and also being available whenever needed. I would also like to thank my family, specifically my parents, Darrell and Roxanne Elliott, for their love and support. I would also like to thank my friends and the chemistry department for their help as well.

Table of Contents

Abstract.....	ii
Acknowledgements.....	iii
Table of Contents.....	iv
List of Figures.....	vi
List of Schemes.....	ix
List of Tables.....	x
1. Introduction to Supramolecular Chemistry, Magnetism, and Polytopic Ligand Design.....	1
1.1 Magnetism and Superexchange.....	1
1.2 Supramolecular Chemistry and Self-Assembly	8
1.3 Ligand Design	17
1.4 Fitting of Magnetic Data for [n×n] Square Grid Systems/Clusters.....	25
2. Experimental Methods.....	34
2.1 Ligand Comments.....	35
2.2 Ligand Synthesis.....	40
2.3 Complexation Reactions.....	66
3 Complexes of Ditopic and Tetratopic Hydrazone Ligands.....	72
3.1 Ditopic Triazole and Benzothiazole Based Ligands and their Complexation Reactions.....	72
3.1.1 Ligands.....	72
3.1.2 Complexation Reactions.....	74

3.1.3	Crystallographic Data.....	75
3.1.4	Magnetic Data.....	97
3.2	Tetratopic Ligands-Towards Larger [n×n] Based Grid Systems	
	(n=4).....	104
3.2.1	Complexation Reactions.....	104
3.2.2	Crystallographic Data.....	106
3.2.3	Magnetic Data.....	107
4	Conclusions.....	112
5	References.....	116

List of Figures

Figure 1: Superexchange exhibited in a linear M-O-M type system.....	5
Figure 2: Superexchange orbital combinations via σ -bonding.....	6
Figure 3: Orbital orthogonality between metal centres.....	7
Figure 4: Molecular cylinder produced by self-assembly.....	10
Figure 5: Crystallographic views of some Mn structures produced by self-assembly.....	12
Figure 6: Representation of the self-assembly process of [2×2], [3×3], and [4×4] grids.....	14
Figure 7: Ni ₄ [2×2] grid and Mn ₉ [3×3] grid structures.....	15
Figure 8: Tetratopic pyridazine based ligand and a Cu(II) [4×4] grid.....	16
Figure 9: Self- Assembly reaction to form a [3×3] grid.....	18
Figure 10: Varying ligand sizes used to produce multimetallic [n×n] grids.....	19
Figure 11: Ligand 2poap and its coordination pockets to form a [3×3] grid.....	20
Figure 12: Possible bonding modes in ditopic ligands.....	21
Figure 13: Crystal structure representation of a Cu ₉ [3×3] grid and a tritopic ligand used.....	22
Figure 14: Self-assembled Cu ₈ pinwheel structure and Mn ₄ chain structure	24
Figure 15: Structures of two hydrazone ligands used in this project.....	24
Figure 16: Magnetic model for an M ₄ tetranuclear square.....	27
Figure 17: *.spk file for a Cu(II) tetranuclear square.....	29
Figure 18: Magnetic profile for a Cu ₄ L ₄ grid.....	31
Figure 19: Magnetic profile for an antiferromagnetically coupled Ni(II) ₄ [2×2] grid.....	32
Figure 20: Synthesis of ligand L2.....	37

Figure 21: Illustration of a triazole hydrazine ligand framework.....	73
Figure 22: Full crystal structure of compound 25	78
Figure 23: Simplified structure of compound 25 depicting coordination at each Cu centre.....	79
Figure 24: Full crystal structure of compound 26	81
Figure 25: Simplified structure of compound 26 depicting coordination at each Cu centre.....	82
Figure 26: Full crystal structure of compound 27	83
Figure 27: Extended lattice structure of compound 27	86
Figure 28: Full crystal structure of compound 28	87
Figure 29: Simplified structure of compound 28 depicting coordination at each Co centre.....	87
Figure 30: Full crystal structure of compound 29	91
Figure 31: Simplified structure of compound 29 depicting coordination at each Co centre.....	91
Figure 32: Full crystal structure of compound 30	93
Figure 33: Simplified structure of compound 30	93
Figure 34: Extended lattice of compound 31	95
Figure 35: Representation of hydrophobic/hydrophilic channels in compound 31	96
Figure 36: Variable temperature magnetic data for compound 26	97
Figure 37: Variable temperature magnetic data for compound 28	99
Figure 38: Variable temperature magnetic data for compound 29	101

Figure 39: Variable temperature magnetic data for compound 30	102
Figure 40: Structure of ligand L1	104
Figure 41: Half substituted ligand synthesized upon reaction of ligand L1 with Mn(II).....	105
Figure 42: Plot of magnetic susceptibility versus temperature for compound 31	107
Figure 43: Ni ₁₆ [4×4] grid structure.....	109
Figure 44: Variable temperature magnetic data for Ni ₁₆ [4×4] grid.....	110

List of Schemes

Scheme 1: Total synthesis of 4,6-dicyanopyrimidine.....	36
Scheme 2: Synthesis of 2-phenylpyrimidine-4,6-dicarbaldehyde.....	39
Scheme 3: Synthesis of compound 14	50
Scheme 4: Synthesis of a ditopic benzothiazole based ligand.....	61

List of Tables

Table 1: Crystallographic data for compounds 25-30	77
Table 2: Important bond distances and angles for compound 25	80
Table 3: Important bond distances and angles for compound 26	82
Table 4: Important bond distances and angles for compound 27	84
Table 5: Important bond distances and angles for compound 28	88

Chapter 1: Introduction to Supramolecular Chemistry, Magnetism, and Polytopic Ligand Design

1.1 Magnetism and Superexchange

All molecular substances are composed of fundamental particles including atoms, which contain protons, neutrons and electrons. It is the electrons in a molecule that define its magnetic properties and how it will behave in a magnetic field. All substances therefore possess some magnetic properties, whether it be diamagnetism or paramagnetism. Diamagnetism is a phenomenon where all the electrons present are paired with electrons of opposite spin, resulting in net diamagnetism and a material which is repelled by an external magnetic field. Paramagnetism on the other hand, is a phenomenon where the substance possesses unpaired electrons, and the material is attracted into a magnetic field.

Many textbooks give a general introduction to molecular magnetism including books by Kahn¹ and Drago² but none better than the book on magnetochemistry by Earnshaw.³ From this discussion on molecular magnetism the following equation defines the magnetic induction of a material, which is used to describe the density of lines of force within a substance;

$$B=H + 4\pi I \quad (1)$$

Where B is the magnetic induction of the substance, H is the magnetic field strength, and I is the intensity of magnetization, which can be described as the magnetic moment per unit volume.³ Division of equation (1) by H, the magnetic field strength, yields;

$$B/H = 1 + 4\pi I/H \quad (2)$$

This equation given can be simplified as the magnetic permeability of a substance per unit volume (P) can be defined as B/H, and the quantity κ can now be defined as $\kappa=I/H$;

$$P = 1 + 4\pi\kappa \quad (3)$$

Where κ represents the susceptibility per unit volume of the substance. Susceptibility measurements are commonly expressed in units of per mass or per mole, as opposed to per unit volume, due to their ease of calculation.³ Therefore this leads to the following expressions for magnetic susceptibility;

$$\chi_g = \kappa/\rho \quad (4)$$

$$\chi_m = \chi_g \cdot M \quad (5)$$

where χ_g is the gram susceptibility of the substance, χ_m is the molar susceptibility of the substance, M is the molar mass of the substance, and ρ is the density of the material.

Substituting equations (4) and (5) into equation (3) yields the following expression;

$$P = 1 + 4\pi\rho\chi_g = 1 + (4\pi\rho\chi_m)/M \quad (6)$$

This equation then allows for two possible situations where the magnetic permeability, P, of a substance is positive or negative. If $P < 1$, then χ_g will be negative as density is a positive property. Therefore, the intensity of lines of magnetic force in the substance will decrease, which yields a magnetic flux that opposes the direction of the external magnetic field applied to the substance. This type of substance is then referred to as diamagnetic, and will be repelled by the external magnetic field. This property of a material deals with the electrons that are paired, and since all matter contains paired electrons somewhere in its structure, all matter will possess a diamagnetic component.³

If the value of the magnetic permeability of a substance is greater than one ($P > 1$), then χ_g will be positive, which will lead to an increase in the magnetic lines of force within the substance. This leads to the production of a magnetic flux in the same direction as the external magnetic field, which results in a paramagnetic substance, which is attracted into the magnetic field. Paramagnetism is defined by materials containing unpaired electrons, and contributes much more to the magnetism of a molecule than diamagnetism.³

Diamagnetic susceptibility values generally range from -1 to -100×10^{-6} e.m.u (electromagnetic units), and are independent of the strength of the magnetic field and temperature. As mentioned previously, all substances contain a diamagnetic component, and this must be corrected for when assessing paramagnetic properties of a material. Paramagnetic susceptibility values generally range between 100 and $100,000 \times 10^{-6}$ e.m.u, and are independent of magnetic field strength. Paramagnetic susceptibility values, however exhibit an inverse dependence upon temperature, and this relationship can be expressed as

$$\chi = \frac{N\beta^2 \mu_e^2}{3kT} \quad (7)$$

Where N is Avogadro's number = 6.023×10^{23} , β is the Bohr magneton = 0.9273×10^{-20} erg gauss⁻¹, k is Boltzmann's constant = 1.381×10^{-16} erg K⁻¹ and T is the temperature expressed in Kelvin. μ_e is the "effective magnetic moment" and can consequently be expressed in units of Bohr magnetons as:

$$\mu_e = 2.828\sqrt{\chi T} \quad (8)$$

When paramagnetic centres, such as transition metal ions containing unpaired electrons, are bridged by a suitable atom or molecule, spin interactions can occur and are referred to as antiferromagnetic or ferromagnetic coupling. In the case of ferromagnetic coupling, the magnetic dipoles of the metal centres are aligned in the same direction below a temperature known as the Curie temperature. Increasing the thermal energy of the spin system will cause the spins to randomize, and once the Curie temperature is surpassed the system will behave like a simple paramagnet, which follows the following relationship known as the Curie-Weiss law (equation):

$$\chi = \frac{C}{T - \theta} \quad (9)$$

where C is the Curie temperature, and θ is the Weiss correction, which is positive for ferromagnetic systems.

In the case of an antiferromagnetically coupled spin system, the magnetic dipoles are aligned antiparallel to one another below a temperature known as the Néel temperature. In this case the observed magnetic susceptibility of the system will decrease, and increasing the thermal energy of the system will randomize the magnetic spins as in the case of ferromagnetic coupling. Once the Néel temperature is surpassed, this spin system will then behave like a simple paramagnet, in agreement with the Curie-Weiss law (equation). The Weiss correction, θ , is negative for antiferromagnetic systems.

In addition, a major difference between both these types of spin systems is that ferromagnetic effects are both temperature and magnetic field dependent, while antiferromagnetic effects are dependent on temperature, but are field independent. A third

phenomenon also exists, in which the unpaired electrons at each metal centre are opposed to one another, but with unequal opposing magnitudes of magnetic moment. This leads to a ferrimagnetic behaviour, which is much less common than the previous two cases.

Superexchange

Spin coupling between metal centres across an intervening atom or molecule (bridge) is known as superexchange. The mathematics behind superexchange is very complex, and therefore the focus of this discussion will just centre on the molecular orbital interactions involved. For a more in depth description of this topic, the Goodenough-Kanamori-Anderson rules provide a mathematical discussion of the wavefunctions associated with superexchange.⁴⁻⁹

Consider a hypothetical dinuclear Cu(II) metal complex, with each metal centre containing one unpaired electron in their corresponding d orbital (e.g. d_{z^2}), and both are bridged by an oxide anion for example. Figure 1 illustrates the system:

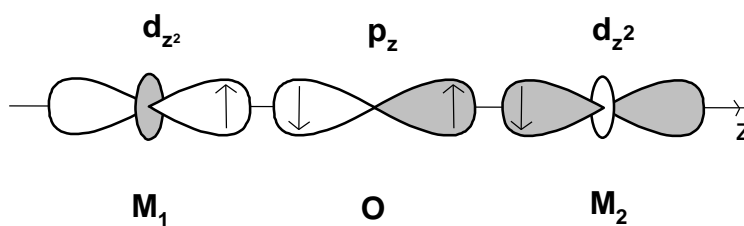


Figure 1: Superexchange exhibited in a linear M-O-M type system.

The metal M_1 contains an unpaired electron in the d_{z^2} orbital, and if it is assumed that the spin of this electron is 'up', upon mixing with an orbital of the oxide bridge of correct symmetry (p_z), a bond is formed, and the resulting effect will cause the electron in the p_z orbital to have a spin of 'down'. The p_z orbital of the oxide bridge will then have

another electron of opposite spin, which then pairs with the electron in the magnetic orbital of the metal M_2 , resulting in another σ -bond, with electron pairing as with the first σ -bond.¹⁰ Therefore, the unpaired electron on M_2 will be spin down, opposite to the unpaired electron on M_1 . This results in antiferromagnetic exchange between M_1 and M_2 .

The scenario illustrated in Figure 1 does not cover all orbital combinations for antiferromagnetic exchange in the linear M-O-M system. Antiferromagnetic exchange can occur via mixing various metal d orbitals with bridging orbitals of appropriate symmetry. Two other possible combinations are illustrated in Figure 2:

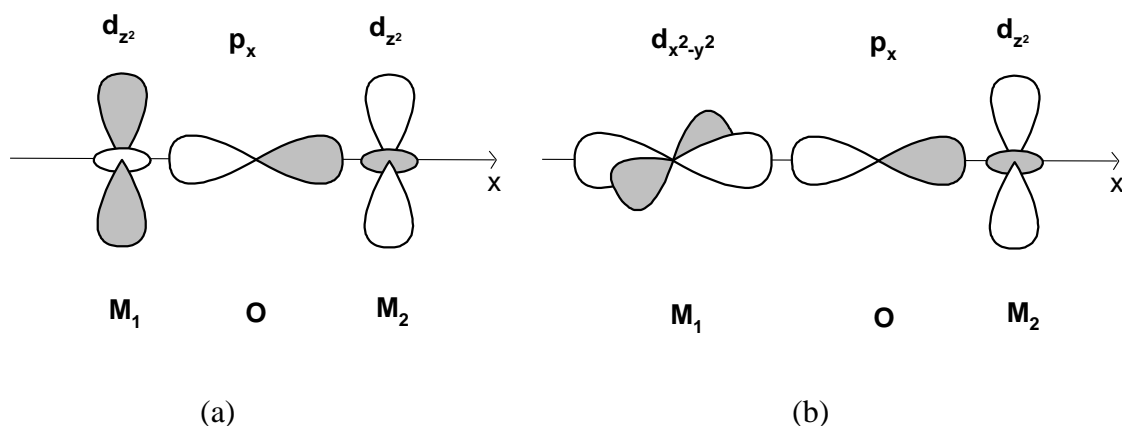


Figure 2: Superexchange orbital combinations via σ -bonding in the linear M-O-M system.

In Figure 2a, the unpaired electron of the metal is again in the d_z^2 orbital, but the major lobes of the metal and oxygen orbitals are at right angles in this case. However, another pathway for antiferromagnetic exchange exists. It occurs through overlap of those d_z^2 lobes of orbitals on M_1 and M_2 that lie in the xy plane with lobes of a p_x orbital on O. In Figure 2b, the overlap of the magnetic ground state orbital of the one metal ($d_{x^2-y^2}$) with the d_z^2 orbital of the other metal centre through the p_x orbital of the oxide bridge

leads to antiferromagnetic exchange as well. These antiferromagnetic interactions will however be small, because the xy component of the d_z^2 orbital is quite small. The coupling constant, J , in antiferromagnetic couplings is negative.

In a scenario where metal orbitals have zero net overlap with each other and with the orbitals of the bridging atom, as in Figure 3, coupling between the two metals is through space and ferromagnetic. The constant, J , in ferromagnetic couplings is positive.¹¹ Figure 3 illustrates a case of orbital orthogonality involving two metal $d_{x^2-y^2}$ orbitals and a bridging p_z orbital:

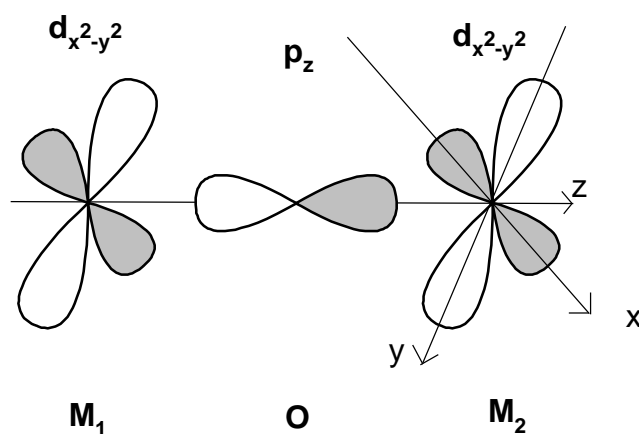


Figure 3: Orbital orthogonality in the linear M-O-M system, which results in ferromagnetism.

In superexchange coupled systems both ferromagnetic and antiferromagnetic couplings contribute to the total coupling. Thus, $J_{\text{total}} = J_{\text{ferro}} + J_{\text{antiferro}}$. In these cases J_{ferro} is frequently smaller and often much smaller than $J_{\text{antiferro}}$. The examples used in this discussion of superexchange use a single atom bridge. However, multiple atom bridges are quite common, as in the case of work done by Thompson et al. For example, Cu(II) atoms with $d_{x^2-y^2}$ magnetic ground states bridged by diazine $-NN-$ bridges exhibit both

antiferromagnetism (via superexchange) and ferromagnetism (orbital orthogonality) as a function of the rotation of the copper magnetic planes about the N-N double bond.^{12,13}

Hatfield et al. also reported a similar result, where a linear relationship was found between the magnitude of the exchange coupling constant (J) and the Cu-O-Cu bond angle in a series of di- μ -hydroxo-bridged Cu(II) complexes.¹⁴ Hatfield explained that only when magnetic orbitals are aligned strictly orthogonally, will ferromagnetism dominate the magnetic exchange between the two Cu(II) centres.¹⁴

1.2 Supramolecular Chemistry and Self-Assembly.

Supramolecular chemistry is a very diverse area in chemistry, and the initial discovery of this field was made by Emil Fischer in 1894 based on his work on enzyme-substrate interactions and the “lock and key” type mechanism.¹⁵ Almost 100 years later after Fischer’s initial discovery Jean-Marie Lehn, Donald J. Cram and Charles J. Pederson were awarded the 1987 Nobel prize in chemistry “for their development and use of molecules with structure-specific interactions of high selectivity”.¹⁶ Lehn, perhaps the largest contributor to this field, described supramolecular chemistry as “chemistry beyond the molecule” in his subsequent Nobel lecture.¹⁷ The area of supramolecular chemistry deals with molecular assemblies held together not only by covalent forces, but also by forces such as hydrogen bonding, van der Waals forces, hydrophobic forces, metal coordination bonds, π - π interactions and electrostatic effects.^{18,19} These interactions are known as non-covalent interactions, and they play a major role in building supramolecular blocks such as the systematic, controlled, and step by step

methodologies that have allowed the construction of large molecular structures from a single DNA strand.²⁰

Inorganic synthesis has made similar progress in developing and synthesizing large architectures, which contain a very large number of metal centres. A major concept in the supramolecular aspect of inorganic synthesis is the idea of molecular self-assembly. Self-assembly can be defined loosely as a collection of small molecular components, which assemble into a large molecular architecture without much direction or planning involved in the reaction, as a result of the non-covalent forces discussed previously. Self-Assembly in the field of inorganic synthesis is generally mediated by the metal centres present, and Stang and coworkers list four components common to all such architectures.²¹ These components include that the assembly be held together by covalent bonds, the assembly is the most stable combination of the components (thermodynamic stability), the assembly can be characterized as a distinct entity separate from its components, and the assemblies are discrete rather than infinite.²¹ This set of conditions has produced some large assemblies, and Figure 4 gives a specific example of one of these compounds:

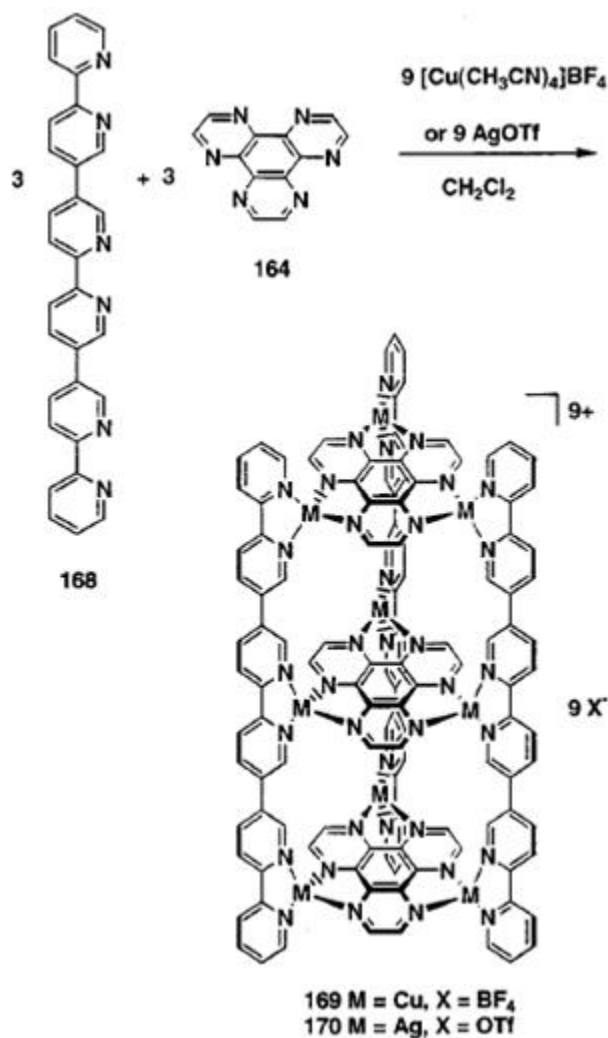


Figure 4: A molecular cylinder produced by self-assembly methods. Reprinted (adapted) with permission from S. Leininger, B. Olenyuk, P. J. Stang, *Chem. Rev.*, **2000**, 100, 853. Copyright (2000) American Chemical Society.²¹

This molecular cylinder was produced from the interaction of the simple organic ligand components which included a hexapyridine linker (compound 168 from Figure 4) and hexaphenylhexaazatriphenylene (compound 164 from Figure 4, with phenyl groups left out for simplicity) with $[\text{Cu}(\text{CH}_3\text{CN})_4]\text{PF}_6$ or AgOTf .²¹ In addition to this cylinder

type compound, this review also reports compounds with various shapes such as rhomboids, polygons, rectangles, cages, and tetrahedra.²¹

Self-assembly methods can be broken down into two separate types. The first is serendipitous self-assembly, which generally occurs with simple, coordinatively unsaturated ligands, which can exhibit varying coordination modes, and with metals that have flexible molecular geometries.²² The second is self-assembly by rational design, which uses an approach where ligands are designed with coordination pockets that match the particular metal coordination environments, and the pockets create an induced fit for the particular metal centre.²³ Serendipitous self-assembly often results because of a mismatch between the ligands' coordination ability and the available coordination sites present on the metal, or by removing ligands from a complex to create empty sites on a metal centre, and the incorporation of exogenous co-ligands.²²

Serendipitous self-assembly can indeed be a very random approach to coordination clusters, but it also has produced many novel structures such as Fe₁₉ oxohydroxide single molecule magnets which display magnetic hysteresis,²⁴ the first reported molecular magnet [Mn₁₂O₁₂(O₂CPh)₁₆(H₂O)₄],²⁵ and [Cr₇M] wheel compounds (M = Mn, Ni, Fe). Powell and coworkers have produced many compounds based on this type of self-assembly, using simple ligands and a wide variety of metal centres. For example, upon use of some simple hydroxy based ligands, a series of clusters built from ferromagnetically coupled mixed oxidation state manganese [Mn(II)₄Mn(III)₆] supertetrahedral units was synthesized. A sample compound of this type was the compound [Mn(III)₆Mn(II)₄(μ₃-O)₄(HL)₆(μ₃-N₃)₃(μ₃-Br)(Br)](N₃)_{0.7}(Br)_{0.3}·3MeCN·

2MeOH, where L is the ligand 3-methyl pentane-1,3,5-triol, where the complex serendipitously self-assembled by mixing the ligand with sodium azide, triethylamine and a Mn(II) salt.²⁷ Figure 5 illustrates the structure of this compound, along with some similar mixed oxidation state compounds produced with similar ligands.

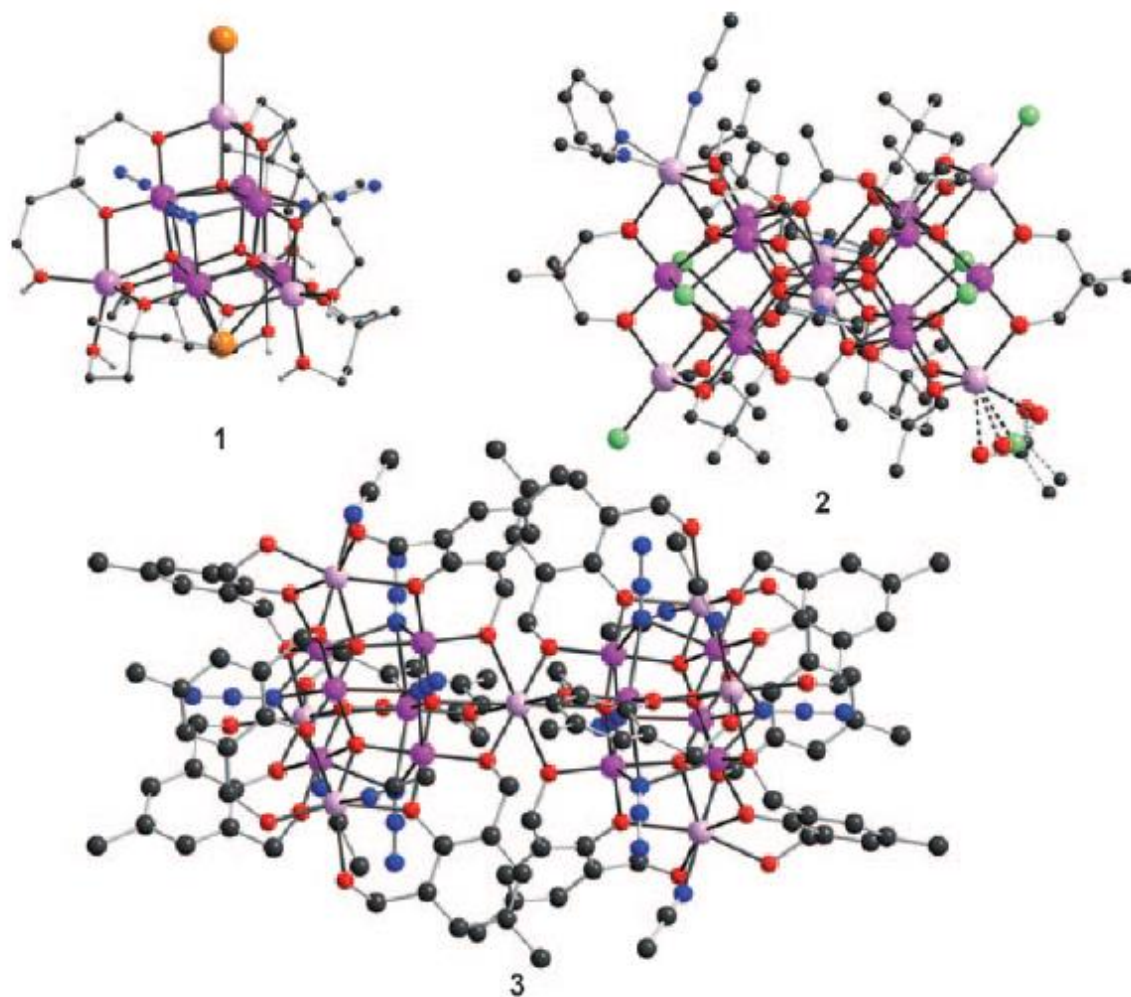


Figure 5: Crystallographic views of some mixed-valence manganese complexes produced via serendipitous self-assembly. Color code: Carbon (black), oxygen (red), nitrogen (blue), manganese(II) (magenta), manganese(III) (pink), bromine (green). Reprinted (adapted) with permission from S. Nayak, M. Evangelisti, A.K. Powell, J. Reedijk, *Chem. Eur. J.*, **2010**, 16, 12865. Copyright (2010) John Wiley and Sons, Inc.²⁷

The polyalcohol based ligands were chosen due to their usefulness in bridging metal centres, and additional bridging ligands such as azide were also added to facilitate the bridging of large numbers of metal ions.²⁷ This was the only planning that occurred during the synthesis of these complexes, and therefore serendipity dominated the outcome of these reactions. Similar compounds produced by this type of chemistry are iron-lanthanide metallo-ring aggregates,²⁸ hexadecacobalt(II) single molecule magnets,²⁹ and a Mn(II)₁₂ partial grid.³⁰

Self-assembly by rational design is a more planned approach to the synthesis of larger inorganic based molecules. The ligands are designed with pockets that have an “induced fit” for the metal centres used, which can accommodate the coordination geometry requirements for the metal centre, whether it be 4, 5 or 6-coordinate. This type of chemistry with ligands having designed pockets for metal centres leads to the formation of [n×n] grids, where n = 2, 3, 4. Figure 6 shows a schematic representation of the self-assembly process in the formation of [2×2], [3×3], and [4×4] grid-type architectures.

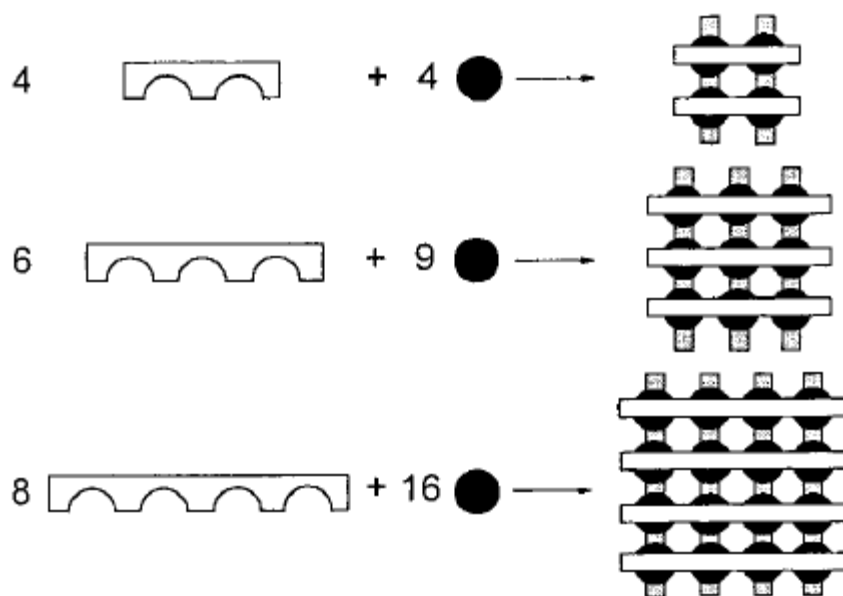


Figure 6: Schematic representation of the self-assembly process of $[2 \times 2]$, $[3 \times 3]$, and $[4 \times 4]$ grid-type architectures. Reprinted (adapted) with permission of E. Bruening, G.S. Hanon, F.J. Romero-Salguero, A.M. Garcia, P.N.W. Baxter, J-M Lehn, E. Wegelius, K. Rissonen, H. Nierengarten, A. van Dorsselaer, *Chem. Eur. J.*, **2002**, 8, 3458. Copyright (2002) John Wiley and Sons, Inc.³¹

In Figure 6, it is shown that two-pocket ligands (n -topic) create $[2 \times 2]$ grids, three pocket ligands create $[3 \times 3]$ grids, and so on. The first grid-type structures were reported using bipyridine-like binding subunits and the tetrahedrally coordinated metal ions Cu(I) and Ag(I).³²⁻³⁵ This logic was then extended to incorporate octahedrally coordinated first row transition metal ions such as Mn(II), Co(II), Ni(II), Cu(II), and also the non-transition metal ion Zn(II), and ligands based on terpyridine/picolinic hydrazone based ligands.^{36,37} Figure 7 illustrates an example of a grid type structure.

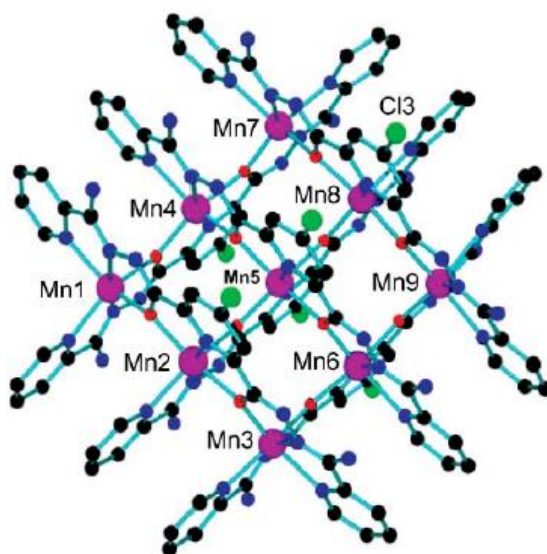


Figure 7: [3x3] Mn(II)₉ grid using a tritopic ligand. Reprinted (adapted) with permission from L. Zhao, C.J. Matthews, L.K. Thompson, S.L. Heath, *Chem. Commun.*, **2000**, 265. Copyright (2000) Royal Society of Chemistry.³⁸

The larger [3×3] grids have been well established with manganese³⁸ and copper³⁹ and use three contiguous *mer* coordination groupings within the tritopic ligands with central pyridine units, which have the potential to bind three six-coordinate metal ions per ligand in an approximately linear fashion.³⁸ The expansion to [4×4] and [5×5] grid-type structures requires that functionality must be added to the ligands either at the ends or in the central position, and this was achieved by using central groups such as 3,6-pyridazine or 4,6-pyrimidine instead of pyridine, and can use hydrazone capping endpieces to create larger tetratopic and pentatopic based ligands.³⁷ Central pyridazine units have been used to create such tetratopic ligands, in addition to using 4,6-pyrimidine based ligands for the synthesis of Pb(II)₁₆ grids,⁴⁰ and Figure 8 gives an example of such a structure.

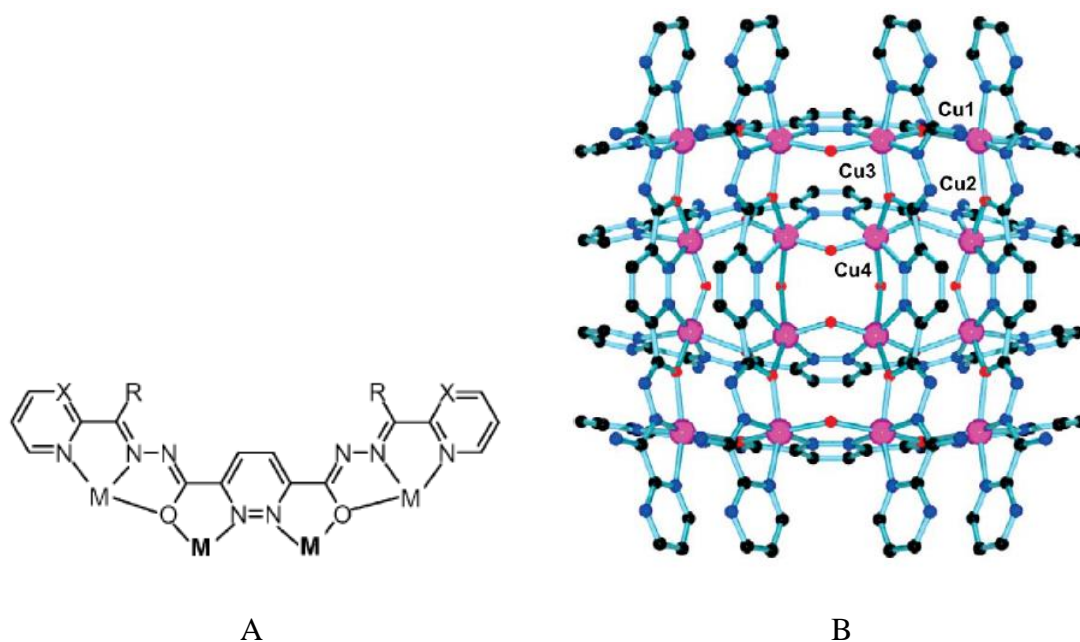


Figure 8: (A) Tetratopic pyridazine based ligand; (B) Cu(II) [4x4] grid produced by rationally designed self-assembly. In the case of this structure the ligand has R = NH₂, X = N. Reprinted (adapted) with permission from L.N. Dawe, L.K. Thompson, *Angew. Chem. Int. Ed.*, **2007**,46, 7440. Copyright (2007) John Wiley and Sons, Inc.³⁹

Self-assembly has proven to be a very powerful tool in the area of complex inorganic synthesis, leading to the synthesis of complex inorganic materials such as self-assembled grids³¹⁻⁴⁰ and supramolecular polymers.⁴¹ Such materials have very complex architectures and properties, but their synthesis can sometimes be very simple from the initial components by the process of self-assembly.

1.3 Ligand Design

Polynuclear grids and clusters are important synthetic targets in modern inorganic synthesis as they create groups of transition metal centres in close proximity, which leads to molecules that can have novel and important magnetic, electrochemical, and spectroscopic properties. These multimetallic complexes also are interesting targets as they could have the unique ability to act as molecular switches, capable of data storage in the range of 10^{12} bits/inch², as theorized by Jean-Marie Lehn,⁴² much higher than comparable data storage media such as modern computer hard drive disks, (disks coated with a magnetic material, which upon applying a voltage can exist in two required on/off states, 10^8 bits/inch²) and DNA (10^{10} bits/inch²).⁴²

Examples of [n×n] grids have been produced with metal ions (e.g. Mn, Fe, Co, Ni, Cu, Zn, Pb) with n = 2-5. These systems, particularly the large ones (e.g. [3×3], [4×4]), have complicated architectures and high molecular weights, and sequential synthesis by adding one piece at a time would be impossible. Therefore, another method is used, self-assembly,^{42,43} which allows the formation of these complexes in one step by the use of rationally designed ligands and transition metal centres of appropriate coordination number and geometry, most notably 4, 5 or 6-coordinate metals. The ligands used to synthesize these grid systems have appropriate donor atoms (such as oxygen or nitrogen) built into their backbone, which form coordinate covalent bonds with the metal centres. The ligands also have coordination pockets which match the geometric requirements of the metal with two or three donor atoms present in each pocket, depending on the metal coordination geometry. The metal centres of adjacent pockets are

then linked by appropriate heteroatom bridges such as oxygen or diazine (-NN-) bridges to form the polynuclear grids. The grids have a square overall geometry and in order for the ligand pockets to be aligned appropriately, the donor pockets are designed to create five-membered chelate rings (vide infra). The basis of self assembly is described in Figure 9, for a tritopic ligand forming a [3x3] square grid:



Figure 9: Diagram depicting the self-assembly procedure which leads to the formation of a [3x3] grid of metal centres. The pink circles are 6-coordinate transition metal centres, and the blue arrows represent coordination pockets of the ligands with three donor atoms.

This method of synthesizing polynuclear transition metal clusters has produced multimetallic grids of various dimensions, including [2x2],^{42,45-49} [3x3],^{4,49-53} [4x4],^{49,54} and [5x5]⁴⁹ examples with various first row transition metals such as Cu(II), Ni(II), Mn(II/III), Fe(II), Co(II), the non-transition metal Zn(II), and varying types of ligands with flexible donor pockets. Similar ligands have also produced lanthanide metal clusters and grids with various metals such as Gd(III), Dy(III), Eu(III), Ho(III) and Yb(III).⁵⁵⁻⁶² The ligands most commonly used are hydrazone based. Figure 10 shows a variety of polytopic ligands used in the formation of grids.

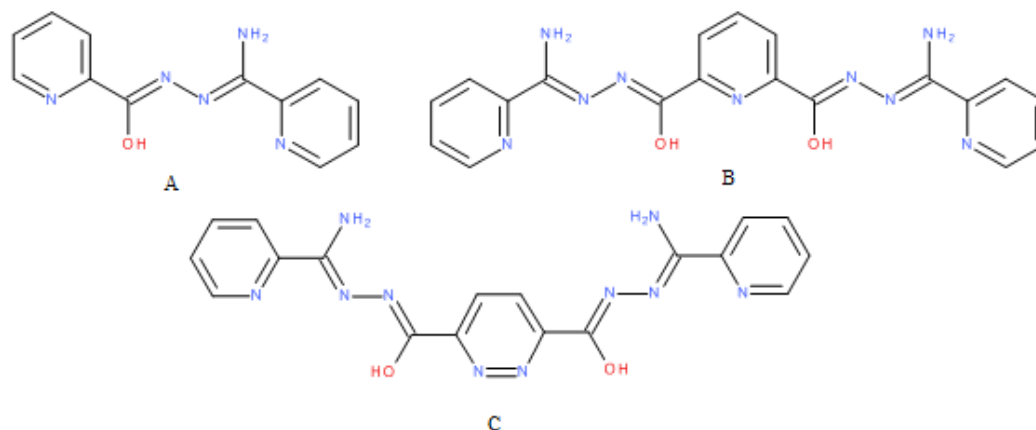


Figure 10: Varying ligand sizes used to produce multimetallic supramolecular grids. (A) Ditopic ligand poap, (B) tritopic ligand 2poap, and (C) tetratopic ligands are illustrated.

The ligands shown in Figure 10 have varying numbers of donor pockets, and are capable of producing $[2 \times 2]$, $[3 \times 3]$, and $[4 \times 4]$ structures respectively by self-assembly.

The hydrazone based ligands used are derived from heteroatom ester compounds (e.g. picolinic compounds), which react with hydrazine to form extended hydrazone based compounds. The hydrazone groups form the “centrepiece” of the ligand, where the central hydrazone oxygen part of the ligand can bridge the metal centres in the structure, via the hydrazine ‘O’ atoms. Reaction of these hydrazone “centrepieces” with an appropriate “endpiece” leads to the ligand framework (Figure 10) with the ligand size being dependent upon the number of hydrazone (HO-C=N-N) functional groups in the compound. The naming system poap was coined from the ligand framework and coordinating atoms, which is pyridine-oxygen-amine-pyridine in the ligand poap. 2poap

refers to the fact that the ligand is tritopic (with a symmetric endpiece on both sides of the centre pyridine).

Grid formation is greatly assisted if the pockets of the ligand which coordinate to the metal line up in a linear fashion, shown by Figure 11:

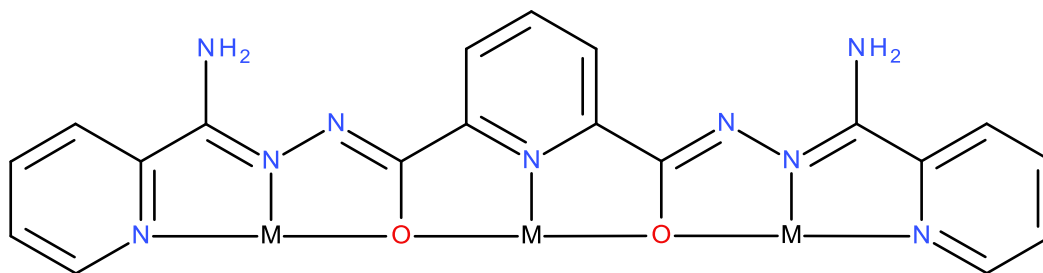


Figure 11: The ligand 2poap and its normal coordination mode for the formation of $[3 \times 3]$ grids. Note the linear arrangement of the pockets and the five-membered chelate rings. Trivial names for the polytopic ligands are based loosely on the arrangement of heterocyclic rings (p), amidrazone oxygen (o) and exocyclic amine groups (a).

In Figure 11, the ligand provides three tridentate pockets for coordination to a metal centre, and upon assembly to the grid compound a homoleptic $[3 \times 3]$ square compound is the major product.^{42,45,49} The coordination mode in Figure 11 is the most common mode for the synthesis of grid complexes, but other coordination modes are possible as well due to the tautomeric flexibility of the ligand. Other possible confirmation modes for ditopic ligands are shown in Figure 12:

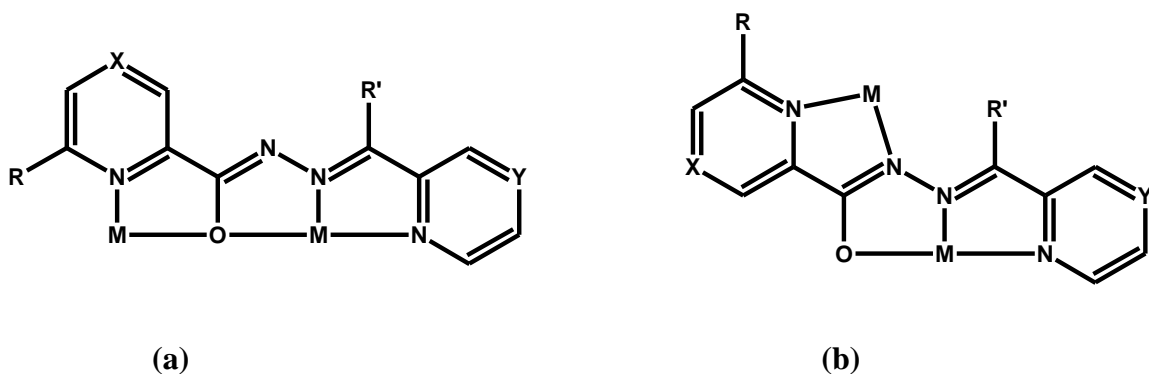


Figure 12: General representation of possible bonding modes in ditopic ligands, showing the formation of 5-membered chelate rings. a) μ -O bonding mode b) NN bonding mode.

As shown in Figure 12, the ligand can bend and twist to form other types of transition metal cluster in addition to the grid compounds, with examples containing mononuclear,^{63,64} dinuclear,⁶⁵⁻⁶⁷ and pentanuclear compounds synthesized with this type of two pocket ligand.^{68,69}

As the number of pockets in the ligand increases, the complexes naturally get larger as well. In a three-pocket ligand such as 2poap, the major products reported have been supramolecular M_9 [3×3] grid complexes,⁵² and four pocket ligands lead to M_{16} [4×4] grids.⁶³ An example of a larger grid complex is the [3×3] grid formed by reaction of the tritopic ligand m2poap with $Cu(NO_3)_2 \cdot 3H_2O$, which spontaneously assembles into a $Cu(II)_9$ [3×3] grid. Figure 13 represents the crystal structure of the complex and the ligand used in the synthesis.⁴⁴

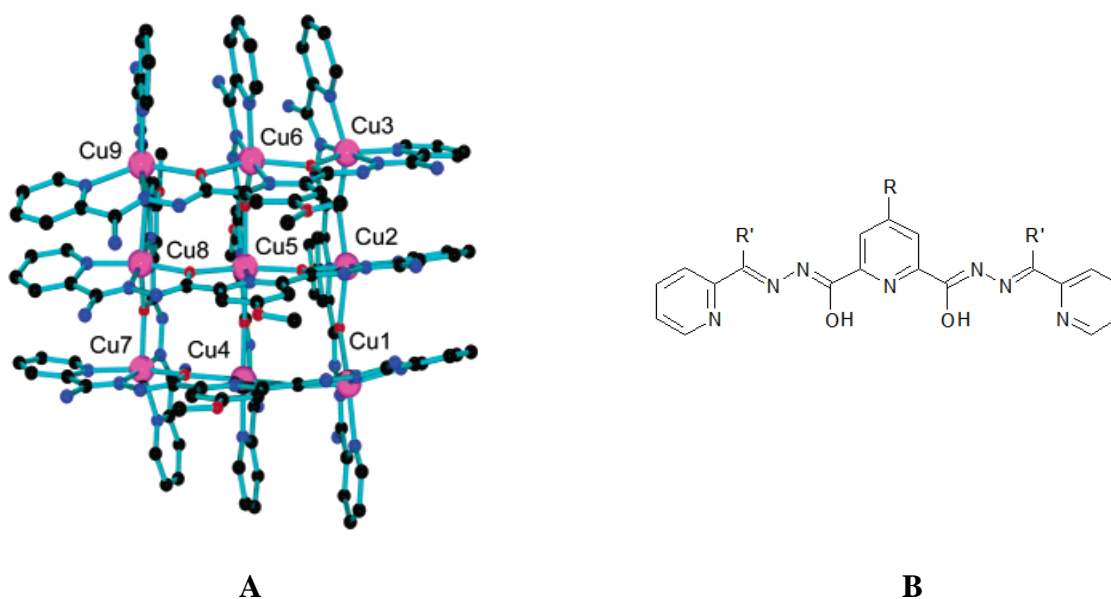


Figure 13: (A) Crystal structure representation of the Cu₉ [3×3] grid. (B) Tritopic ligands to create some [3×3] grids. 2poap (R = H, R' = NH₂), Cl2poap (R = Cl, R' = NH₂), m2poap (R = OMe, R' = NH₂), Cl2pomp (R = Cl, R' = CH₃), 2pomp (R = H, R' = CH₃). Reprinted (adapted) with permission from V.A. Milway, V. Niel, T.S.M. Abedin, Z. Xu, L.K. Thompson, H. Grove, D.O. Miller, S.R. Parsons, *Inorg. Chem.*, **2004**, 43, 1874. Copyright (2004) American Chemical Society.⁴⁴

The Thompson research group has synthesized a large group of ligands with potential to form [3×3] grid systems, based on ligands derived from 2poap, which upon complexation with a metal cation self-assemble into nonanuclear grids with metals such as copper, manganese, cobalt, zinc, and nickel. The grids are composed of nine metal cations and six ligands, which are arranged in such a manner that one group of three ligands is orthogonal to the other group of three, above and below the grid pseudo-plane. From Figure 13, one can see that the ligand m2poap is derived from a pyridine centrepiece, with two endpieces derived from reaction of the intermediate bis-hydrazone with appropriate pyridine based groups. The ligands are all similar in structure, and by

changing the nature of the “R” and “R’” groups from Figure 13, many different ligands with potential for [3×3] grid formation can be synthesized.⁴⁴

Similar to the ligands derived from ditopic ligands such as poap, these higher order polytopic ligands can also spontaneously self-assemble into other supramolecular structures such as clusters,⁴⁶ boxes,⁴⁸ horse shoes,⁷² chains,⁴⁹ pinwheels,^{44,74} rings,⁷⁴ and helicates^{75,76} (ditopic ligands like poap produce mononuclear complexes and also pentanuclear clusters can be formed). These more complex self-assembled multi-metallic structures show the spontaneity that arises from self-assembly reactions, and the many different types and shapes of products that can be formed in large measure as a result of tautomeric flexibility of the ligand. Figure 14 gives structural representations of two alternative supramolecular structures based on tritopic and tetratopic ligands.

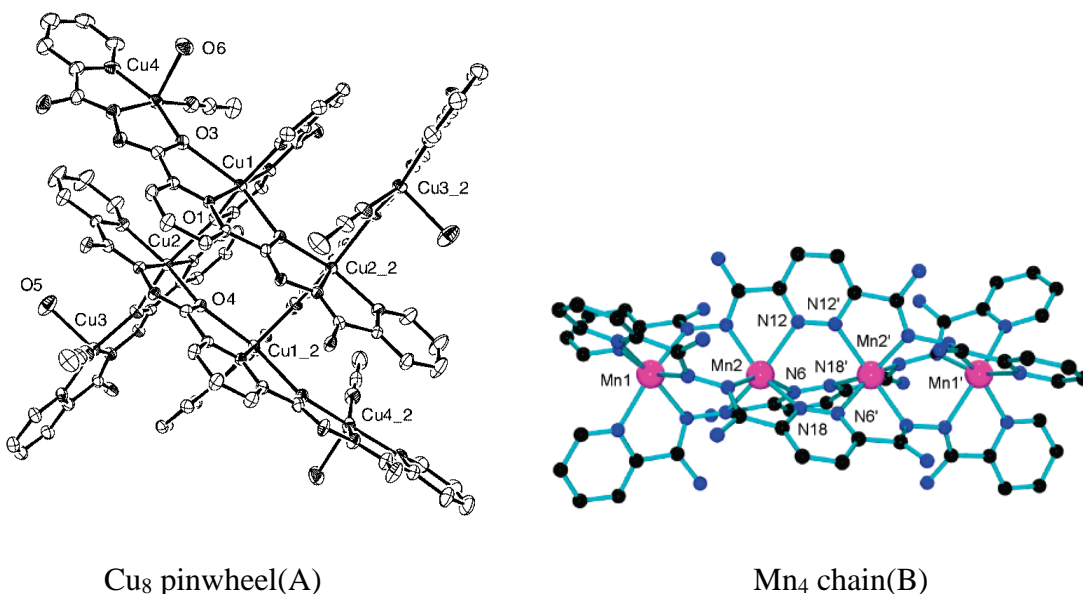


Figure 14: (A) Structural representation of the cation [Cu₈(2poap)₄](CH₃OH)₄(CH₃CN)₄. (B) Structural representation of the cation Mn₄ chain derived from a pyridine based ligand with pyridine endpieces. Reprinted with permission from V.A. Milway, V. Niel, T.S.M. Abedin, Z. Xu, L.K. Thompson, H. Grave, D.O. Miller, S.R. Parsons, *Inorg. Chem.*, **2004**, 43, 1874 and S.K. Dey, T.S.M. Abedin, L.N. Dawe, S.S. Tandon, J.L. Collins, L.K. Thompson, A.V. Postnikov, M.S. Alam, *Inorg. Chem.*, **2007**, 46, 7767. Copyright (2004, 2007) American Chemical Society.^{44,49}

The current study focuses on two new classes of ditopic and tetratopic ligands (Figure 15 A/B) based on pyrimidine and benzothiazole based hydrazones. These ligands have the potential to form [2×2] and [4×4] grids, with the possibility also of other cluster formation:

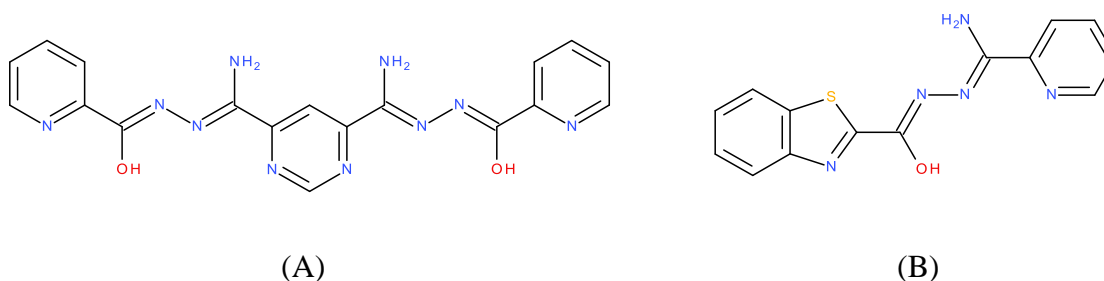


Figure 15: Structures of two hydrazone based ligands synthesized during this project.

Ligand (A) from Figure 15 is a tetratopic pyrimidine based ligand, and produced the first reported Ni₁₆ [4×4] square grid, a 4 × [2×2] heteroleptic grid. This structure will be discussed in more detail in the results section of this thesis, with a comparison to a similarly synthesized compound. The complex consists of four [2×2] Ni₄ squares at each corner, which are linked together through the ligand N-C-N bridge from the pyrimidine ring. Each individual Ni₄ square subunit is bridged by the hydrazone μ-O bridge from the ligand endpieces as well.⁷⁶ Ligand (B) is a ditopic benzothiazole ligand, and ligands in this class have produced a series of trigonal bipyramidal Mn(II) and Co(II) complexes which will be discussed in much more detail later in this thesis.⁷⁷

1.4 Fitting of Magnetic Data for [n×n] Square Grid Systems/Clusters

The fitting of magnetic data for [n×n] square grids is a process which involves a series of steps. The initial step in the fitting of any experimental magnetic data for any polynuclear cluster is the definition of a Heisenberg spin Hamiltonian to model the magnetic exchange in the cluster, and to determine all of the spin states and their energies associated with the system. The general formula for a Heisenberg spin Hamiltonian, which includes spin coupling between all metal centres, ligand field effects, and Zeeman splitting is a summation over all states, and is given in equation 10:³

$$H = -\sum_{i<j} J_{ij} \cdot S_i \cdot S_j + \sum_i S_i \cdot D_i \cdot S_i + \mu_B \sum_i S_i \cdot g_i \cdot B \quad (10)$$

However, the most significant contribution is the first term, appropriate for an isotropic spin coupled system, and the other ligand field and Zeeman terms are ignored. Therefore, a simplified spin Hamiltonian can now be written, and is illustrated in equation 11:³

$$H = -\sum_{i<j} J_{ij} \cdot S_i \cdot S_j \quad (11)$$

This simplified spin Hamiltonian can now be used to obtain magnetic information about the polynuclear cluster such as the total spin quantum numbers, S' , along with their corresponding energies $E(S')$. The next step in the fitting of the magnetic data is to substitute the quantum numbers along with their energies into the Van Vleck equation, which calculates the magnetic susceptibility of the polynuclear system as a function of temperature. Equation 12 gives the general form of the Van Vleck equation:

$$\chi_M = \frac{N\beta^2 g^2}{3kT} \frac{\sum S'(S'+1)(2S'+1)\Omega(S')e^{-E(S')/kT}}{\sum (2S'+1)\Omega(S')e^{-E(S')/kT}} \quad (12)$$

Where N is Avogadro's number ($6.022 \times 10^{23} \text{ mol}^{-1}$), g is the Landé splitting factor, k is Boltzmann's constant ($1.381 \times 10^{-23} \text{ JK}^{-1}$), β is the Bohr magneton, T is temperature (K), S' is the spin quantum number, $E(S')$ is the energy of the associated quantum number, and $\Omega(S')$ gives the degeneracy of each energy state with the associated quantum number. The calculated χ_M term is normally corrected such that the Van Vleck expression can include a term for paramagnetic impurity (ρ), a Weiss correction for temperature (θ) and a temperature independent paramagnetism term (TIP). The modified form of equation 12 is shown in equation 13:

$$\chi_M = \frac{N\beta^2 g^2}{3k(T-\theta)} \frac{\sum S'(S'+1)(2S'+1)\Omega(S')e^{-E(S')/kT}}{\sum (2S'+1)\Omega(S')e^{-E(S')/kT}} (1-\rho) + \frac{N\beta^2 g^2 S(S+1)\rho}{3kT} + TIP \quad (13)$$

The spin states and energies derived from the exchange Hamiltonian are calculated using three different mathematical methods: vector coupling method,⁷⁸ irreducible tensor operators, and full matrix diagonalization.⁷⁹ The method of full matrix diagonalization is the method used in the software package MAGMUN4.1,⁸⁰ which calculates all the spin states and their associated energies and substitutes them directly into the Van Vleck equation.

The program uses an output file (*.spk), which contains the total spin states and energies for the cluster in question. This output file is generated from an input file (OW01.ini), which accounts for the magnetic model in question, using an executable program (OW01.exe), which employs the full matrix diagonalization method. The first step in using the program is to formulate a magnetic model for the system, and in the case of an M_4 tetranuclear $[2 \times 2]$ grid, Figure 16 illustrates the model, where J_1 , J_2 , J_3 represent the coupling constants between adjacent metal centres.

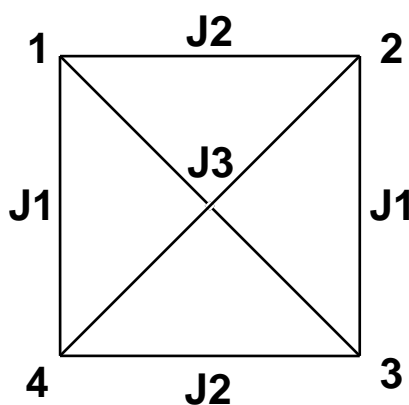


Figure 16: Magnetic model for an M_4 tetranuclear square.

The input file is then used to define the spin state corresponding to the number of unpaired electrons present at each metal centre, their connectivity via a bridging atom, and the relative strengths of the coupling between each metal centre (JX). In the case of Cu(II), which will be used for the example, the spins of the metal centres will be $S = \frac{1}{2}$ (d^9), and the model will assume that there is no cross-coupling across the square ($J3 = 0$), and that the exchange between each adjacent metal centre is equal in magnitude ($J1 = J2$). The exchange coupling constant (J) and other parameters are determined by non-linear regression of the data in the input file to the modified Van Vleck equation (13).

The executable program OW01.exe then uses the input (.ini) file to calculate the spin states and energies for the system, which will eliminate the need to derive an exchange equation for the data. The output *.spk file is then generated, which contains the required $E(S')$ values. The *.spk file for the example of a Cu(II) tetranuclear square is shown in Figure 17.

```

MDA 01.00 SPK 00
#PROGRAM:
  Program OWOL, (c) Oliver Waldmann, Version 11.5.01
#HAMILTONIAN:
  Heisenberg Hamiltonian
#SYSTEM:
  Spins = 1/2 1/2 1/2 1/2
  Couplings = 1-2 2-3 3-4 1-4
#PARAMETER:
  Strengths = -1 -1 -1 -1
  Emin = -2
#COMMENT:
  sorted spektrum with classification
#DATA:
0          0      0      ← Magnetic ground state
1          2      0      ← Next highest lying energy state
2          0      1
2          2      1
2          2      2
3          4      0

```

Figure 17: *.spk file for a Cu(II) tetranuclear square. The first column defines normalized relative energies while the second defines the spin states ($2S'$).

Upon writing this file, the *.spk file, along with the experimental data, can be fitted to the modified Van Vleck equation (Eqn. 13) using the MAGMUN4.1 program. The output from MAGMUN4.1, which contains the fitted data, is worked up using an Excel spreadsheet, with data presented as temperature, experimental and calculated χ , χT , and μ values. The magnetic moment of a complex is proportional to the number of unpaired electrons, and considering the definition of magnetic susceptibility:

$$\chi = (Ng^2\beta^2/kT) \sum M_S^2/(2S + 1) \quad (14)$$

Which can be simplified to:

$$\chi = (Ng^2\beta^2/kT) S(S + 1) \quad (15)$$

The molar magnetic susceptibility varies as C/T from the Curie-Weiss law, with the constant C depending on the spin multiplicity of the ground state. Sometimes the magnetic susceptibility is given in terms of temperature dependence of the so-called effective magnetic moment μ_{eff} defined by:

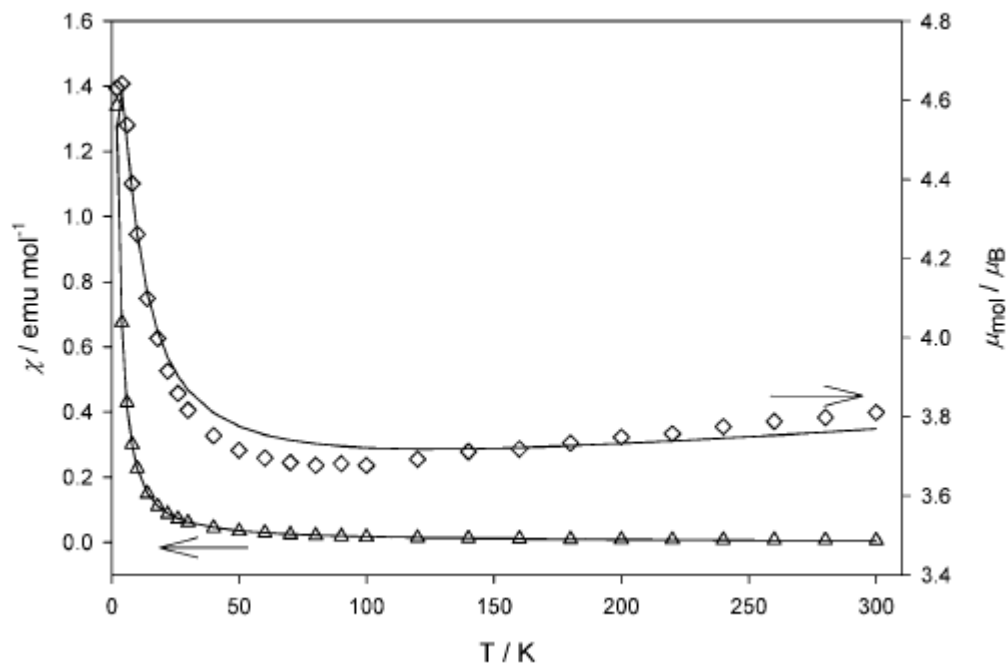
$$\mu_{\text{eff}} = (3kT \chi/N\beta^2)^{1/2} \quad (16)$$

This equation can be simplified for ease of calculation of experimental data by employing the appropriate constant terms:

$$\mu_{\text{eff}} = 2.828 (\chi T)^{1/2} \quad (17)$$

which defines the magnetic moment of the compound, in units of the Bohr magneton (μ_{B}).

A plot of magnetic susceptibility (per mole) and magnetic moment versus temperature for a ferromagnetically coupled Cu_4L_4 grid can be seen in Figure 18, where L is a tetradentate ditopic pyridine-hydrazone ligand.



$$H_{\text{ex}} = -J(S_1 \cdot S_2 + S_2 \cdot S_3 + S_3 \cdot S_4 + S_1 \cdot S_4)$$

Figure 18: Magnetic profile for a Cu_4L_4 grid, along with the appropriate isotropic exchange Hamiltonian used to model the system. Reprinted (adapted) with permission from C. J. Matthews, K. Avery, Z. Xu, L. K. Thompson, L. Zhao, D. O. Miller, K. Biradha, K. Poirier, M. J. Zaworotko, C. Wilson, A. E. Goeta, J. A. K. Howard, *Inorg. Chem.*, **1999**, 38, 5266. Copyright (1999) American Chemical Society.⁸¹

The magnetic profile shows a slight decrease in the magnetic moment as temperature drops, followed by a sharp increase at 25 K, along with the corresponding increase in susceptibility around 7 K. This is indicative of the system being dominated by intramolecular ferromagnetic coupling. Fitting using MAGMUN4.1 gave $g = 2.07(0)$, $J = 7.2(8) \text{ cm}^{-1}$, $\text{TIP} = 475 \times 10^{-6} \text{ cm}^3 \text{ mol}^{-1}$, $\theta = -0.5 \text{ K}$. The fitted positive coupling constant ($J = 7.2 \text{ cm}^{-1}$) indicates ferromagnetic exchange.⁸¹

The other case would be a system which is dominated by intramolecular antiferromagnetic coupling, and would show a different magnetic profile and fit using MAGMUN4.1. The magnetic profile for an antiferromagnetically coupled Ni₄L₄ square is given in Figure 19, using the same magnetic model and exchange Hamiltonian as the Cu₄L₄ cluster. However, in this case $S = 2/2$. (1)

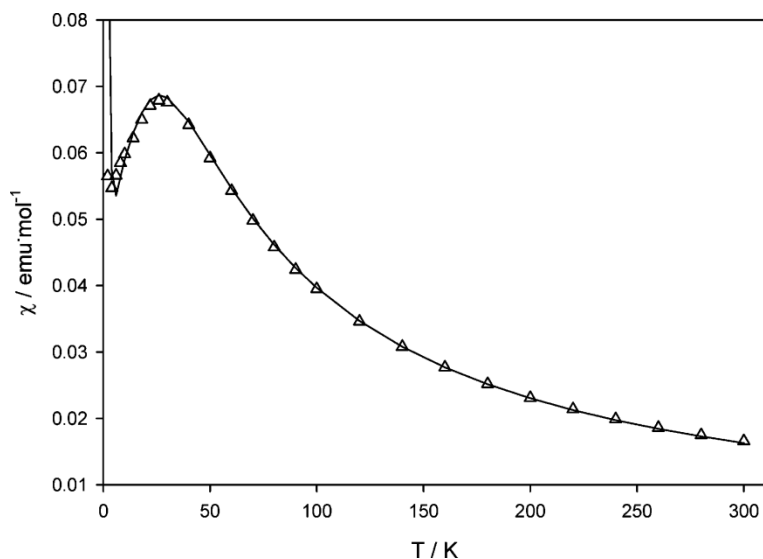


Figure 19: Magnetic profile for an antiferromagnetically coupled Ni(II)₄ [2×2] grid. C. J. Matthews, K. Avery, Z. Xu, L. K. Thompson, L. Zhao, D. O. Miller, K. Biradha, K. Poirier, M. J. Zaworotko, C. Wilson, A. E. Goeta, J. A. K. Howard, *Inorg. Chem.*, **1999**, 38, 5266. Copyright (1999) American Chemical Society.⁸¹

The plot of susceptibility versus temperature shows a maximum at around 35 K, which indicates the presence of antiferromagnetic coupling. The solid line represents the fit from the Van Vleck equation, while the triangles represent the experimental data for $g = 2.25(1)$, $J = -13.3(8) \text{ cm}^{-1}$, $\text{TIP} = 800 \times 10^{-6} \text{ cm}^3 \text{ mol}^{-1}$, $\theta = -1 \text{ K}$. The negative value of the coupling constant, $J = -13.3 \text{ cm}^{-1}$, also indicates antiferromagnetic exchange.⁷³ As

shown by the magnetic profiles for both the Cu(II) and Ni(II) tetranuclear squares, MAGMUN4.1 can use the same magnetic model and exchange Hamiltonian (Van Vleck expression) to fit the magnetic data of two very different systems in terms of their coupling and magnetism.

Chapter 2: Experimental Methods

Solvents and chemicals used were purchased from commercial sources, and were used without further purification. Dry methanol was used in some reactions, and was distilled over magnesium from commercially available methanol.

Infrared (IR) spectra were obtained as Nujol mulls between KBr discs using a Mattson Polaris FT-IR instrument. Mass spectra were taken on an Agilent 1100 Series LC/MSD in atmospheric pressure chemical ionization positive (APCI+) mode with methanol-acetonitrile mixtures as solvents. NMR spectra were obtained on a Bruker 500 MHz instrument with deuterium labelled solvents that are commercially available. Elemental analysis was collected by Canadian Microanalytical Service in Delta, British Columbia. Melting point data were obtained on a Fischer-Johns melting point apparatus. In some of the elemental analysis', the %H had some discrepancies, which is not uncommon. This is possibly due to the sample being damp when sent away for collection.

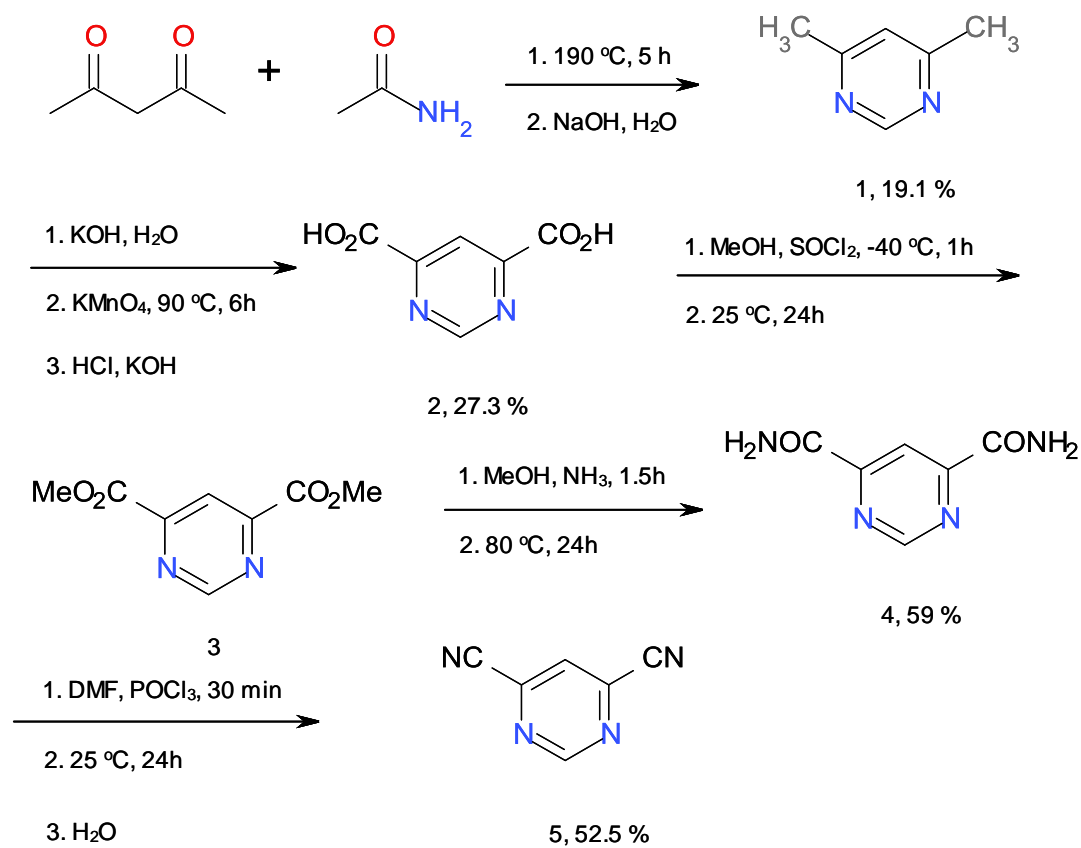
Variable temperature magnetic data were collected with a Quantum Design MPMS5S Squid Magnetometer using field strengths of 0.1-5 T and in the temperature range of 2-300 K. Background corrections for the sample holder assembly and diamagnetic components of the complexes were applied.

Crystallographic structural data were collected using an AFC8-Saturn 70 single crystal X-ray diffractometer from Rigaku/MSK, equipped with an X-stream 2000 low temperature system and a SHINE optic source. Crystal clear software was used for data collection and processing. Crystallographic structural data were collected, solved and refined by Dr. Louise Dawe.

The physical characteristics of some synthesized organic intermediates led to difficulty during the isolation process (e.g. product was wet or obtained in low yield). Therefore, some compounds are only characterized using one or two methods and compared to previous sample spectra to maximize the amount of ligand synthesized in the final product.

2.1 – Ligand Comments

Four tetratopic based organic ligands were successfully synthesized and characterized (via liquid chromatography mass spectrometry, infrared spectroscopy, and selected NMR spectra and melting points). These larger polytopic ligands were in general more difficult to synthesize than their corresponding ditopic and tritopic counterparts, and the yields of these reactions were generally much lower than with the smaller ligands. For these larger ligands, the main challenge for their successful synthesis was synthesis of the centrepiece 4,6-dicyanopyrimidine, which was very difficult. The synthesis of cyano substituted heterocycles such as bipyridines, pyrimidines, pyridazines, and imidazoles has been covered extensively.⁸²⁻⁸⁶ The synthesis of 4,6-dicyanopyrimidine took five steps,⁸⁷ and in general gave low yields of around 5%. The total synthesis of 4,6-dicyanopyrimidine, and the reagents used in its synthesis can be seen in Scheme 1. Figure 20 shows how this compound can be used to synthesize tetratopic ligands:



Scheme 1: Total synthesis of 4,6-dicyanopyrimidine.⁸⁷

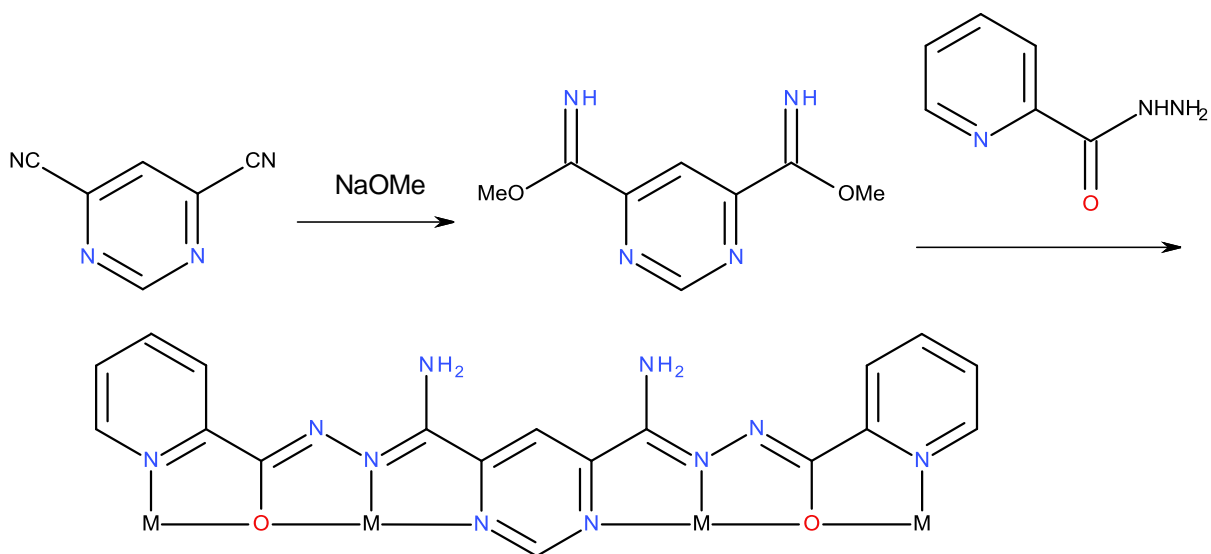


Figure 20: Synthesis of a tetratopic ligand from 4,6-dicyanopyrimidine (L2).

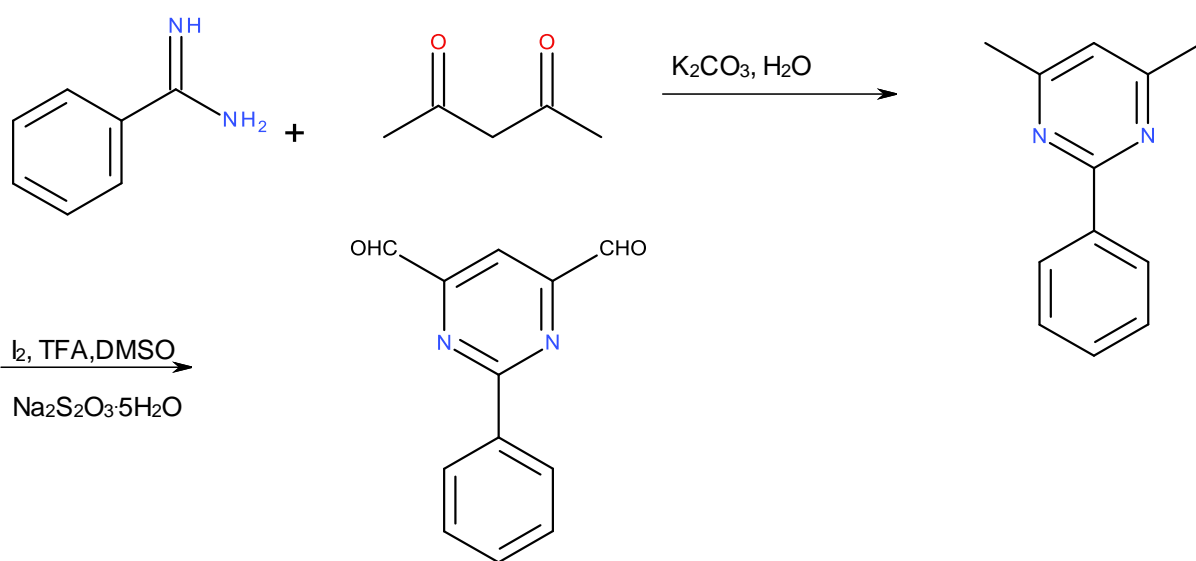
The ligands were synthesized using the technique of converting the nitrile functional groups of the pyrimidine ring to the di-iminoesters by reaction with sodium methoxide.⁸⁸ This was achieved using a solution of sodium methoxide generated *in situ* by dissolving metallic sodium in distilled methanol at a known concentration, such that the solution volume needed could be calculated. The nitrile groups on the pyrimidine ring react with the sodium methoxide to form the iminoester *in situ*. The further reaction with an appropriate hydrazone endpiece would lead to the desired ligand in a condensation reaction, with the release of methanol. Many reactions of this type were carried out, monitoring the amount of time for the iminoester formation to occur, and the temperature required. It was found that the best conditions for iminoester formation were around 30 minutes of reaction time, where a colour change from purple to orange/red was observed

at a refluxing temperature. Overall, the synthesis of four tetratopic ligands (L1, L2, L3 and L4) was attempted, by changing the hydrazone endpiece of the ligand.

The size of the polytopic ligands targeted using this approach was a cause for concern, because the larger ligands become, the lower the yield is likely to be. This is most likely due to the hydrolysis of imine N-C bonds by the presence of trace water in the reaction. This possibility was minimized by excluding water as a solvent or using dry solvents as much as possible. Complexation reactions of the ligand with a metal can also lead to ligand hydrolysis, but because harsh conditions such as high temperatures or acidic conditions were avoided, this possibility was also minimized. The solids recovered were characterized using LCMS and infrared spectroscopy, and were assumed to be the correct structure unless characterization strongly proved otherwise. The ligand solids were then mixed with a solution of a transition metal compound using various reaction conditions, and the resulting solution mixtures left for slow evaporation of the solvent for crystal formation.

Due to the difficulty of the synthesis of 4,6-dicyanopyrimidine (*vide supra*), another way to generate a similar centrepiece was investigated. The synthesis of a suitable building block, 2-phenylpyrimidine-4,6-dicarbaldehyde, was published by the Lehn research group.⁸⁴ This was a two-step process, first involving the synthesis of 2-phenyl-4,6-dimethylpyrimidine, using the method of Haley and Maitland,⁸⁵ using the starting materials acetyl acetone and benzamidine. This compound is then converted to the precursor aldehyde according to the published method by Lehn, by oxidation of the methyl groups using iodine and trifluoroacetic acid.⁸⁵ This seemingly simple two-step

process appeared to be much easier than the previous method, and should give higher yielding ligand products due to the aldehyde functional groups of the pyrimidine ring being much more reactive towards the hydrazone compounds than the corresponding nitrile functional groups of 4,6-dicyanopyrimidine. Scheme 2 illustrates the synthesis of this compound:



Scheme 2: Synthesis of 2-phenylpyrimidine-4,6-dicarbaldehyde. TFA refers to trifluoroacetic acid and DMSO refers to dimethyl sulfoxide.^{84,85}

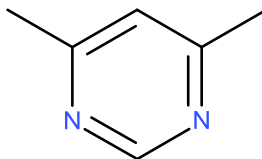
However, this synthesis of the precursor aldehyde proved to be very difficult, as the method published did not seem to work under the published conditions. Targeted ligands using this compound could not be synthesized, despite their potential for the formation of [4×4] based grid systems. This area of the project was studied extensively, with the reaction conditions modified from the reported procedure and tried due to the high potential of the ligand framework for square grid formation. Although the desired

success was not obtained in this area, there is still high potential for extended research in this class of ligands with high potential for cluster formation. Of course, this area can only be explored if the synthesis of the ligand can be performed to isolate the ligand in desirable yields, but the potential is there.

2.2 Ligand Synthesis

Building blocks for the construction of polytopic ligands based on a 4,6-disubstituted pyrimidine centrepiece.

2.2.1 - Compound 1. 4,6-Dimethyl pyrimidine

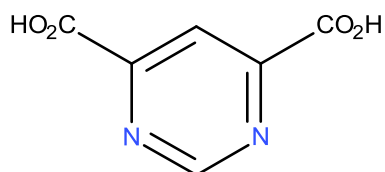


1

Acetylacetone (80.0 mL, 0.784 mol) and formamide (200 mL, 5.04 mol), were mixed in an Erlenmeyer flask to form a clear yellow solution. A three-necked round bottom flask was then equipped with a water condenser, air condenser, and a dropping funnel. The contents of the yellow solution were placed in the dropping funnel, and an additional 200 mL of formamide was added to the flask. An oil bath was pre-heated to 190°C, and the formamide solution was then immersed in the oil. Dropwise addition of the yellow solution into the hot formamide was then carried out over a period of 4-5 hours, into the refluxing reaction mixture. Upon full addition of the formamide/acetylacetone solution to the flask, a dark brown solution was obtained. The dark brown solution was neutralized with NaOH (9.00 g, 0.225 mol) in 80 mL of H₂O, and then transferred into a separatory funnel. The product was extracted with

3×150 mL aliquots of chloroform, and the organic layer was then reduced in volume to approximately 70 mL under reduced pressure. The organic layer was then vacuum distilled, and the product was collected in four different fractions at a temperature range of 40-60 °C and a pressure of 80 mm Hg. 4,6-Dimethylpyrimidine (**1**, 16.21 g, 19.1 % yield), a clear, colourless liquid, was the resulting product from the distillation.⁸⁷ Mass Spectrum (m/z): 109.1 (M+H).

2.2.2-Compound 2. 4,6-pyrimidine dicarboxylate

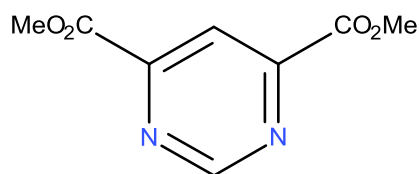


2

4,6-Dimethylpyrimidine (10.6 g, 0.0981 mol) and KOH (1.00 g, 0.0179 mol) were dissolved in 200 mL of H₂O to yield a cloudy, colourless mixture, which was placed in a three-necked round bottomed flask and heated to a temperature of 90 °C. KMnO₄ (60.00 g, 0.380 mol) was added as a solid in small portions to the dimethylpyrimidine solution, followed by rinsings with water. When the purple colour of the permanganate dissipated more KMnO₄ was added. The addition was carried out over a period of 2 hours, and the mixture refluxed for an additional 4 hours. A brown/black solid byproduct (MnO₂) was then separated by suction filtration, and the clear filtrate collected to be worked up. The clear solution was concentrated under reduced pressure to a volume of 70 mL, followed by addition of concentrated HCl until the pH of the solution was approximately 2. At this point a thick white solid formed and the

mixture was cooled in an ice bath to produce more product. The white solid was collected by suction filtration, and washed with water. The solid was then suspended in 50 mL of water in a round bottomed flask, and an aqueous solution of 4.00 g of KOH was added dropwise with slight heating. Upon completion of the addition, methanol was added until a white solid came out of solution (6.54 g, 27.3% yield) which was isolated by suction filtration, and washed with methanol.⁸⁷ Mass Spectrum (m/z): 169.1 (M+H), 245.1, IR (ν/cm^{-1}): 3384 (ν OH), 1621 (ν CO), 929 (ν pym).

2.2.3-Compound 3. 4,6-dimethyl pyrimidine dicarboxylate

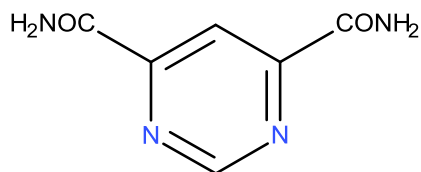


3

Compound **2** (3.99 g, 0.0163 mol) was slurried in 120 mL of methanol in a three-necked round bottomed flask, and the slurry was cooled to $-40\text{ }^{\circ}\text{C}$ with a dry ice/ethanol bath. The flask was equipped with a drying tube, stopper, and a dropping funnel. SOCl_2 (5.82 g, 0.0489 mol) was then added dropwise over a period of 1 hour, with no change in the reaction appearance. The white suspension was then warmed to room temperature and stirred at room temperature for 24 hours. The white solid, KCl, was then suction filtered, and the clear yellow filtrate was concentrated under reduced pressure to yield a pale yellow solid. Upon drying under vacuum, the yellow solid diester was still very wet, and difficult to isolate. Therefore, the product was used as is for the next step of the synthesis

immediately following this reaction (estimated mass of approximately 4.00 g).⁸⁷ Mass Spectrum (m/z): 197.1 (M+H), IR (v/cm⁻¹): 3384 (v OH), 1621 (v CO), 929 (v pym).

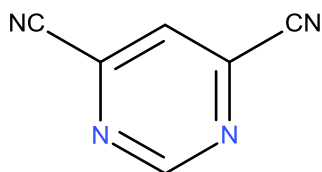
2.2.4-Compound 4. 4,6-pyrimidine diamide



4

The wet yellow solid (**3**), isolated from the previous step, was dissolved in 225 mL of methanol in a three-necked round bottomed flask. The flask was fitted with a condenser, stopper, and a gas bubbling connection which was attached to a cylinder of NH₃ gas. NH₃ was slowly bubbled through the methanolic solution for 1.5 hours, or until the solution was saturated with the gas, and the bubbler removed from the flask and replaced with a stopper. A white slurry formed, which was refluxed for 24 hours to ensure the reaction had been completed. The white solid (**4**, 2.00 g, ~59.0% yield) was then isolated by suction filtration, and washed with copious amounts of methanol and ether (an exact yield for this reaction could not be obtained as the starting ester was used from the previous reaction, with its exact mass unknown).⁸⁷ Mass Spectrum (m/z): 168.1 (M+H), IR (v/cm⁻¹): 3434, 3407, 3230 (v NH), 1704 (v CO), 929 (v pym).

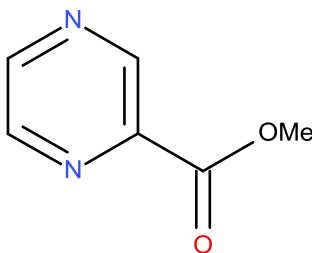
2.2.5-Compound 5. 4,6-pyrimidine dicyanitrile



5

Compound **4** (5.05 g, 0.0304 mol) was added to 45 mL of DMF in a round bottom flask to yield a cloudy white slurry. A dropping funnel was then attached to the flask, and 8.00 mL of POCl₃ (0.0858 mol) was placed in the funnel, and added dropwise over a period of 30 minutes. A brown slurry formed, which was then stirred at room temperature for 24 hours. A dark brown/black solution formed, which was then treated slowly with 7 mL of H₂O as the process is very exothermic. An additional 40 mL of water was added, and the solution was then extracted with 3×100 mL of chloroform. The clear yellow organic layer was then concentrated under reduced pressure to yield a clear, orange oil, which was then placed under vacuum to isolate the product. The oil was sublimed under reduced pressure to give a brown solid, which was recrystallized from chloroform to yield 2.08 g of pure compound **5** (52.5% yield).⁸⁷ Mass Spectrum (m/z): 131.1 (M+H) IR (ν/cm⁻¹): 1562, 1525 (ν CN), 910 (ν pym).

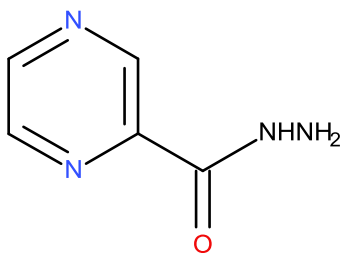
2.2.6-Compound 6. 2-methylpyrazine carboxylate



6

2-Pyrazine carboxylic acid (10.0 g, 0.0800 mol), was dissolved in 80 mL of methanol in a round bottomed flask, to yield a colourless solution. 5 drops of thionyl chloride were then added to the methanolic solution to yield a clear, colourless reaction mixture. The thionyl chloride was added as a source of H^+ , as it activates the carboxylic acid to form an acid chloride intermediate, which is then more susceptible to nucleophilic attack by the methanol in solution. The solution was then refluxed for three days. The resulting clear brown solution was concentrated under reduced pressure on a rotary evaporator to yield a pink solid (which turned brown upon standing).^{69,81} The product was very hard to isolate as it was stuck to the inside of the flask. Consequently, it was re-dissolved in methanol to yield a brown solution, which was concentrated again. The same problem existed, so a small sample of the product was taken for characterization, and the rest was left in the flask for the next reaction. Mass spectrum (m/z): 139.0 ($M+H$), 107.0, IR (ν/cm^{-1}): 1720 (ν CO ester), 954 (ν pyrazine).

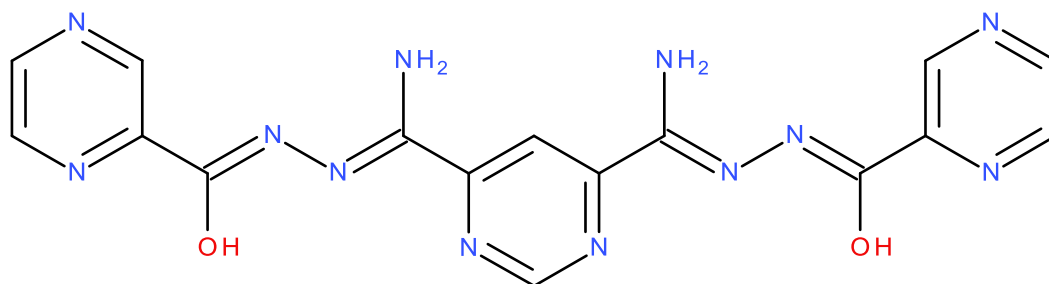
2.2.7-Compound 7. 2-pyrazine hydrazide



7

Compound **6** was re-dissolved in 200 mL of methanol in a round bottomed flask to yield a clear brown solution. To this, a solution of hydrazine monohydrate (4.97 g, 0.0993 mol) in 10 mL of methanol was added (just enough solvent to dissolve the hydrazine), which yielded no colour change. The resulting brown reaction mixture was then refluxed for 24 hours, at which time, an off-white precipitate formed in the brown solution. The very fine solid (8.97 g, estimated 81.2% yield) was isolated by suction filtration and washed with 2×10 mL of methanol, followed by air drying.^{69,81} Mass spectrum (m/z): 139.0 (M+H), 121.0, 193.0, IR (ν/cm^{-1}): 3305 (ν NH), 3226 (ν NH), 1647 (ν CO amide), 961 (ν pyrazine).

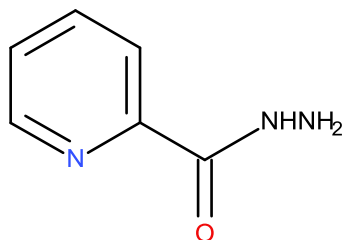
2.2.8-Compound 8. Ligand L1



8

Compound **5** (0.60 g, 0.0046 mol) was dissolved in 20 mL of dry methanol in a three necked round bottomed flask, and the solution was purged with N₂ gas and kept under a N₂ atmosphere. 1.5 mL of a solution of 0.29 M sodium methoxide in dry methanol was added to the reaction, forming the diiminoester of compound **5** *in situ*. The initial appearance was a deep purple solution, and following 40 minutes of reaction the colour was a red/orange colour indicating formation of the iminoester. 2-pyrazine hydrazone (1.34 g, 0.00971 mol) was then added, resulting in the formation of a yellow slurry, which was heated gently over a period of 8 hours. A bright yellow slurry was observed after 8 hours, and the yellow solid (0.82 g, 44% yield) was isolated by suction filtration and washed with methanol. Mass spectrum (m/z): 407.2 (M+H), 397.4, IR (ν/cm⁻¹): 3414 (ν OH), 3259 (ν OH), 3173 (ν NH), 1679 (ν CO amide), 955 (ν pyrazine).

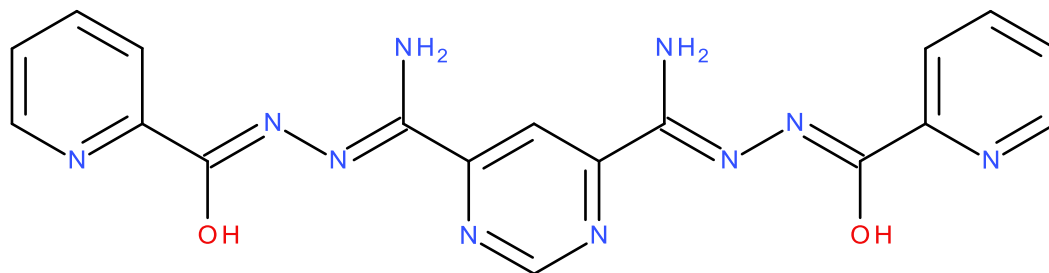
2.2.9-Compound 9. Picolinic hydrazide



9

Ethyl picolinate (2.00 g, 0.0132 mol) was dissolved in 30 mL of methanol to yield a colourless solution. $\text{N}_2\text{H}_4\cdot\text{H}_2\text{O}$ (0.79 g, 0.0158 mol) was added, and the resulting colourless solution was refluxed for 72 hours. The solution was then concentrated under reduced pressure to yield a clear yellow oil. The yellow oil was put under vacuum on a vacuum line to remove volatile impurities, which resulted in the formation of a pale yellow solid (1.78 g, 99.0% yield).^{69,81} Mass Spectrum (m/z): 168.1 (M+H), IR (ν/cm^{-1}): 3400 (ν OH) 3250, 3175, (ν NH), 1692 (ν CO).

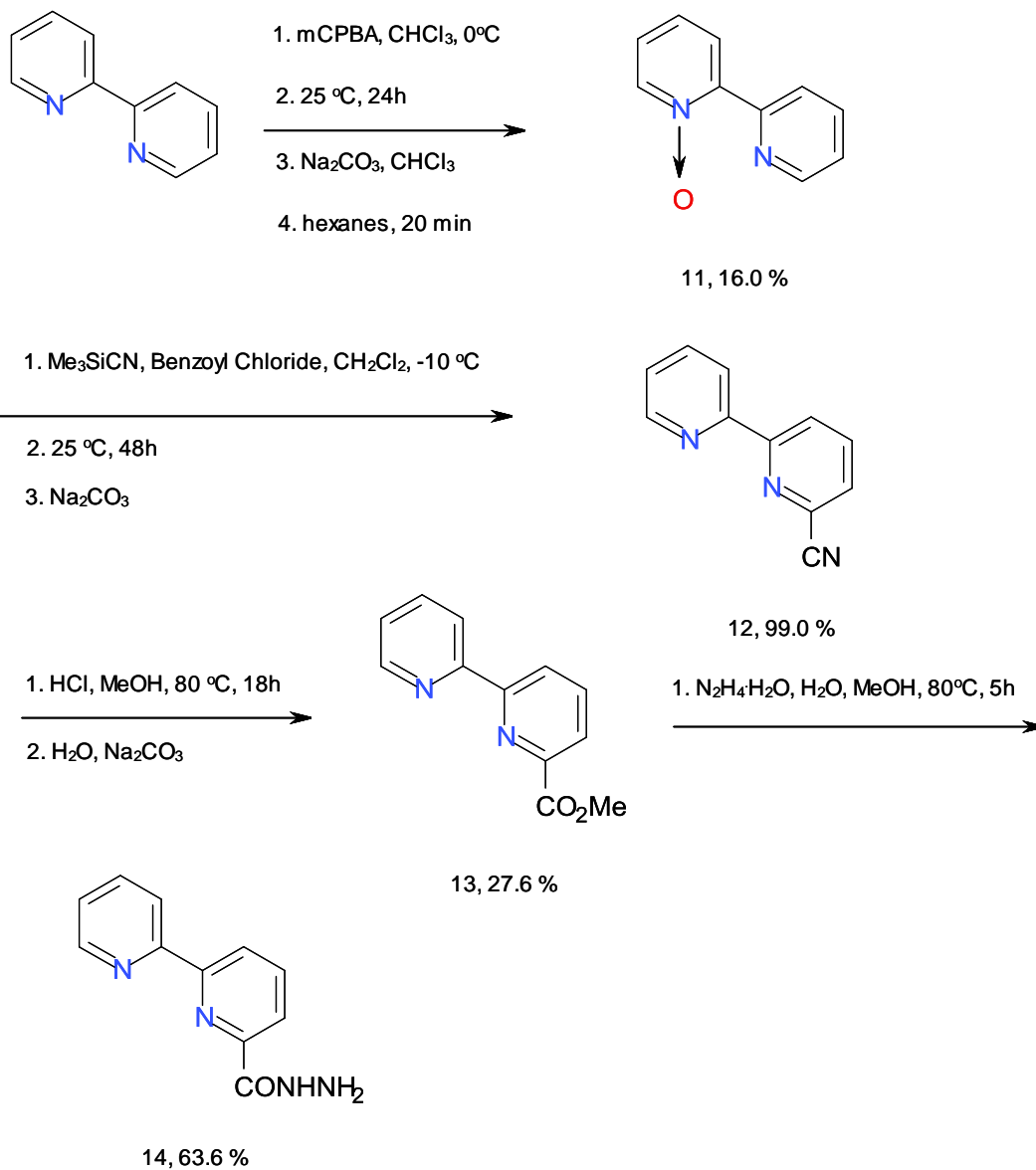
2.2.10-Compound 10. Ligand L2



10

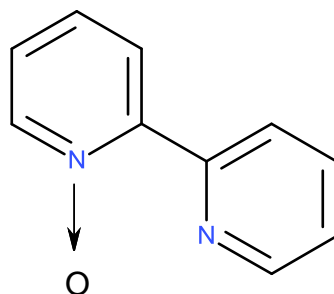
Compound **5** (0.60 g, 4.61 mol) was dissolved in 20 mL of dry methanol in a three necked round bottomed flask, and the solution was purged with N₂ gas and kept under a N₂ atmosphere. 1.3 mL of a solution of 0.29 M sodium methoxide in dry methanol was added to the reaction, forming a diiminoester of compound **5** *in situ*. After 40 minutes of reaction the colour was red/orange, typical of the iminoester. Compound **9** (1.32 g, 9.70 mol) was then added, resulting in the formation of a yellow slurry, which was heated gently over a period of 8 hours. A bright orange slurry was observed after 8 hours, and the orange solid (0.77 g, 41% yield) was isolated by suction filtration and washed with methanol.¹⁰⁸ Mass spectrum (m/z): 405.1 (M+H), IR (ν/cm⁻¹): 3405 (ν OH), 3253 (ν OH), 3169 (ν NH), 1680 (ν CO amide).

Scheme 3 illustrates the synthesis of compound **14** used to synthesize tetratopic ligand L3.



Scheme 3: Synthesis of bipyridine hydrazide (**14**). mCPBA refers to *m*-chloroperoxy benzoic acid, Me₃SiCN refers to trimethylsilyl cyanide, and MeOH refers to methanol.

2.2.11-Compound 11. 2,2'-bipyridine N - oxide

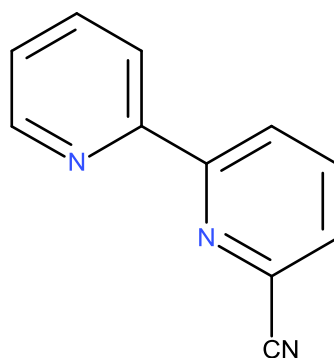


11

Bipyridine (17.43 g, 0.112 mol) was dissolved in 40 mL of CHCl_3 in a round bottomed flask to yield a clear yellow solution, which was chilled in an ice bath. Meta-chloroperoxybenzoic acid (mCPBA, 25.00 g, 0.145 mol) was dissolved in 160 mL of CHCl_3 , and half of this solution was added dropwise to the bipyridine solution with stirring. The resulting clear yellow solution was then stirred for 30 minutes, and the remaining mCPBA solution was added dropwise to the reaction. The resulting clear yellow solution was then stirred at room temperature for 24 hours, and concentrated under reduced pressure to a volume of 100 mL, which was transferred into a separatory funnel. The solution was washed with $2 \times 75\text{mL}$ of 5% Na_2CO_3 until CO_2 evolution had ceased, and then the aqueous layer was kept and washed with $2 \times 50\text{ mL}$ of CHCl_3 . The CHCl_3 extracts were then combined and concentrated to remove all remaining CHCl_3 . After pumping off the excess CHCl_3 under vacuum, 200 mL of hexane was added, and the mixture refluxed for 20 minutes to precipitate the excess bipyridine. The excess bipyridine was filtered off, and the solution was left to crystallize. A brown wet solid (**11**, 3.16 g, estimated 16% yield) was then isolated by

suction filtration. The wet nature of the solid made characterization difficult, so the next step was carried out in the procedure with this crude sample.

2.2.12-Compound 12.

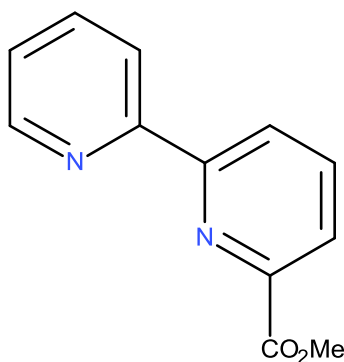


12

2,2'-bipyridine N - oxide (Compound 11) (3.16 g, 0.0184 mol) was dissolved in 70 mL of CH_2Cl_2 in a three necked round bottomed flask to yield a clear brown solution. Trimethylsilyl cyanide (12 mL, 0.0959 mol), was added to the flask with no change in solution appearance. The flask was equipped with a bubbler, a vacuum line connection, and a dropping funnel. The brown solution was purged with N_2 gas, and then cooled to $-10\text{ }^\circ\text{C}$ with a dry ice/ethanol bath. Benzoyl chloride (4.2 mL, 0.0362 mol), was placed into the dropping funnel and added dropwise with stirring to the reaction solution over a period of 15 minutes. The cooling bath was then removed, and stirring at room temperature continued over a period of 48 hours. 40 mL of 10% aqueous Na_2CO_3 was added carefully, and stirring continued for 40 minutes. Two washings with 20 mL of 10% aqueous Na_2CO_3 were then carried out in a separatory funnel, after which the organic layer was a red solution and the aqueous layer was

clear and colourless with a very high pH. The organic layer was separated and concentrated under reduced pressure to a very low volume, after which a brown/yellow crude solid formed, which was then filtered off and placed under vacuum in a round bottomed flask to remove impurities. The crude yellow product was then re-dissolved in 35 mL of warm CH₂Cl₂ to yield a brown solution, which was placed in an ice bath. Upon cooling, a brown solid (**12**, 3.22 g, estimated 99% yield) was isolated by suction filtration, and washed with diethyl ether. Mass spectrum (m/z): 176.0 (M+H), IR (v/cm⁻¹): 2233, 1581 (v CN).

2.2.13-Compound 13.

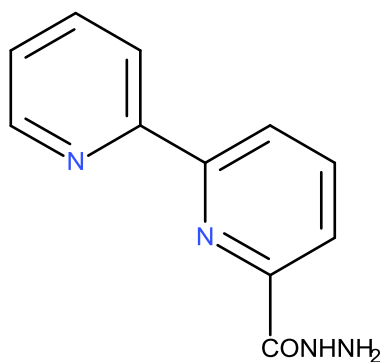


13

Compound **12** (3.36 g, 0.0186 mol) was dissolved in 250 mL of methanol in a round bottomed flask to yield a clear orange solution. 70 mL of concentrated HCl was added to the orange solution with no change in appearance. This solution was then purged with N₂ gas, and refluxed under N₂ for 18 hours. The volume of the resulting brown/red solution was decreased under reduced pressure to 80 mL, and then 200 mL of H₂O was added and the flask quickly placed in an ice bath to cool. Addition of

solid Na_2CO_3 followed to bring the solution to neutral pH, resulting in CO_2 evolution. Upon reaching neutral pH, a fine brown precipitate came out of solution, which was filtered off. The remaining reaction solution was then placed in a separatory funnel, and extracted with 4×80 mL portions of CHCl_3 , and the clear brown organic extracts were combined and concentrated to low volume to yield a dark brown solid, which was isolated by suction filtration. Upon removing volatile impurities under vacuum, the brown solid (**13**, 1.10 g, 27.6%) was collected. Mass spectrum (m/z): 215.1 (M+H) IR (ν/cm^{-1}): 1720 (ν CO).

2.2.14-Compound 14.

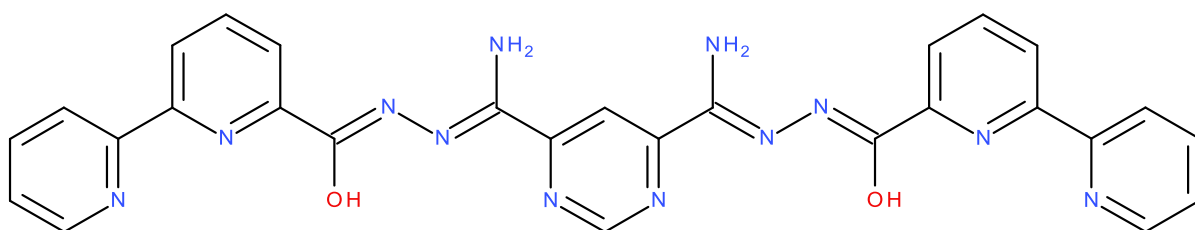


14

Compound **13** (1.10 g, 0.00512 mol) was dissolved in 40 mL of methanol in a round bottomed flask to yield a clear brown solution. $\text{N}_2\text{H}_4\cdot\text{H}_2\text{O}$ (0.31 g, 0.00614 mol) in 5 mL of methanol was added to the reaction mixture, and the clear brown solution refluxed for 5 hours. Upon completion of the heating, a pale yellow precipitate was present in the reaction mixture. The yellow solid (0.70 g, 63.6%) was

then isolated by suction filtration, and washed with methanol and ether. Mass spectrum (m/z): 215.1 (M+H) IR (ν/cm^{-1}): 3322, 3266 (ν NH), 1680 (ν CO).

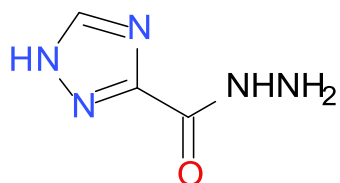
2.2.15-Compound 15. Ligand L3



15

Compound **5** (0.30 g, 0.00231 mol) was dissolved in 10 mL of dry methanol in a three necked round bottomed flask, and the solution was purged with N_2 gas and kept under a N_2 atmosphere. 0.8 mL of a solution of 0.29 M sodium methoxide in dry methanol was added to the reaction mixture via syringe, such that the diiminoester of compound **5** would form *in situ*. The resulting red solution was then neutralized with 2 drops of glacial acetic acid in dry methanol. Compound **14** (0.70 g, 3.26 mol) was then added, resulting in the formation of a pale red slurry, which was heated gently over a period of 24 hours. A bright yellow slurry was observed after 12 hours, and a yellow solid (0.20 g, 15.5% yield) was isolated by suction filtration and washed with methanol. Mass spectrum (m/z): 559.3(M+H), 541.3 IR (ν/cm^{-1}): 3453 (ν OH), 3371, 3328, 3308 (ν NH) 1671 (ν CO).

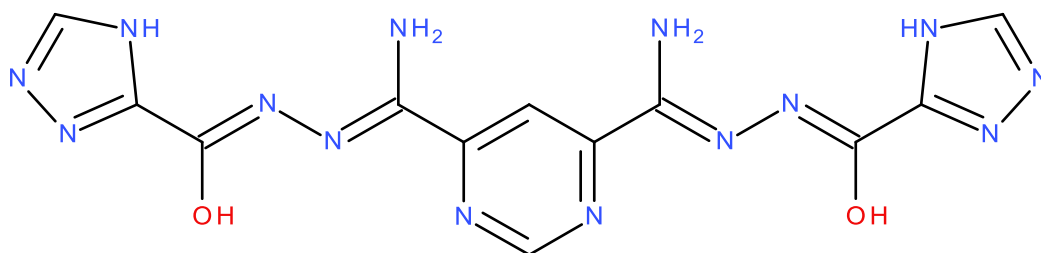
2.2.16-Compound 16. 1,2,4-triazole-5-hydrazide



16

Methyl-1H-1,2,4-triazole-3-carboxylate (10.00 g, 0.0787 mol) was placed in a round bottomed flask, and then dissolved in 175 mL of methanol to yield a colourless solution. $\text{N}_2\text{H}_4\cdot\text{H}_2\text{O}$ (4.92 g, 0.0983 mol) was dissolved in 25 mL of methanol, added to the ester solution, and the mixture refluxed for a period of 24 hours. After one hour of reaction, the result was a thick, white slurry. The resulting white solid (9.90 g, 99.0% yield) was isolated by suction filtration, and washed with methanol and ether. Mass spectrum (m/z): 128.1(M+H), 110.1, IR (v/cm^{-1}): 3299, 3218, 3147 (v NH), 1644 (v CO).

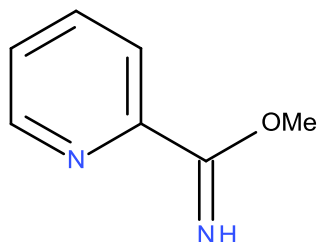
2.2.17-Compound 17. Ligand L4



17

Compound **5** (0.40 g, 0.00307 mol) was dissolved in 30 mL of dry methanol in a three necked round bottomed flask, and the solution was purged with N₂ gas and kept under a N₂ atmosphere. 0.6 mL of a solution of 0.29 M sodium methoxide in dry methanol was added to the reaction mixture via syringe, forming a diiminoester of compound **5** *in situ*. After 40 minutes, the resulting red solution was then neutralized with 2 drops of glacial acetic acid in dry methanol. Compound **16** (0.84 g, 6.61 mol) was added, resulting in the formation of a milky white slurry, which was heated gently over a period of 24 hours. The slurry became yellow after 12 hours, and the yellow solid (**17**, 0.87 g, 74% yield) was isolated by suction filtration and washed with methanol. Mass spectrum (m/z): 385.3(M+H), IR (v/cm⁻¹): 3444 (v OH), 3347, 3254 (v NH), 1665 (v CO).

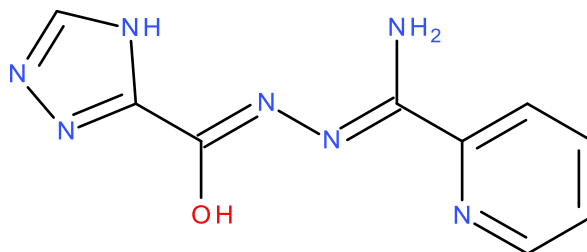
2.2.18-Compound 18.



18

2-Cyanopyridine (0.64 g, 0.0061 mol) was added to a colourless solution of sodium methoxide which was generated *in situ* by adding 0.09 g of sodium metal to 75 mL of methanol. The resulting colourless solution was stirred at room temperature with a drying tube attached to the round bottomed flask for 8 hours. The reaction mixture was then neutralized with glacial acetic acid, and was used in a subsequent reaction without isolating the product. Previous mass spectral studies of this product showed that there is a peak at 137.1 (M+H), corresponding to the molecular ion of **18**. However, due to the unstable nature of this product, it is normally generated *in situ*.⁸⁸

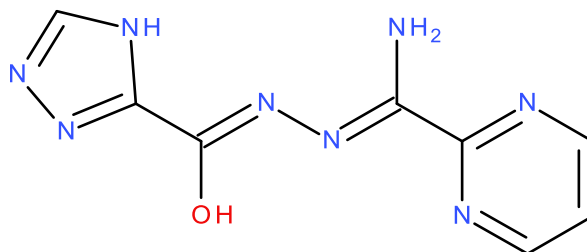
2.2.19-Compound 19. Ligand L5



19

The imidate ester of 2-cyanopyridine (Compound **18**, estimated 0.00679 mol) was prepared in 70 mL of dry methanol in a round bottomed flask, and compound **16** (0.75 g, 0.00590 mol) was added to the flask, resulting in a milky white slurry. An additional 30 mL of dry methanol was added, and the mixture was refluxed for 18 hours resulting in a thick yellow slurry. The yellow solid (**19**, 0.86 g, estimated 63.0% yield) was isolated by suction filtration, and washed with copious amounts of methanol and ether. Mass Spectrum (major mass peaks, m/z): 233 ($M + 2H$), 164. 1H NMR (ppm, DMSO- d_6) 3.17 (s) (CH), 7.06 (s) (NH), 8.49 (s) (NH), 10.5 (s) (OH), 7.49–8.61 (d, t, m) (CH aromatic). Selected IR data (Nujol, cm^{-1}): (ν NH) 3396, 3316 cm^{-1} , (ν CO amide) 1681, (ν CN) 1639 cm^{-1} . Anal. (%) Calcd. (Found) for $C_9H_9N_7O$: C, 46.76 (46.74); H, 3.84 (3.93); N, 42.85 (42.41).

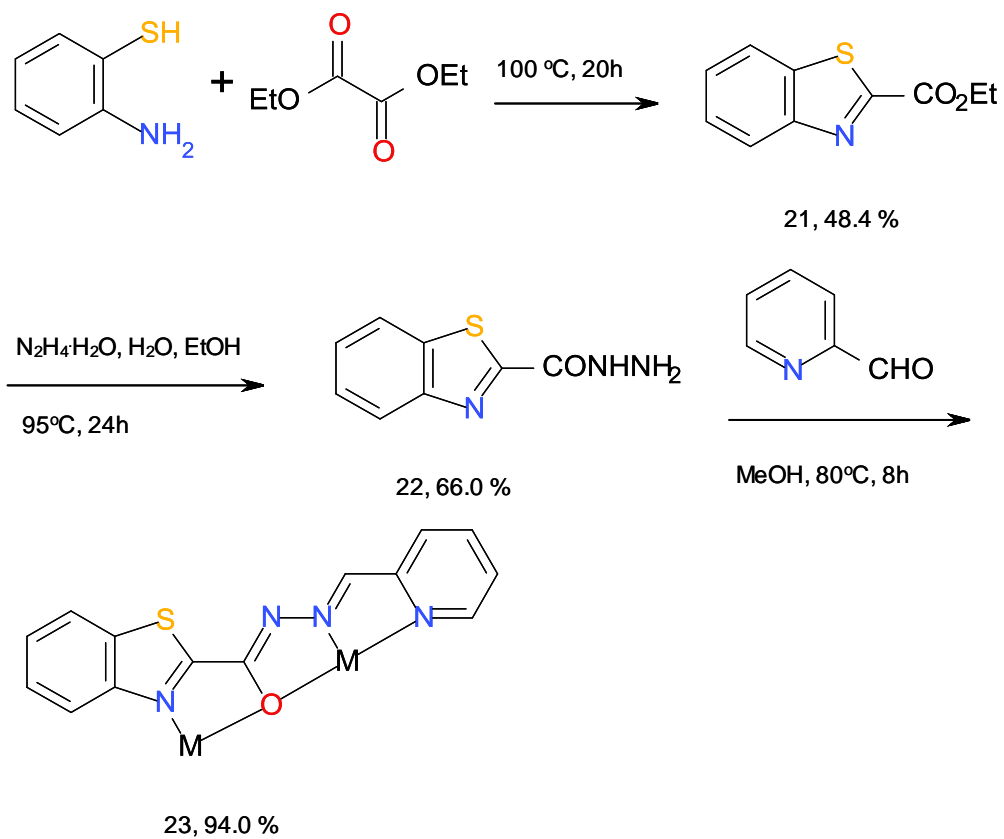
2.2.20-Compound 20. Ligand L6



20

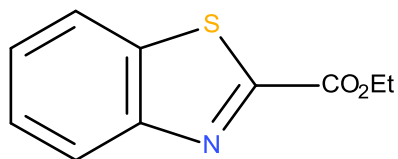
The imidate ester of 2-cyanopyrimidine (4.52 mmol, prepared by the same procedure as Compound **18**) in 50 mL of dry methanol in a round bottomed flask as a clear colourless solution. Compound **16** (0.50 g, 3.93 mmol) was added to the flask, resulting in a milky white slurry. An additional 30 mL of dry methanol was added, and the mixture was refluxed for 24 hours. After refluxing the mixture, the result was a thick, bright yellow slurry. The yellow solid (**20**, 0.88 g, 96.7% yield) was isolated by suction filtration, and washed with copious amounts of methanol and ether. Mass spectrum (m/z): 223.1 ($M+H$), (ν/cm^{-1}): 3396, 3316 (ν NH), 1640 (ν CO). Anal. (%) Calcd. (Found) for $C_9H_9N_7O$: C, 41.41 (41.38); H, 3.55 (3.45); N, 48.74 (48.28).

Scheme 4 illustrates the synthesis of ligand L7.



Scheme 4: Synthesis of the ditopic benzothiazole based ligand L7 depicting its two pocket coordination mode.

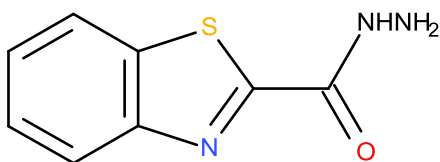
2.2.21-Compound 21. Benzothiazole ethyl ester



21

The preparation was done based on a previous method by Yale et al.⁸⁹ 2-aminothiophenol (5.00 g, 0.0399 mol) and diethyl oxalate (11.68 g, 0.0799 mol) were mixed in a round bottomed flask, resulting in a clear yellow solution. The yellow solution was then refluxed for 20 hours. Upon completion of the reaction, a purple/brown solid was present. This crude solid was isolated by suction filtration, and then immediately recrystallized using boiling hexanes, and chilled in an ice bath. A grey solid (4.00 g, 48.4% yield) crystallized out of solution, and was then isolated by suction filtration. M.pt. 58-61 °C, literature value 60-62 °C.⁸⁷ Mass spectrum (m/z): 208.1 (M+H), IR (ν/cm^{-1}): 1747 (ν CO), 3372, 3311, (ν NH).

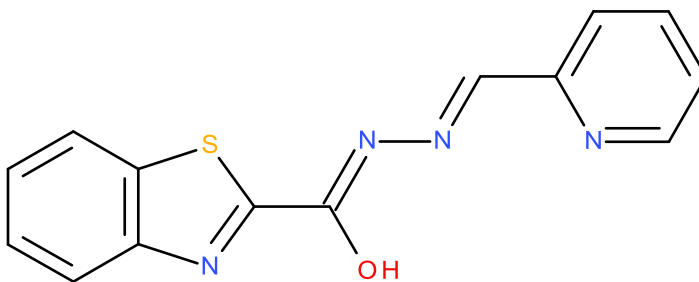
2.2.28-Compound 22. Benzothiazole hydrazide



22

Compound **21** (1.00 g, 0.00482 mol) was slurried in 50 mL of ethanol in a round bottomed flask to yield a grey slurry. $\text{N}_2\text{H}_4\cdot\text{H}_2\text{O}$ (0.28 g, 0.00555 mol) was added to the reaction flask, and upon swirling the colour of the slurry immediately changed to yellow. The yellow slurry was then refluxed over a period of 24 hours. Upon completion of the reaction, a yellow precipitate was present in a clear colourless solution. The yellow solid (0.61 g, 66% yield) was then collected by suction filtration, and washed with copious amounts of methanol. Mass spectrum (m/z): 193.1 (M+H), IR (v/cm^{-1}): 1677 (v CO), 3284, 3195 (v NH).

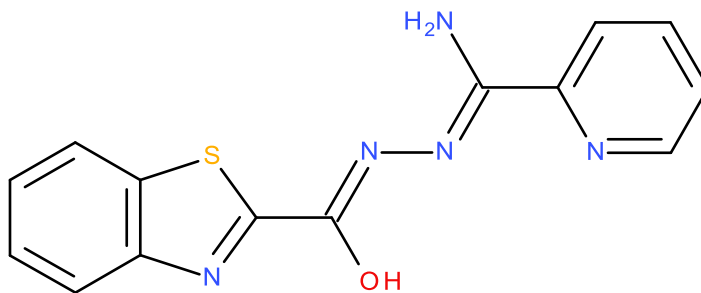
2.2.23-Compound 23. Ligand L7



23

Compound **22** (0.61 g, 0.00316 mol) was placed in a round bottomed flask, and 50 mL of methanol was added. 2-Pyridine carboxaldehyde (0.39 g, 0.00363 mol) was then added to the yellow slurry of **22**, with immediate change to a milky white slurry upon stirring. An additional 25 mL of methanol was added, and the white slurry was then refluxed for 8 hours. Upon completion of the reaction, a pale white solid was present in a clear yellow solution. The white solid (0.84 g, 94% yield) was then collected using suction filtration, and washed with methanol and diethyl ether. Mass Spectrum (major mass peaks m/z): 283 (M+H) ^1H NMR (ppm, DMSO- d_6) 1.23 (s) (CH), 8.71 (s) (NH), 7.44–8.65 (d, t, m) (CH aromatic). Selected IR data (Nujol, cm^{-1}): (ν NH) 3156 cm^{-1} , (ν CO amide) 1697 cm^{-1} . Anal. (%) Calcd. (Found) for $\text{C}_{14}\text{H}_{10}\text{N}_4\text{SO}$: C, 58.81 (58.50); H, 3.67 (3.45); N, 19.61 (20.19).

2.2.24-Compound 24. Ligand L8



24

The imidate ester of 2-cyanopyridine (Compound **18** (0.00647 mol)) was prepared in 70 mL of dry methanol in a round bottomed flask as before. Compound **22** (1.00 g, 0.00518 mol) was added to the colourless iminoester solution, followed by addition of 20 mL of extra methanol. The result was a bright yellow slurry, which was refluxed for a period of 24 hours. Upon completion of the reaction, a bright yellow precipitate was present in a clear, faintly yellow solution. The yellow solid (0.95 g, 62% yield) was then collected by suction filtration, and washed with methanol. Mass Spectrum (m/z): 298 (M+H), 280.0 (M - H₂O). ¹H NMR (ppm, DMSO-d₆) 7.24 (s) (NH), 8.64 (s) (NH), 7.53–8.31 (d, t, m) (CH aromatic). Selected IR data (Nujol, cm⁻¹): (ν NH) 3430, 3313 cm⁻¹, (ν CO amide) 1681 cm⁻¹, (ν CN) 1639 cm⁻¹. Anal. (%) Calcd. (Found) for C₁₄H₁₁N₅SO: C, 54.90 (54.85); H, 3.92 (3.61); N, 22.87 (22.50).

2.3 Complexation reactions

General Comments:

A variety of reaction conditions were chosen initially to optimize the best approach to complex formation. Ligand to metal ratios were varied, and reaction mixtures were filtered and the mother liquor left to crystallize by slow evaporation at room temperature. For example, when attempting to synthesize a [2×2] square grid, using a ditopic ligand, the stoichiometric ratio of metal to ligand of 1:1 was used, as in such a complex there are four ligands acting as potential Lewis base donors for four metals; solvent molecules or metal salt counter-ions would fill the additional coordination sites of the metal. For most complexation reactions, approximately 0.05 g of the ligand and an appropriate molar amount of metal salt, with a mixture of solvents such as methanol, acetonitrile, and water were used. For each ligand synthesized, a reaction with transition metal salts of Cu(II), Mn(II), Co(II), and Ni(II) was generally attempted. Evaporation of solvent at room temperature yielded either powdered products, which were re-dissolved in an attempt to produce crystalline materials, or crystals which were submitted for X-ray diffraction to determine a structure of the compound.

Complexes synthesized

2.3.1-[Cu₄(L5)₄](CF₃SO₃)₅(H₃O)(H₂O)₆ (25)

Copper(II) triflate (0.090 g, 0.00025 mol) was dissolved in 15 mL of methanol in a round bottomed flask to yield a blue solution. Compound **19** (Ligand L5) (0.050 g, 0.00022 mol) was added to the blue solution with stirring, and the result was an immediate colour change to a dark green solution. This green solution was then warmed and stirred for a period of 16 hours. The clear green reaction mixture was then gravity filtered into an Erlenmeyer flask and left to concentrate by slow evaporation at room temperature. A small quantity of green crystals suitable for X-ray structural determination were present after one week, which were then submitted for X-ray analysis. The hygroscopic nature of the crystals of this compound made characterization very difficult, and therefore the X-ray structure was the only major method of characterization used. An estimate of the mass of product obtained was about 30 mg. The Cambridge Crystallographic Data Centre (CCDC) number for this structure is 807494.

2.3.2-[Cu₄(L5)₄](H₂O)₄(ClO₄)₄ (26)

Copper(II) perchlorate hexahydrate (0.090 g, 0.00025 mol) was dissolved in 15 mL of methanol in a round bottomed flask to yield a clear blue solution. Compound **19** (Ligand L5) (0.050 g, 0.00022 mol) was added to the blue solution with stirring, resulting in an immediate colour change to a clear, dark green solution. A small amount of precipitate also formed, which readily dissolved upon addition of 3 mL of H₂O. The solution was then warmed and stirred for a period of 12 hours. The clear green reaction mixture was then gravity filtered into an Erlenmeyer flask, and left to concentrate by slow evaporation

at room temperature. Green crystals suitable for X-ray structural determination were present after one week, and then submitted for X-ray analysis. (0.040g, 25% yield) Anal. (%) Calcd (Found) for $[\text{Cu}_4(\text{C}_9\text{H}_{10}\text{N}_7\text{O})_4](\text{ClO}_4)_4(\text{H}_2\text{O})_5$ - C, 26.06 (26.06); H, 2.55 (1.93); N, 23.65 (23.62). The CCDC number for this structure is 807492.

2.3.3-Co(L7)₂(BF₄)₂ (27)

Cobalt(II) tetrafluoroborate (0.11 g, 3.1×10^{-4} mol) was dissolved in 15 mL of methanol in a round bottomed flask to yield a clear pink solution. Compound **23** (Ligand L7) (0.080 g, 2.8×10^{-4} mol) was added to the pink solution with stirring, and the result was an immediate colour change to a clear, dark red solution. After a period of one hour, 2 mL of H₂O was added to dissolve a small amount of precipitate that came out of solution. This red solution was then warmed and stirred for a period of 3 hours. The clear red reaction mixture was then gravity filtered into an Erlenmeyer flask, and left to concentrate by slow evaporation at room temperature. Red crystals suitable for X-ray structural determination were present after 3 days, and then submitted for X-ray analysis (0.03 g, 30% yield). Anal. (%) Calcd (Found) for $\text{Co}(\text{C}_{14}\text{H}_9\text{N}_4\text{SO})_2\text{BF}_4$ - C, 43.09 (42.93); H, 3.35 (2.52); N, 14.36 (14.64). The CCDC number for this structure is 807490.

2.3.4-[Co₅(L8)₆](BF₄)₂(SiF₆) (28)

Cobalt(II) tetrafluoroborate (0.10 g, 3.0×10^{-4} mol) was dissolved in 17 mL of methanol in a round bottomed flask to yield a clear pink solution. Compound **24** (Ligand L8) (0.080 g, 2.7×10^{-4} mol) was added to the pink solution with stirring, and the result was an immediate colour change to a red/orange slurry. 3 mL of methanol and 3 mL of H₂O was then added in an attempt to dissolve this precipitate. After a period of one hour, the

precipitate dissolved and the result was a clear, dark red solution. This red solution was then warmed and stirred for a period of 2 hours. The clear red reaction mixture was then gravity filtered into an Erlenmeyer flask, and the resulting solution left to evaporate slowly at room temperature. Red crystals suitable for X-ray structural determination were present after 3 days, and then submitted for X-ray analysis (0.01 g, 21% yield). Anal. (%) Calcd (Found) for $\text{Co}_5(\text{C}_{14}\text{H}_{10}\text{N}_5\text{SO})_6(\text{BF}_4)_2(\text{SiF}_6)(\text{H}_2\text{O})_{10}$ C, 39.26 (38.91); H, 3.14 (2.57); N, 16.36 (16.42). The CCDC number for this structure is 807491.

2.3.5-[Co₅(L8)₆](NO₃)₄ (29)

Cobalt(II) nitrate (0.10 g, 3.0×10^{-4} mol) was dissolved in 15 mL of methanol in a round bottomed flask to yield a clear pink solution. Compound **24** (Ligand L8) (0.08 g, 2.7×10^{-4} mol) was added to the pink solution with stirring, and the result was an immediate colour change and the formation of a red/orange slurry. 3 mL of methanol and 3 mL of H₂O was then added in an attempt to dissolve this precipitate. After a period of one hour, the precipitate dissolved and the result was a dark red solution. This red solution was then warmed and stirred for a period of 2 hours. The red solution was then gravity filtered into an Erlenmeyer flask, and left to evaporate slowly at room temperature. Red crystals suitable for X-ray structural determination were present after 10 days, and then submitted for X-ray analysis (0.01 g, 24% yield). Anal. (%) Calcd (Found) for $\text{Co}_5(\text{C}_{14}\text{H}_{10}\text{N}_5\text{SO})_6(\text{NO}_3)_4(\text{H}_2\text{O})_{15}$ C, 38.67 (38.87); H, 4.14 (2.72); N, 18.45 (18.26). There is no CCDC number for this structure as it is an unpublished sample.

2.3.6-[Mn₅(L8)₆](OAc)₄ (30)

Manganese(II) acetate tetrahydrate (0.050 g, 1.9×10^{-4} mol) was dissolved in 10 mL of acetonitrile and 5 mL of H₂O in a sample vial to yield a clear, pink solution. Compound **24** (Ligand L8) (0.050 g, 1.7×10^{-4} mol) was added to the vial, resulting in an orange solution with a small amount of unreacted ligand. The slurry was stirred for 20 minutes, after which a red solution was obtained. Stirring was continued for a period of 2 hours, and then the red solution was gravity filtered into another sample vial, and left to evaporate slowly at room temperature. Red crystals suitable for X-ray structural determination were present after 2 weeks, and then submitted for X-ray analysis (0.007 g, 24% yield) Anal. (%) Calcd (Found) for Mn₅(C₁₄H₁₁N₅SO)₆(OAc)₄(H₂O)₁₂ C, 43.99 (43.70); H, 4.10 (3.41); N, 16.74 (16.54). There is no CCDC number for this structure as it is an unpublished sample.

2.3.7-[Cu₁₆(L1)₈(H₂O)₁₆](CF₃SO₃)₁₆(H₂O)₁₇ (31)

Copper(II) triflate (0.10 g, 2.6×10^{-4} mol) was dissolved in 10 mL of methanol in a round bottomed flask to yield a clear blue solution. Compound **8** (Ligand L1) (0.050 g, 1.2×10^{-4} mol) was added to the clear blue solution, resulting in the formation of a clear, deep red solution. This solution was then stirred and heated gently for a period of 3 hours after addition of 3 mL of H₂O. The resulting clear red solution was then gravity filtered into an Erlenmeyer flask, and left to evaporate slowly at room temperature. Small red crystals were obtained, and the crystals were then sent to the Advanced Light Source synchrotron facility in Cincinnati, Ohio for structural determination, which did not yield a definitive structure. The crystals did not diffract well enough for a structural solution

using routine X-ray diffraction studies (*vide supra*) (0.010 g, 11% yield). Anal. (%) Calcd (Found) for $[\text{Cu}_{16}(\text{C}_{16}\text{H}_{15}\text{N}_{12}\text{O}_2)_8(\text{H}_2\text{O})_{16}](\text{CF}_3\text{SO}_3)_{16}(\text{H}_2\text{O})_{17}$ - C, 23.86 (23.73); H, 2.57 (1.84); N, 18.56 (18.19).

Chapter 3: Complexes of Ditopic and Tetratopic Hydrazone Ligands

3.1 Ditopic Triazole and Benzothiazole Based Ligands and their Complexation Reactions

3.1.1-Ligands

Two triazole and two benzothiazole ditopic hydrazone based organic ligands were successfully synthesized and characterized (via APCI mass spectrometry, infrared spectroscopy, and selected NMR spectra). These smaller ligands are simple two pocket ligands (ditopic), targeted for the formation of polynuclear square [2×2] grids (Figure 21). In general, these smaller ligands are much simpler to synthesize than their tritopic/tetratopic counterparts, and the yields of these reactions are generally much higher and involve smaller numbers of reaction steps. Two main hydrazide compounds (central backbone of the ligand framework) were examined: triazole carboxylic acid hydrazide and benzothiazole carboxylic acid hydrazide. Both of these hydrazone based precursors were fairly simple to synthesize and, upon addition of “endpieces”, the corresponding ditopic ligands were synthesized. For example, in the triazole based ligand L5, the hydrazide fragment was the portion of the ligand derived from the triazole hydrazide, and the “endpiece” was derived from 2-cyanopyridine. Figure 21 illustrates this concept:

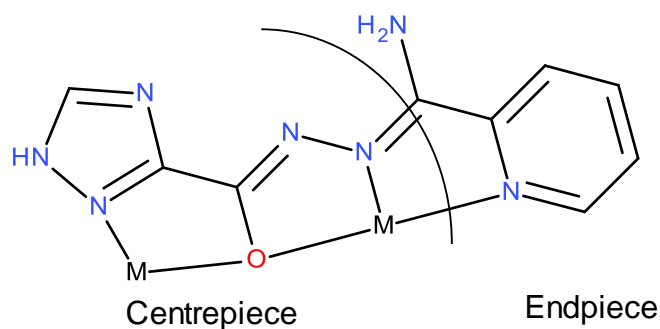


Figure 21: Illustration of the hydrazide backbone (centrepiece) and “endpiece” of triazole based ligand L5.

As seen in the introduction section, these ditopic ligands can adopt various coordination modes, either for the formation of tetranuclear [2×2] grids or in some cases mononuclear, dinuclear, and pentanuclear complexes. The formation of [2×2] square grids is facilitated by the formation of stable five-membered chelate rings in the ligand pockets upon coordination with the metal centre. The resulting grid complex is heteroleptic in nature, as the presence of a bidentate pocket in addition to the tridentate pocket of the ligand leads to coordinative unsaturation for a typical six-coordinate metal centre, and the four additional sites are filled by solvent or anionic ligand molecules present in the reaction mixture. The formation of mononuclear and dinuclear complexes sometimes occurs with certain metal ions, as an alternative structural arrangement.⁶³ The formation of homoleptic pentanuclear clusters can also occur with typical ditopic ligands. These ligands generally form heteroleptic [2×2] grids with octahedral metal centres, with solvent or anionic ligands (e.g. NO_3^-) filling the remaining coordination sites. However, in the case of poor anionic donor co-ligands (e.g. BF_4^-), co-ligand competition is reduced, and homoleptic oligomeric M_5L_6 trigonal bipyramidal clusters can result.^{46,68,90}

Two ditopic triazole and two ditopic benzothiazole ligands were synthesized and are discussed in this thesis. Both ligand types were synthesized by very similar procedures, via a hydrazide precursor, followed by the addition of an aldehyde or cyano based endpiece. These endpieces proved to be very reactive with hydrazide based nucleophiles, and these reactions proceeded very smoothly under very simple reaction conditions, with high percent yields.

In addition, similar bidentate ligands were synthesized using benzothiazole as a component of a series of ditopic ligands with the potential formation of [2×2] grid systems. The synthesis of these ligands first involved the formation of the benzothiazole ring from the reaction of 2-aminothiophenol and diethyl oxalate, followed by the simple synthesis of a hydrazide based compound from this ester. Upon addition of an “endpiece” to the resulting benzothiazole hydrazide, the desired ligand was recovered, as aldehyde and cyano based endpieces proved to be very reactive towards benzothiazole hydrazides. Scheme 4 in chapter 2 illustrated the synthesis of a ligand from this class.

3.1.2-Complexation Reactions

Six crystalline coordination complexes were successfully synthesized during this portion of the project, using self-assembly methods, and have been successfully characterized by X-ray diffraction. The structures will be discussed, in addition to their variable temperature magnetic properties. Two Cu(II) [2×2] grids, one Co(III) mononuclear compound, two Co(II) pentanuclear clusters, and one Mn(II) pentanuclear cluster, which forms a metal-organic framework type structure, will all be discussed.

Compound **25**, a Cu(II)₄ [2×2] grid, was produced by reaction of compound **19** (Ligand L5) with copper(II) triflate, to spontaneously self-assemble into the square grid structure. Ligand L5 also underwent a reaction with copper(II) perchlorate to form a second [2×2] Cu(II)₄ grid (compound **26**). The structures of both of these tetranuclear grids will be discussed. Ligand L9 underwent reaction with cobalt(II) tetrafluoroborate to produce a mononuclear Co(III) compound (compound **27**) by aerial oxidation. Ligand L10 produced two pentanuclear Co(II)₅ clusters, the first on reaction with cobalt(II) tetrafluoroborate (compound **28**), and the second upon reaction with cobalt(II) nitrate (compound **29**). Finally, ligand L10 also underwent reaction with manganese(II) acetate to yield a Mn(II)₅ pentanuclear cluster, which showed a metal-organic framework type structure, upon examining the extended lattice of the crystal structure. The X-ray crystal structures of all compounds will be discussed in the next section.

3.1.3-Crystallographic Data

The collection and processing of all crystal structures was done using CrystalClear (Rigaku)⁹¹ The structures of all compounds were solved using direct methods,⁹² expanded using Fourier techniques⁹³ with all non-hydrogen atoms refined anisotropically. Hydrogen atoms were refined by introducing them into a difference map or calculated positions and were refined positionally with fixed displacement ellipsoids, or refined using the riding model. In some cases, the protons corresponding to lattice solvent molecules could not be located in difference map positions, and were omitted from the structure models. These atoms were included in the formulas for the calculation of intensive properties. Neutral atom scattering factors were taken from

Cromer and Waber,⁹⁴ anomalous dispersion effects were taken from Creagh and McAuley,⁹⁵ and values for the mass attenuation coefficients are those of Creagh and Hubbell.⁹⁶ All calculations were done using the CrystalStructure⁹⁷ crystallographic software package, excluding refinement which was performed using SHELXL-97.^{98,99} In addition, disordered lattice solvent electron density for some structures was removed via Platon's SQUEEZE procedure.¹⁰⁰

The crystallographic data for all six compounds (Compounds **25**, **26**, **27**, **28**, **29**, and **30**) are listed in Table 1.

Table 1: Crystallographic data for compounds **25-30**.

	25	26	27	28
Empirical Formula	C ₁₄ H ₄₇ Cu ₄ F ₁₅ N ₂₈ O ₂₆ S ₅	C ₃₆ H ₄₀ Cl ₄ Cu ₄ N ₂₈ O ₂₄	C ₂₈ H ₁₈ BCoF ₄ N ₈ O ₂ S ₂	C ₈₄ H ₈₀ Co ₅ N ₃₀ O ₁₆ B ₂ F ₁₄ SiS ₆
Mol wt	2047.45	1644.88	708.36	2568.46
Cryst syst	Triclinic	Tetragonal	Monoclinic	Monoclinic
Space group	P1 (#1)	I4 ₁ /a (#88)	C 2/c (#15)	P2 ₁ /c (#14)
Crystal color, habit	Green prism	Green prism	Red prism	Brown prism
Cryst. dimensions/mm	0.29 x 0.29 x 0.22	0.21 x 0.14 x 0.13	0.15 x 0.12x 0.09	0.21 x 0.05 x 0.04
<i>a</i> /Å	10.659(9)	14.7586(16)	21.057(3)	13.132(8)
<i>b</i> /Å	13.767(1)		16.647(2)	29.758(3)
<i>c</i> /Å	14.415(2)	27.279(3)	17.450(3)	27.266(3)
α /deg	68.669(8)	90.00	90	90.00
β /deg	89.741(1)	90.00	104.873(3)	104.665(7)
γ /deg	68.154(7)	90.00	90	90.00
<i>V</i> /Å ³	1808(0)	5941.8(11)	5912.0(15)	10308(3)
ρ_{calcd} /(g cm ⁻³)	1.880	1.839	1.592	1.655
<i>T</i> /K	153(2)	153(2)	153(2)	153(2)
<i>Z</i>	1	4	8	4
no. of reflns collected	16694	26011	36228	132880
total, unique, <i>R</i> _{int}	12719, 0.0204	3084, 0.0267	5498, 0.0473	21346, 0.0947
obsd (<i>I</i> > 2.00 σ (<i>I</i>))	12633	2978	5343	17835
final <i>R</i> 1, <i>wR</i> 2 ^a	0.0444, 0.1230	0.0813, 0.2390	0.0836, 0.2351	0.0965, 0.2244

$$^a R1 = \sum ||Fo| - |Fc|| / \sum |Fo|$$

$$wR2 = [\sum (w(Fo^2 - Fc^2)^2) / \sum w(Fo^2)^2]^{1/2}$$

	29	30*
Empirical Formula	C ₉₀ H ₈₄ Co ₅ N ₃₄ S ₆ O ₂₄	C ₉₀ H ₆₆ Mn ₅ N ₃₀ O ₆ (OAc) ₄ (H ₂ O) _x
Mol wt	2512.89	
Cryst syst	Monoclinic	Cubic
Space group	P2 ₁ /c (#14)	Ia-3d (#230)
Crystal color, habit	Red prism	Red prism
Cryst. dimensions/mm	0.21 x 0.16 x 0.02	
<i>a</i> /Å	12.980(6)	58.2223(8)
<i>b</i> /Å	28.594(1)	58.2223(8)
<i>c</i> /Å	30.941(1)	58.2223(8)
α /deg	90.00	90.00
β /deg	90.147(7)	90.00
γ /deg	90.00	90.00
<i>V</i> /Å ³	11484(8)	

$\rho_{\text{calcd}} / (\text{g cm}^{-3})$	1.453	
T/K	153(2)	153(2)
Z	4	
no. of reflns collected	21288	
total, unique, R_{int}	21288, 0.0816	
obsd ($I > 2.00\sigma(I)$)	14237	
final $R1, wR2^a$	0.0893, 0.2943	0.2114

$$^a R1 = \sum ||F_o| - |F_c|| / \sum |F_o|$$

$$wR2 = [\sum (w(F_o^2 - F_c^2)^2) / \sum w(F_o^2)^2]^{1/2}$$

*Compound **30** currently is under final refinement.

The molecular structure of the tetranuclear square cation in $[\text{Cu}_4(\text{L5})_4](\text{CF}_3\text{SO}_3)_5$ ($\text{H}_3\text{O})(\text{H}_2\text{O})_6$ (compound **25**) is shown in Figure 22, the core structure illustrating the geometry of the metal centres in Figure 23, and important bond distances and bond angles are listed in Table 2.

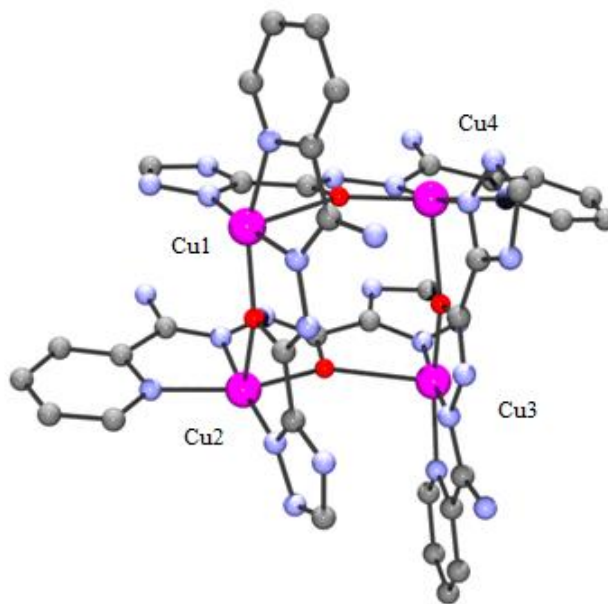


Figure 22: Structural representation of $[\text{Cu}_4(\text{L5})_4](\text{CF}_3\text{SO}_3)_5(\text{H}_3\text{O})(\text{H}_2\text{O})_6$ (Compound **25**) (ball and stick projection, developed from ORTEP thermal ellipsoids), with triflate anions, hydronium ions, water molecules and hydrogen atoms removed for clarity. Colour code: Cu(II) (magenta), carbon (grey), nitrogen (blue), oxygen (red). ORTEP (Oak Ridge Thermal-Ellipsoid Plot Program). K. Johnson Carroll, 1965. "ORTEP: A FORTRAN Thermal-Ellipsoid Plot Program for Crystal Structure Illustrations".

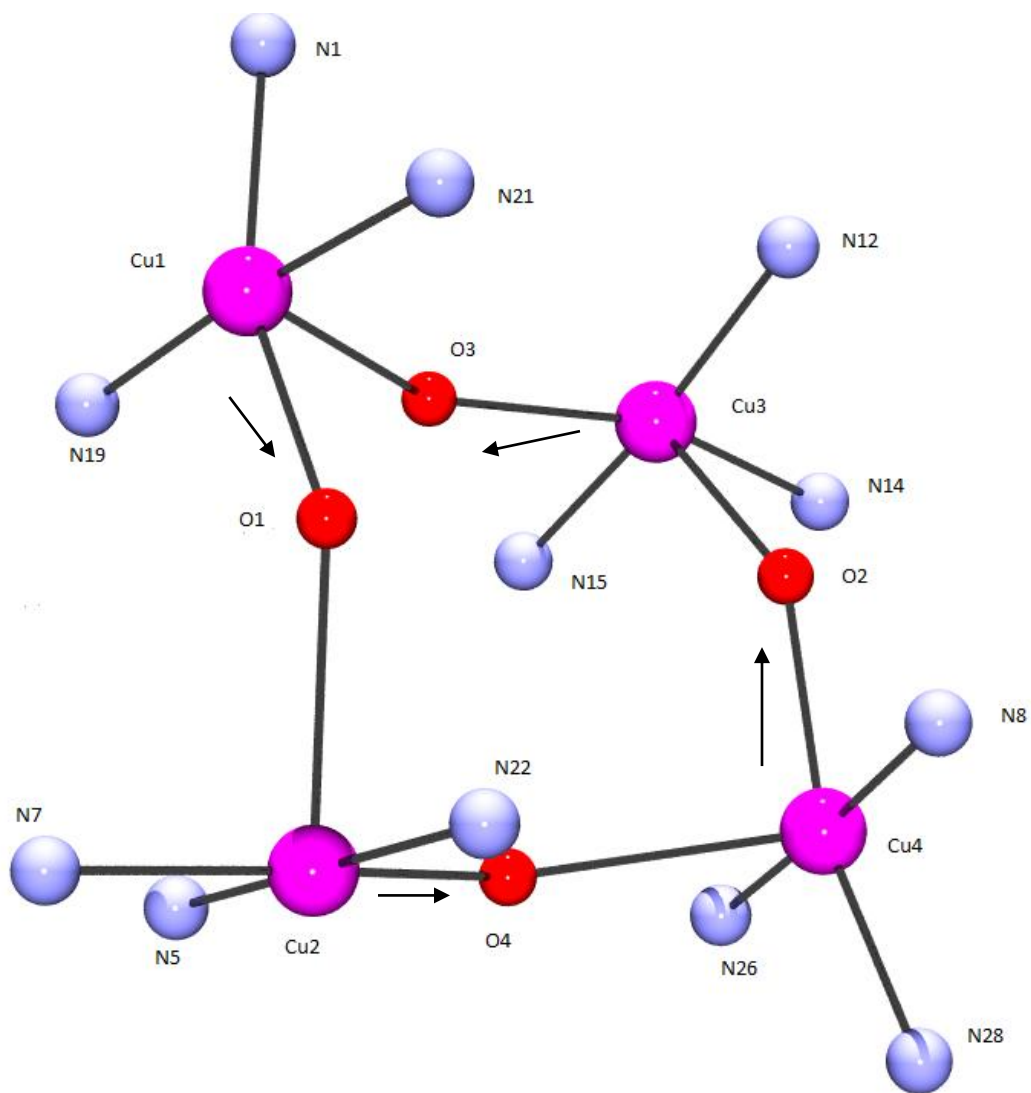


Figure 23: Cu(II)₄ core of [Cu₄(L5)₄](CF₃SO₃)₅(H₃O)(H₂O)₆ (Compound **25**), depicting the square pyramidal coordination environment at each Cu(II) centre. Colour code: Cu(II) (magenta), nitrogen (blue), oxygen (red). The arrows indicate directions of the long Jahn-Teller distortion axes.

Table 2: Important bond distances (Å) and angles(°) for compound **25**.

Cu1-N19	1.914(5)	Cu3-O3	2.446(3)
Cu1-N1	1.949(5)	Cu4-N26	1.943(5)
Cu1-O3	1.990(4)	Cu4-N8	1.965(5)
Cu1-N21	2.029(5)	Cu4-N28	2.030(5)
Cu1-O1	2.533(3)	Cu4-O4	2.033(4)
Cu2-N5	1.924(4)	Cu4-O2	2.316(4)
Cu2-N22	1.953(4)	Cu1-O1-Cu2	143.71(13)
Cu2-O1	1.996(4)	Cu1-O3-Cu3	141.12(13)
Cu2-N7	2.023(5)	Cu2-O4-Cu4	145.16(14)
Cu2-O4	2.731(3)	Cu3-O2-Cu4	138.99(13)
Cu3-N12	1.913(5)		
Cu3-N15	1.979(5)		
Cu3-O2	2.008(4)		
Cu3-N14	2.031(5)		

Compound **25** consists of a Cu(II)₄ [2×2] grid, with the four copper ions bridged by deprotonated μ-O hydrazone oxygen atoms in a square arrangement. The copper ions are square pyramidal in geometry, with long axial Cu-O contacts to oxygen atoms from the ligand oxygen ranging from 2.316-2.731 Å highlighting the Jahn-Teller axis of each copper centre (Figure 23). In addition to these long contacts, short in-plane Cu-O contacts range from 1.990-2.030 Å, which are also ligand oxygen atoms. Cu-O-Cu angles are in the range of 138.9-145.2°, and the Cu-Cu separations are 4.052-4.551 Å. The alternating

arrangement of axial (long) and basal (short) Cu-O contacts within the $\text{Cu}_4-(\mu\text{-O})_4$ square leads to strict orbital orthogonality, suggesting dominant intramolecular ferromagnetic behavior (*vide infra*). This is consistent with a similar reported Cu(II) $[2 \times 2]$ grid published with the same ligand (Compound **26**).⁷⁷

The molecular structure of $[\text{Cu}_4(\text{L5})_4](\text{H}_2\text{O})_4(\text{ClO}_4)_4$ (Compound **26**) is shown in Figure 24, the core structure illustrating the geometry of the metal centres in Figure 25, and important bond distances and bond angles listed in Table 3.

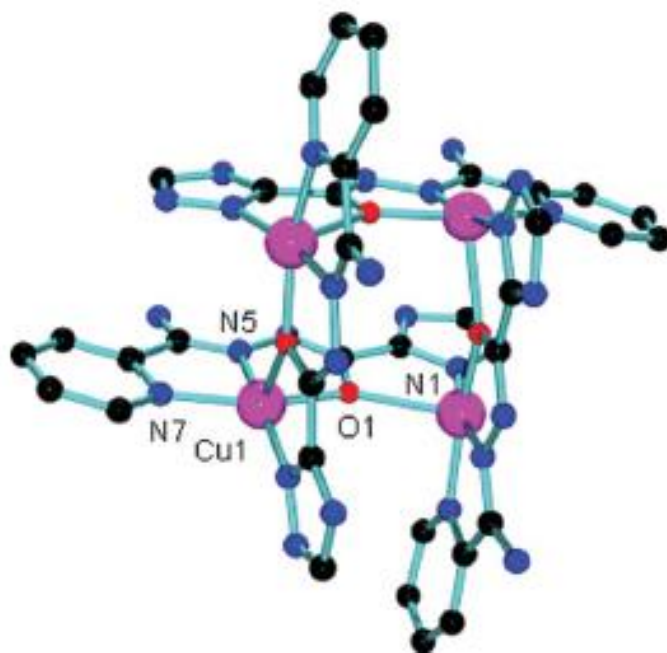


Figure 24: Structural representation of $[\text{Cu}_4(\text{L5})_4](\text{H}_2\text{O})_4(\text{ClO}_4)_4$ (Compound **26**, ball and stick projection, developed from ORTEP thermal ellipsoids), with perchlorate anions, water molecules and hydrogen atoms removed for clarity. Colour code: Cu(II) (magenta), carbon (black), nitrogen (blue), oxygen (red).

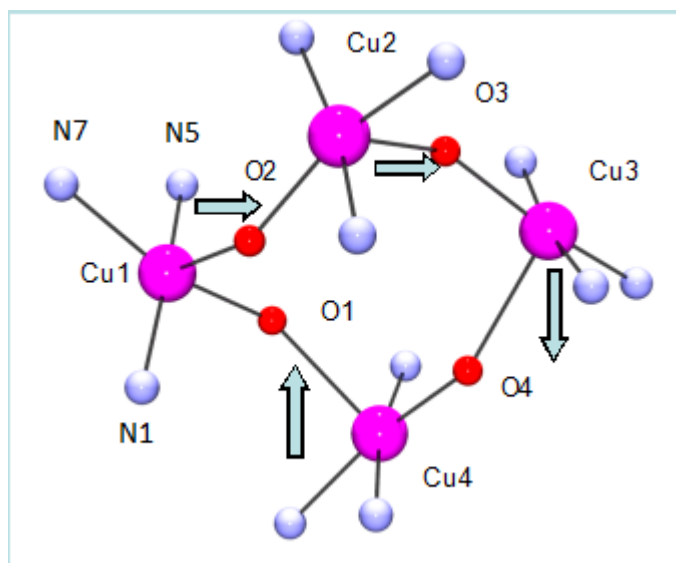


Figure 25: Cu(II)₄ core of [Cu₄(L5)₄](H₂O)₄(ClO₄)₄ (Compound **26**), depicting the square pyramidal coordination environment at each Cu(II) centre. Colour code; Cu(II) (magenta), nitrogen (blue), oxygen (red).

Table 3: Important bond distances (Å) and angles (°) for compound **26**.

Cu1-N5	1.907(5)
Cu1-O1	1.973(4)
Cu1-N1	1.981(4)
Cu1-N7	2.023(5)
Cu1-O1	2.331(3)
Cu1-O1-Cu2	138.40(2)

Compound **26** consists of a Cu(II)₄ [2×2] square grid arrangement which is very similar to compound **25**, with the four copper ions bridged by deprotonated μ-O hydrazone oxygen atoms from the ligands in a strictly square arrangement (four-fold symmetry). The copper ions are square pyramidal in geometry, with long axial Cu-O contacts to oxygens O1-O4 (2.331(3) Å), via the ligand molecules, coinciding with the Jahn-Teller

axis of each copper centre. In addition to these long contacts, short basal plane Cu-O contacts are 1.973(4) Å. Cu-O-Cu angles are 138.4°, and the Cu-Cu separations are 4.03 Å. The alternating arrangement of axial (long) and basal (short) Cu-O contacts within the Cu₄-(μ-O)₄ square (Figure 25) leads to strict orbital orthogonality, suggesting dominant intramolecular ferromagnetic behavior (vide infra). All bond distances at angles were essentially the same at each Cu centre, so only the properties for one Cu centre were included in Table 3.

The molecular structure of Co(L7)₂(BF₄)₂ (Compound **27**) is shown in Figure 26 and important bond distances and bond angles are listed in Table 4.

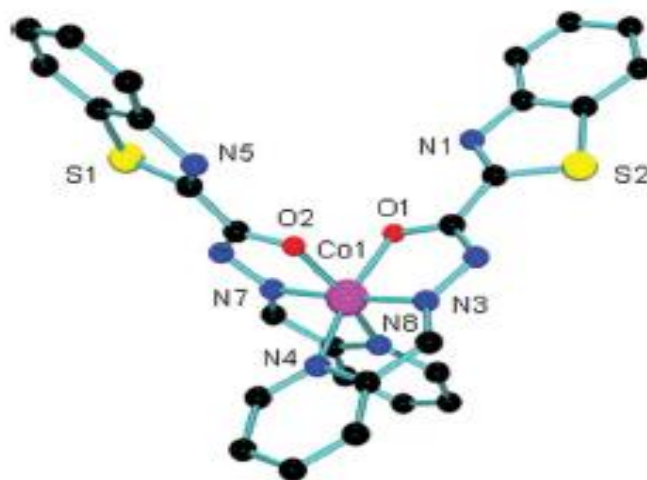


Figure 26: Structural representation of Co(L7)₂(BF₄)₂ (Compound **27**, ball and stick projection, developed from ORTEP thermal ellipsoids), with tetrafluoroborate anions and hydrogen atoms removed for clarity. Colour code: Co(III) (magenta), carbon (grey), nitrogen (blue), oxygen (red), sulphur (yellow).⁷⁷

Table 4: Important bond distances (Å) and angles (°) for compound **27**.

Co1-N2	1.852(4)	O1-Co1-O2	89.71(14)
Co1-N6	1.854(4)	N2-Co1-N5	100.41(18)
Co1-O1	1.902(3)	N6-Co1-N5	82.69(18)
Co1-O2	1.906(3)	O1-Co1-N5	90.67(15)
Co1-N5	1.924(4)	O2-Co1-N5	165.54(16)
Co1-N1	1.936(4)	N2-Co1-N1	82.56(17)
N2-Co1-N6	176.05(18)	N6-Co1-N1	99.82(16)
N2-Co1-O1	83.07(16)	O1-Co1-N1	165.63(15)
N6-Co1-O1	94.50(15)	O2-Co1-N1	90.88(15)
N2-Co1-O2	93.98(15)	N5-Co1-N1	92.32(16)
N6-Co1-O2	82.87(16)		

The structure of compound **27** is mononuclear with an octahedral, *bis-mer* CoN₄O₂ arrangement of two ligands around the Co(III) ion, involving just the pyridine imine endpieces of the ligands. The benzothiazole ring in both ligands remains uncoordinated to the metal centre, except for the deprotonated hydrazone oxygen atom, which binds terminally to the Co atom (Co-O 1.906(3), 1.902(3) Å). Co-ligand bond distances are generally very short for the complex (1.85-1.94 Å) indicating the initial Co(II) salt oxidized to a Co(III) oxidation state. This was due to the reaction mixture being exposed to air. The reaction was also performed when air was excluded from the reaction vessel by using a N₂ atmosphere. However, the same product was achieved, except the Co(II) salt used was cobalt(II) nitrate as opposed to cobalt(II)

tetrafluoroborate, but the same mononuclear type Co(III) compound was achieved with the same ligand. This should lead to this compound having no paramagnetism, as Co(III) compounds are generally low spin d^6 compounds, leading to a diamagnetic sample. Two BF_4^- ions are found in the lattice of compound **27**, but they are each only present at half occupancy, indicating that each ligand does in fact lose one proton, in agreement with the charge assessment of the complex. The uncoordinated benzothiazole rings sit well outside the metal coordination sphere, and present opportunities for inter-ring π contacts. The extended structure of compound **27** does reveal some π overlap between the benzothiazole rings, with the shortest ring-ring contacts being $\sim 3.5 \text{ \AA}$.⁷⁷ Figure 27 illustrates a portion of the extended structure.

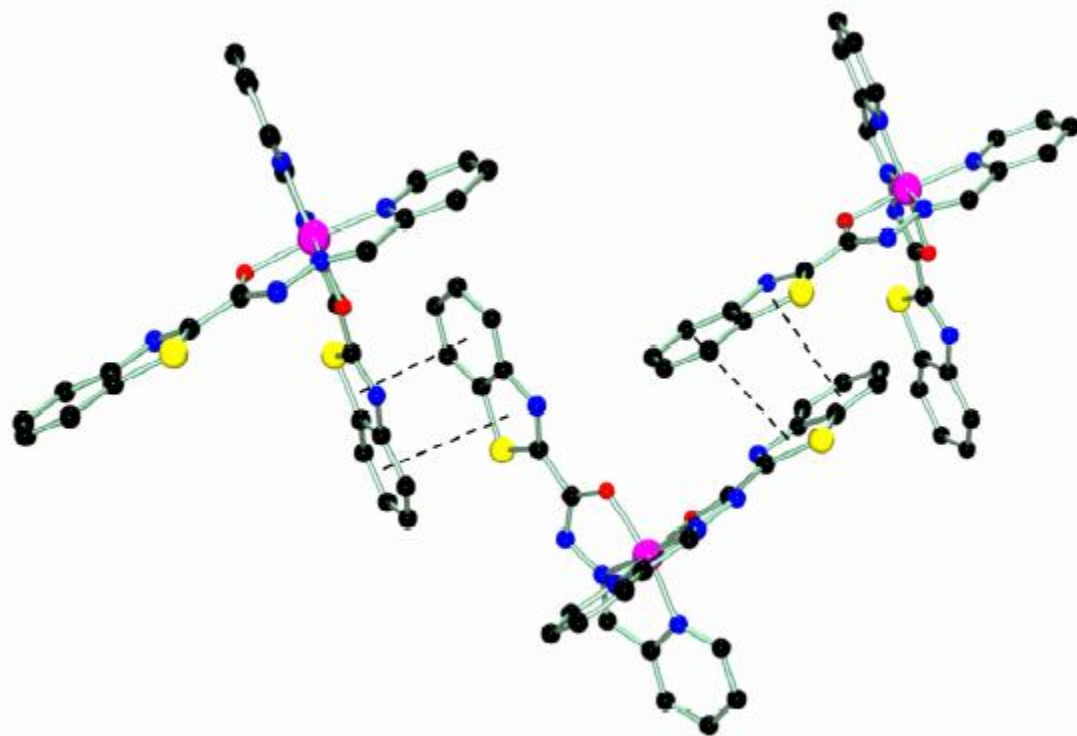


Figure 27: Extended lattice structure of compound **27**, showing the π - π interactions between the benzothiazole rings.⁷⁷

The molecular structure of $[\text{Co}_5(\text{L}8)_6](\text{BF}_4)_2(\text{SiF}_6)$ (Compound **28**) is shown in Figure 28, the core structure showing the metal-ligand bonding is shown in Figure 29, and important bond distances and bond angles are listed in Table 5.

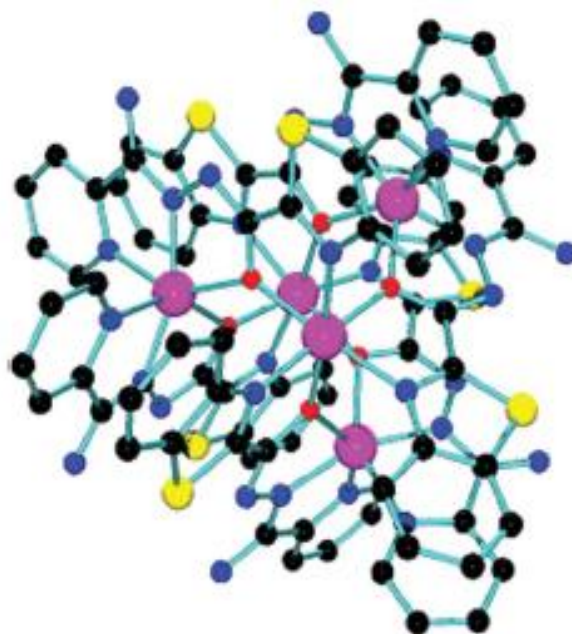


Figure 28: Structural representation of $[\text{Co}_5(\text{L}8)_6](\text{BF}_4)_2(\text{SiF}_6)$ (Compound **28**, ball and stick projection, developed from ORTEP thermal ellipsoids), with anions and hydrogen atoms removed for clarity. Colour code: Co(II) (magenta), carbon (black), nitrogen (blue), oxygen (red), sulphur (yellow).⁷⁷

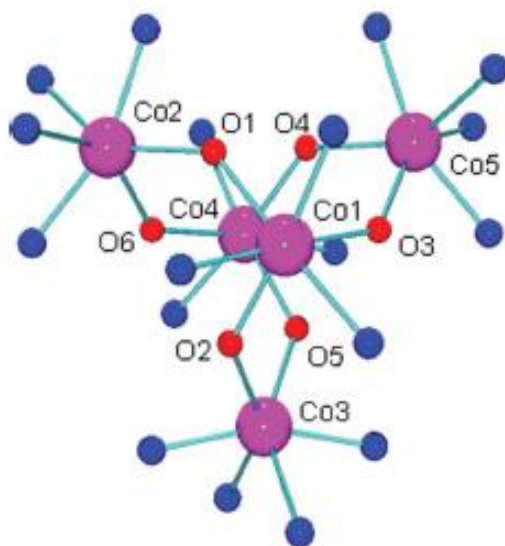


Figure 29: $\text{Co}(\text{II})_5$ core of $[\text{Co}_5(\text{L}8)_6](\text{BF}_4)_2(\text{SiF}_6)$ (Compound **28**), depicting the octahedral coordination environment at each Co(II) centre. Colour code: Co(II) (magenta), nitrogen (blue), oxygen (red).

Table 5: Important bond distances (Å) and angles (°) for compound **28**.

Co1-O2	2.086(4)	Co4-O5	2.094(4)
Co1-O3	2.102(4)	Co4-O4	2.101(4)
Co1-O1	2.114(4)	Co4-O6	2.101(4)
Co1-N1	2.129(5)	Co4-N26	2.127(5)
Co1-N6	2.138(5)	Co4-N21	2.136(5)
Co1-N11	2.157(5)	Co4-N16	2.145(5)
Co2-N28	2.033(5)	Co5-N18	2.011(5)
Co2-N3	2.036(5)	Co5-N13	2.015(5)
Co2-O6	2.143(4)	Co5-O3	2.160(4)
Co2-O1	2.175(4)	Co5-O4	2.165(4)
Co2-N30	2.209(5)	Co5-N15	2.223(5)
Co2-N5	2.224(5)	Co5-N20	2.246(5)
Co3-N23	2.016(6)	Co1-O1-Co2	137.60(19)
Co3-N8	2.018(5)	Co1-O2-Co3	136.2(2)
Co3-O2	2.143(4)	Co1-O3-Co5	137.9(2)
Co3-O5	2.161(4)	Co4-O4-Co5	136.0(2)
Co3-N25	2.205(5)	Co4-O5-Co3	136.3(2)
Co3-N10	2.206(5)	Co4-O6-Co2	136.6(2)

Compound **28** consists of a trigonal-bipyramidal cluster of Co(II) ions within a group of six tetradentate ligands. Each ligand bridges a pair of cobalt centres via the μ -O

hydrazone oxygen atom, and all six ligands coordinate in a similar fashion, with a hydrazone nitrogen, pyridine nitrogen and benzothiazole nitrogen filling the other coordination sites of the octahedral metal centres, resulting in a homoleptic cluster. Normally ditopic ligands of this type form heteroleptic [2×2] squares with six-coordinate metal ions (*vide infra*), with coordination of co-ligands, frequently anionic ligands, at the four vacant metal sites. In cases where anions are poor donors co-ligand competition is reduced, and other oligomeric cluster combinations are possible.¹⁰¹ The next highest homologue in the series would be a 5:6 (metal:ligand) homoleptic combination, and other examples of related trigonal-bipyramidal clusters with similar ligands have already been reported with Mn(II), Co(II) and Zn(II).^{101,102} In these systems, as is true in the present case, five six-coordinate metal ions are bonded to six ligands which each fill five metal coordination sites.¹⁰²

The core structure of compound **28** is illustrated in Figure 29, which shows the trigonal bipyramidal metal Co₅L₆ polyhedron, with the apical metal centres (Co1, Co4) bridged to three other Co(II) cations (Co2, Co3, Co5) via the hydrazone oxygen atoms, while these centres are only bridged via μ -O linkages to two adjacent metal ions. Co-L distances are relatively long, and range from 2.01-2.25 Å, which is typical of Co(II). Co-O-Co bond angles also fall in the range of 136-138°, similar to another Co(II)₅ cluster reported.^{101,102} The unexpected presence of SiF₆²⁻ in the lattice was also a bit surprising, since none of this counterion was added to the reaction medium. However, BF₄⁻ anions are known to hydrolyze to BF₃OH⁻ and HF,¹⁰³ which could explain presence of SiF₆²⁻

resulting from the etching of silicon from the glass round bottomed flask used during the synthesis from a reaction involving HF.

The individual Co(II) ions are also highly distorted, indicated by the wide variety of Co-L bond distances and L-Co-L bond angles at each metal centre. The apical CoN₃O₃ ions (Co1, Co4) have three Co-O distances which are comparable, and less than corresponding Co-N distances, and a slight rhombic distortion of the six-coordinate ligand environment. On the other hand, the equatorial CoN₄O₂ centres are highly distorted, with two very short Co-N bond distances (2.01-2.04 Å), with much longer contacts to the remaining coordinated atoms. Rhombic distortion is not as evident than it is at the apical Co(II) centres.¹⁰⁴

The molecular structure of compound **29**, [Co₅(L8)₆](NO₃)₄, is shown in Figure 30, the core structure showing the metal-ligand bonding is shown in Figure 31, and important bond distances and bond angles are listed in Table 5.

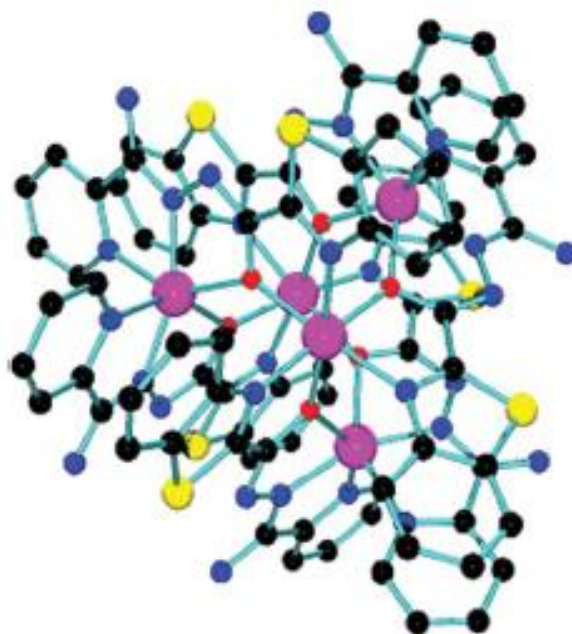


Figure 30: Structural representation of $[\text{Co}_5(\text{L}8)_6](\text{NO}_3)_4$ (Compound **29**) (ball and stick projection, developed from ORTEP thermal ellipsoids), with nitrate anions and hydrogen atoms removed for clarity. Colour code: Co(III) (magenta), carbon (black), nitrogen (blue), oxygen (red), sulphur (yellow).

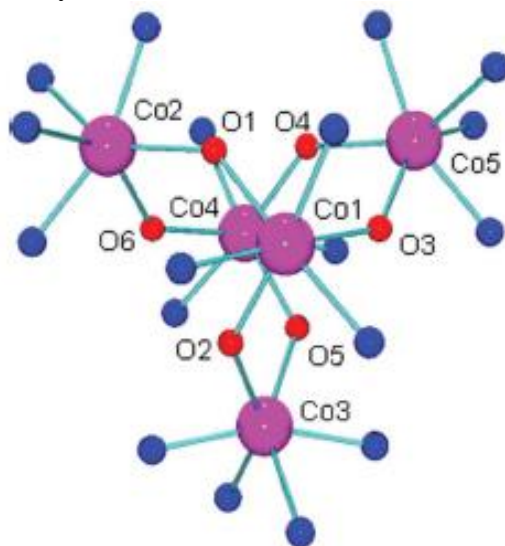


Figure 31: $\text{Co}(\text{II})_5$ core of $[\text{Co}_5(\text{L}8)_6](\text{NO}_3)_4$ (Compound **29**), depicting the octahedral coordination environment at each Co(II) centre. Colour code: Co(II) (magenta), nitrogen (blue), oxygen (red).

Compound **29** is almost identical in structure to compound **28** (Co-N and Co-O bond distances, along with Co-O-Co bond angles all fall in the same range as in compound **28**), as it also consists of a trigonal-bipyramidal cluster of Co(II) ions within a group of six tetradentate ligands. Each ligand again bridges a pair of cobalt centres via the μ -O bridged oxygen atom. The six ligands satisfy the octahedral coordination sphere of each Co(II) centre, resulting in a similar homoleptic complex.

The core structure of compound **29** is identical in nature to compound **28**, which is illustrated in Figure 31. This compound is again a trigonal bipyramidal polyhedron. Co-L bond distances and Co-O-Co bond angles are similar to previously reported Co(II)₅ complexes.^{101,102}

The molecular structure of compound **30**, [Mn₅(L8)₆](OAc)₄, is shown in Figure 32, the core structure showing the metal-ligand bonding is shown in Figure 33. Metric parameters are absent at the present time because the structure still requires complete refinement.

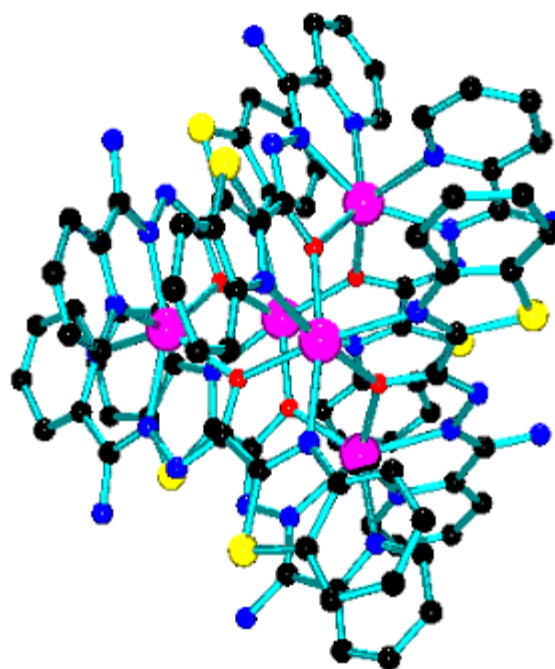


Figure 32: Structural representation of $[\text{Mn}_5(\text{L}8)_6](\text{OAc})_4$ (Compound **30**, ball and stick projection, developed from ORTEP thermal ellipsoids), with acetate anions and hydrogen atoms removed for clarity. Colour code: Mn(II) (magenta), carbon (black), nitrogen (blue), oxygen (red), sulphur (yellow).

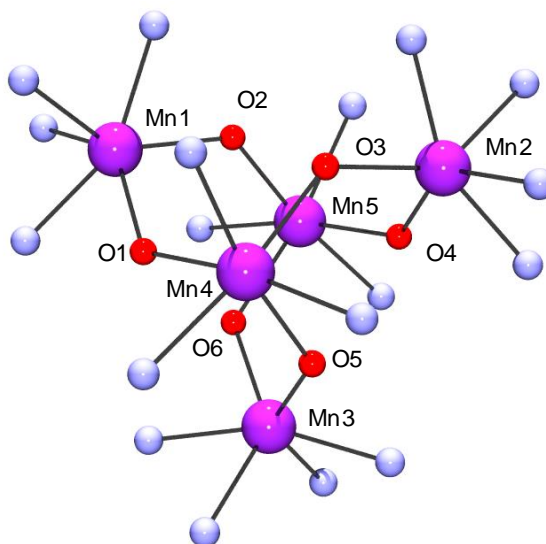


Figure 33: Mn(II)₅ core of $[\text{Mn}_5(\text{L}8)_6](\text{OAc})_4$ (Compound **30** depicting the octahedral coordination environment at each Mn(II) centre. Colour code: Mn(II) (magenta), nitrogen (blue), oxygen (red).

The structure of compound **30** reveals a homoleptic pentanuclear cation which is not fully refined. Therefore, the exact bond distances and bond angles in this structure are still to be determined. An approximation of the structural properties of compound **30** will be discussed, as opposed to the exact values. Six tetradentate ligands are bound to a trigonal bipyramidal $[\text{Mn}_5-(\mu\text{-O})_6]$ core cluster, such that there is again an exact match between the bonding capacity of the six ligands and the coordination requirements of the five octahedral metal ions. This self-assembled structure has been observed before with $\text{Mn}(\text{II})$ ^{93,94} and is an alternative to the $[2 \times 2]$ heteroleptic Mn_4 grid structure commonly observed with this class of ligand. Anion and solvent donor competition are regarded as the primary influences in the cluster outcome, with the weakly coordinating acetate anion favouring the formation of the trigonal bipyramidal cluster as opposed to the $[2 \times 2]$ grid. Mn–L bond distances and Mn–O–Mn bond angles are similar to those reported in related $\text{Mn}(\text{II})_4$ and $\text{Mn}(\text{II})_5$ compounds.^{101,102}

This complex is an example for which ordered self-assembly creates the primary polymetallic cluster but serendipitous self-assembly produces a very large novel extended metal-organic framework (MOF) type structure with distinct hydrophobic/hydrophilic channels. The hydrophobic channels have the aromatic rings pointing into the channel, while the hydrophilic channels have the $-\text{NH}_2$ groups from the ligand pointing in which undergo hydrogen bonding with solvent molecules. Figure 34 illustrates the MOF nature of the structure:

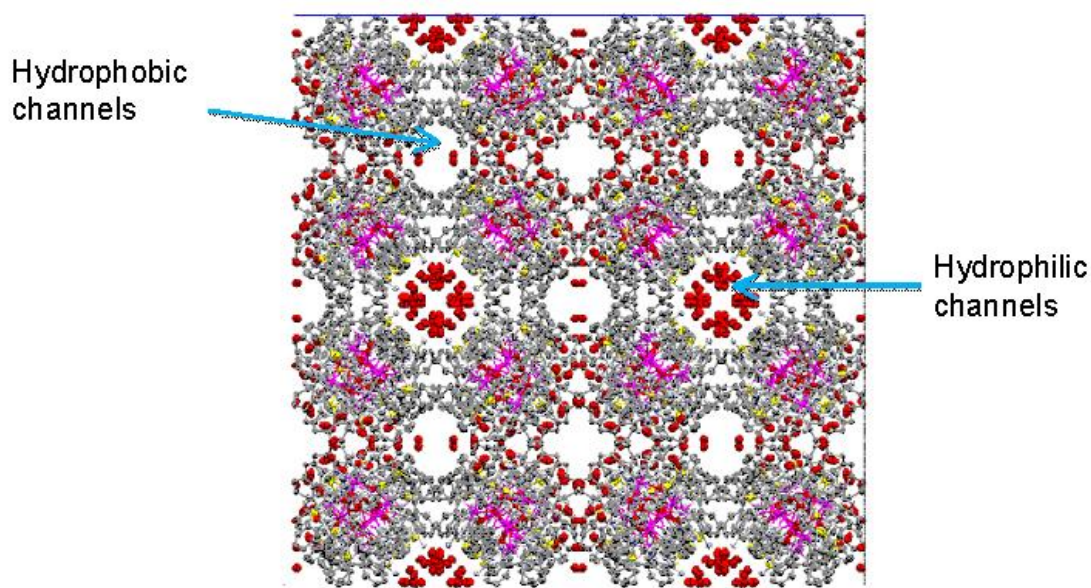


Figure 34: Expanded lattice of compound **30** which illustrates the hydrophobic/hydrophilic channels responsible for the assembly to a MOF type structure.

Mn(II) framework type structures have been reported¹⁰⁵ with much simpler ligands than the ligands used for the synthesis of compound **30** but the present structure illustrates that ordered self-assembly creates the primary cluster, but in addition a little serendipity leads to a large MOF type structure.¹⁰⁶ Figure 35 shows an expanded representation of the hydrophobic/hydrophilic channels of the structure:

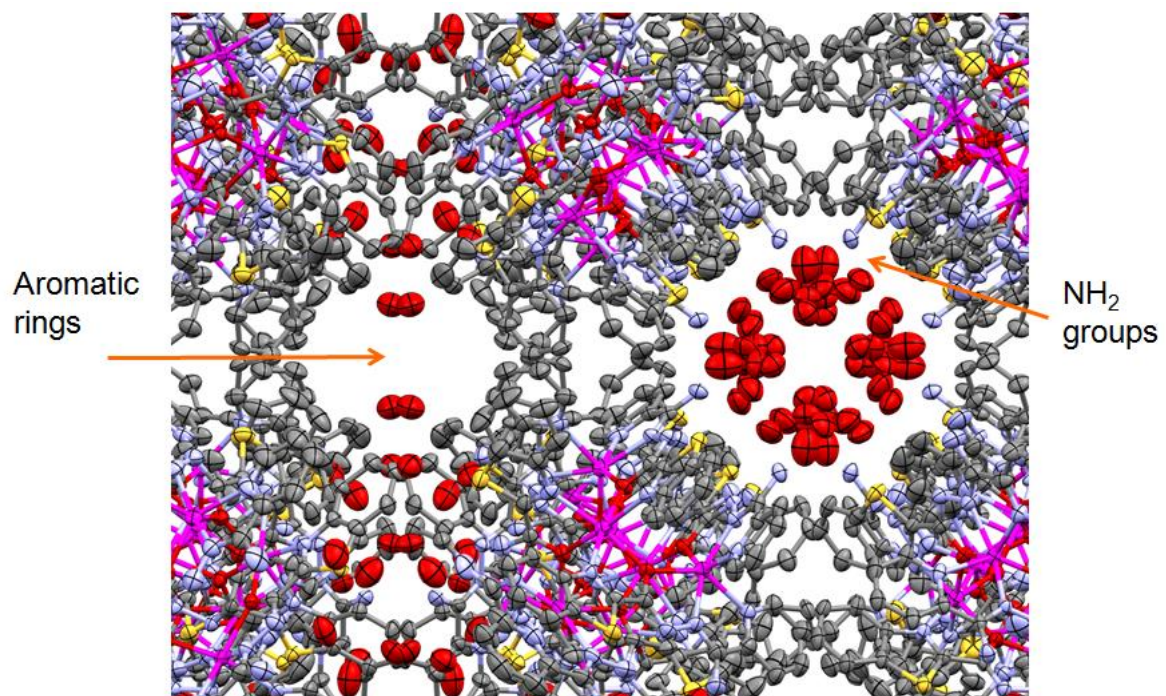


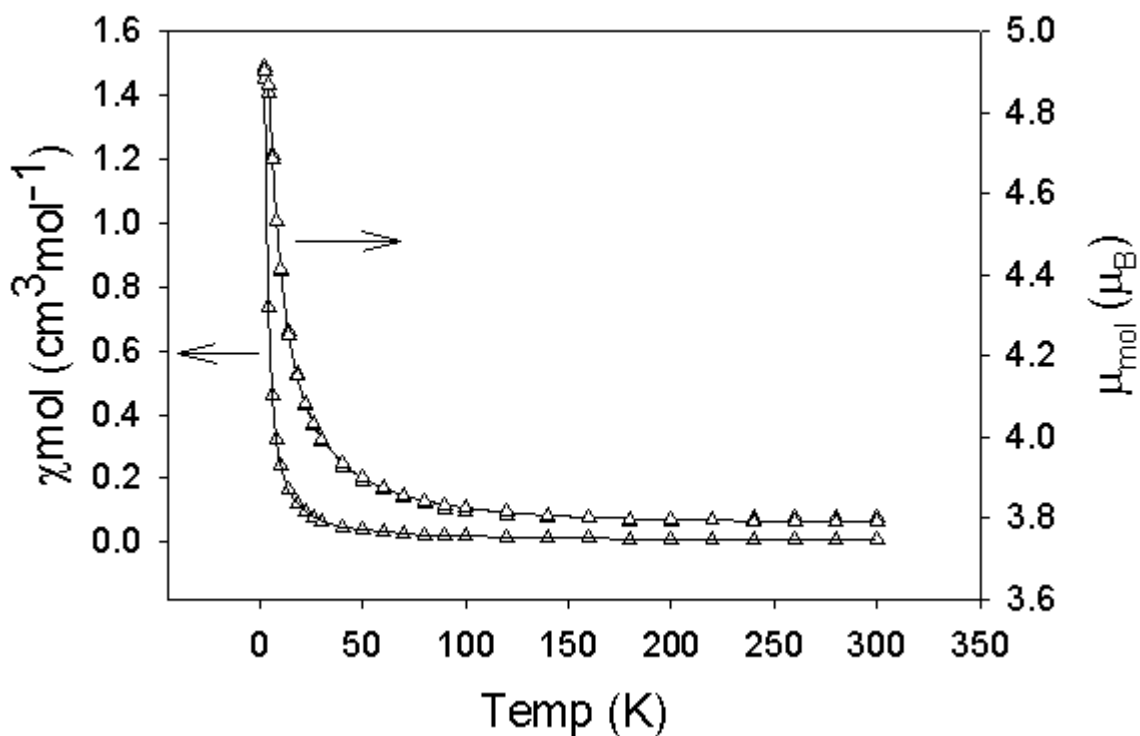
Figure 35: Close up representation of the hydrophobic/hydrophilic channels in compound **30**.

3.1.4-Magnetic Data

Variable temperature DC magnetic data for the polynuclear complexes were obtained in the temperature range 2-300 K at a magnetic field strength of 0.1 T.

Compound **27**, $\text{Co(L9)}_2(\text{BF}_4)_2$, has a Co(III) centre, based on Co-L distances, and is diamagnetic. Unless otherwise stated, data fitting was carried out using the generalized fitting procedures available in MAGMUN4.1.

Figure 36 illustrates the variable temperature magnetic data for compound **26**, shown as plots of moment per mole and susceptibility per mole versus temperature:



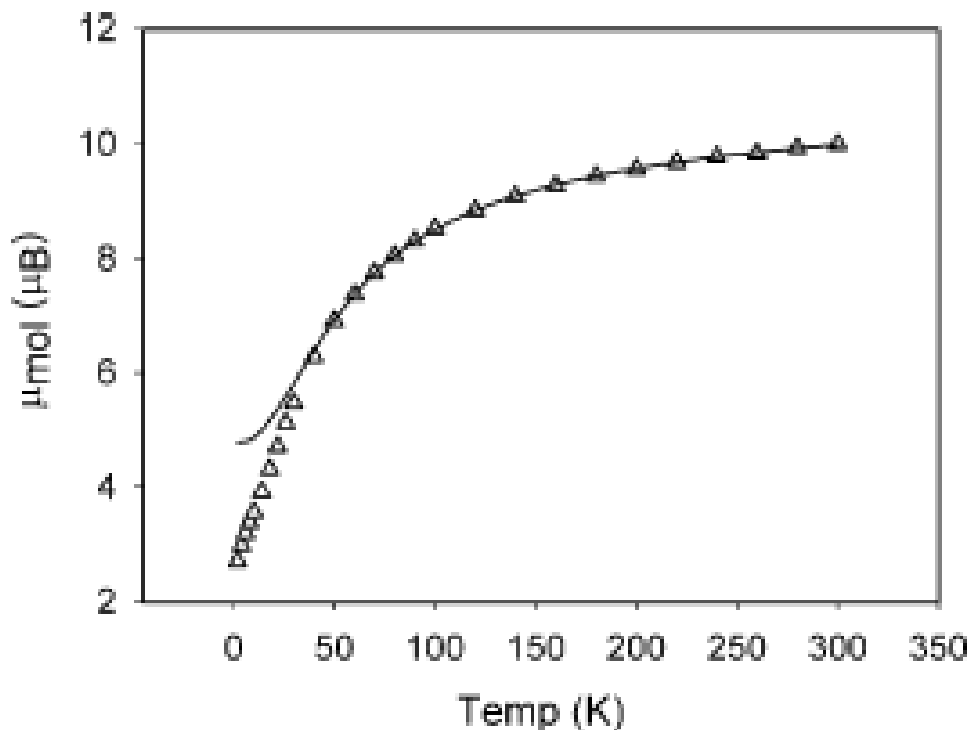
$$H_{ex} = -J\{S_1 \cdot S_2 + S_2 \cdot S_3 + S_3 \cdot S_4 + S_1 \cdot S_4\} \quad (18)$$

Figure 36: Variable temperature magnetic data (Δ) for compound **26**. See the text for the fitted parameters.

The magnetic moment of **26** is roughly constant ($3.8 \mu_B$) on cooling from 300 K to 50 K, followed by an increase in the moment to $4.7 \mu_B$ at 25 K, suggesting the presence of intramolecular ferromagnetic coupling. The data were fitted to the exchange Hamiltonian shown in equation 18, for four $S = \frac{1}{2}$ spin Cu(II) centres. A good fit for the data was obtained for $g = 2.15(1)$, $J = 6.6(7) \text{ cm}^{-1}$, $\text{TIP} = 150 \times 10^{-6} \text{ cm}^3 \text{ mol}^{-1}$, $\theta = -0.3 \text{ K}$ (Weiss correction for temperature), $10^2 R = 0.33$ ($R = [\sum(\chi_{\text{obs}} - \chi_{\text{calc}})^2 / \sum \chi_{\text{obs}}^2]^{1/2}$). The solid lines in Figure 36 were calculated using these parameters. Ferromagnetic coupling is confirmed by the positive coupling constant. The ferromagnetic exchange in this system is typical where the Jahn-Teller axes are misaligned within the square, leading to alternating axial/equatorial magnetic connections and strict magnetic orbital orthogonality between the Cu(II) ions, which have a $d_{x^2-y^2}$ ground state.⁹⁹ The J value for this complex is also comparable with a structurally similar ferromagnetic Cu(II)₄ square grid complex.¹⁰²

The variable temperature magnetic data of compound **25** could not be obtained, as the bulk sample was sticky, and could not be dried to a powder suitable for magnetic study. Due to the similar arrangement of the Jahn-Teller axis in this compound to compound **26**, this should lead to orthogonal magnetic orbital connections within the square, and will also lead to the dominance of intramolecular ferromagnetism, as seen in **26**.

The variable temperature magnetic data for compound **28** are shown in Figure 37 as a plot of moment per mole versus temperature.



$$H_{ex} = -J\{S_1 \cdot S_2 + S_1 \cdot S_3 + S_1 \cdot S_4 + S_2 \cdot S_5 + S_3 \cdot S_5 + S_4 \cdot S_5\} \quad (19)$$

Figure 37: Variable temperature magnetic data (Δ) for compound **28**. See text for fitted parameters.

The pronounced drop from 9.96 μ_B at 300 K to 2.7 μ_B at 2 K clearly indicates the presence of intramolecular antiferromagnetic coupling, but the value at 2 K is much less than expected on the basis of the spin-only model for such a system with an odd number of metal centres ($S = 3/2$), and indicates the necessity for considering a system with a spin of $S = 1/2$ (Kramer's doublet) contribution at low temperature.¹ The initial data fitting was attempted using an isotropic $S = 3/2$ cluster model, using the exchange Hamiltonian shown in equation 2, but as expected fitting could not be achieved over the full

temperature range. However, once a system with $S = 1/2$ was considered in the low temperature regime (<50 K), an excellent fit could be obtained for the temperature range 50-300 K to give $g_{\text{avg}} = 2.474(2)$, $J = -11.28 \text{ cm}^{-1}$, $\text{TIP} = 745 \times 10^{-6} \text{ cm}^3\text{mol}^{-1}$, showing the presence of significant antiferromagnetic exchange.

The lower experimental moments at <50K are a clear indication of contributions in this temperature regime from $S = 1/2$ individual ground terms, and the value at 2 K suggests a molecular spin ground state approaching $S_{\text{T}} = 1/2$, expected for an odd number of spin centres. No fit was attempted for temperatures <50 K. Magnetization data as a function of field at 2 K give a value of $2.2 N\beta$ at 5 T, consistent with a system with a net spin of between one and two electrons ($g = 2.47$). The high 'g' is consistent with the high degree of distortion at the Co(II) centres, and the J value is consistent with exchange in related systems^{101,102}

Figure 38 illustrates the variable temperature magnetic data for compound **29**, $[\text{Co}_5(\text{L10})_6](\text{NO}_3)$, as a plot of magnetic moment per mole versus temperature:

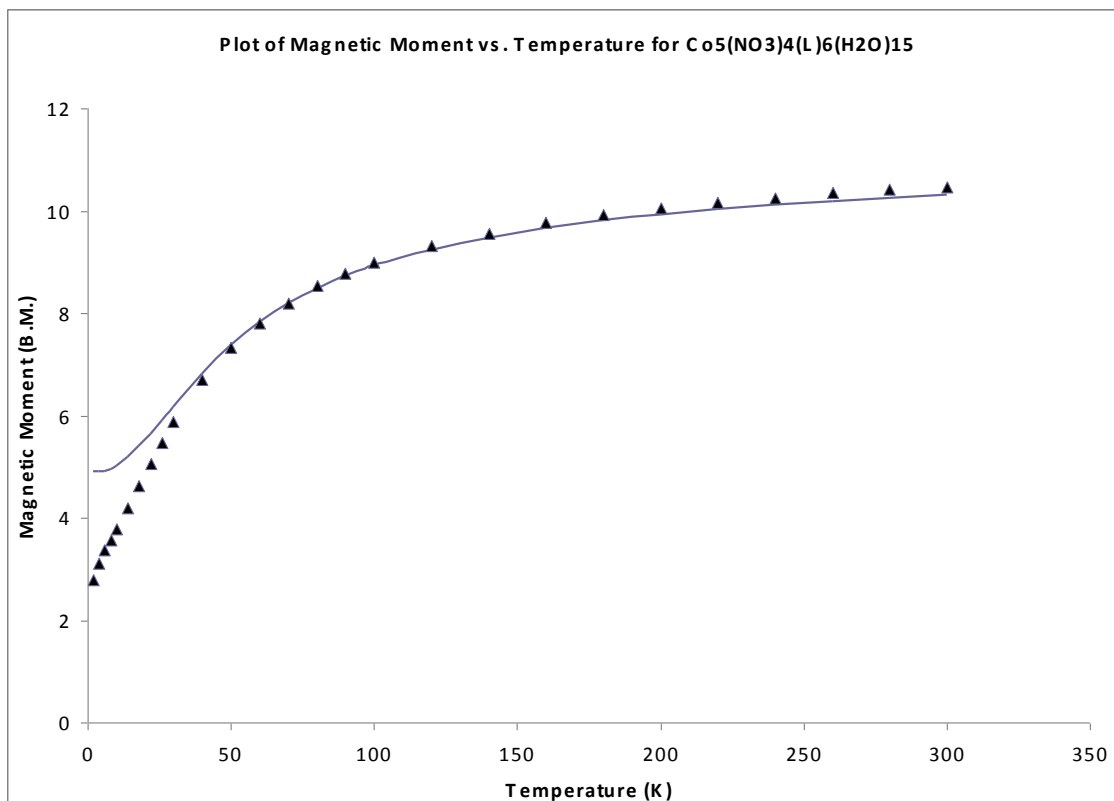


Figure 38: Variable temperature magnetic data (Δ) for **29**. See text for fitted parameters.

The pronounced drop in moment from $10.47 \mu_B$ at 300 K to $2.8 \mu_B$ at 2 K clearly indicates the presence of intramolecular antiferromagnetic coupling, but the value at 2 K is again much less than expected on the basis of the spin-only model for such a system with an odd number of metal centres ($S = 3/2$), and indicates the necessity for considering a system with a spin of $S = 1/2$ (Kramer's doublet) contribution at low temperature. The initial data fitting was attempted using an anisotropic $S = 3/2$ cluster model, using the exchange Hamiltonian shown by equation (19), and as expected fitting could not be achieved over the full temperature range. However, once a system with $S = 1/2$ was considered, an excellent fit was obtained for the temperature range 50-300 K to give

$g_{\text{avg}} = 2.530(6)$, $J = -10.01 \text{ cm}^{-1}$, $\text{TIP} = 980 \times 10^{-6} \text{ cm}^3 \text{ mol}^{-1}$, showing the presence of significant antiferromagnetic exchange.

Figure 39 shows the variable temperature magnetic data for compound **30**, $[\text{Mn}_5(\text{L10})_6](\text{OAc})_4$, as plots of moment per mole and susceptibility per mole versus temperature:

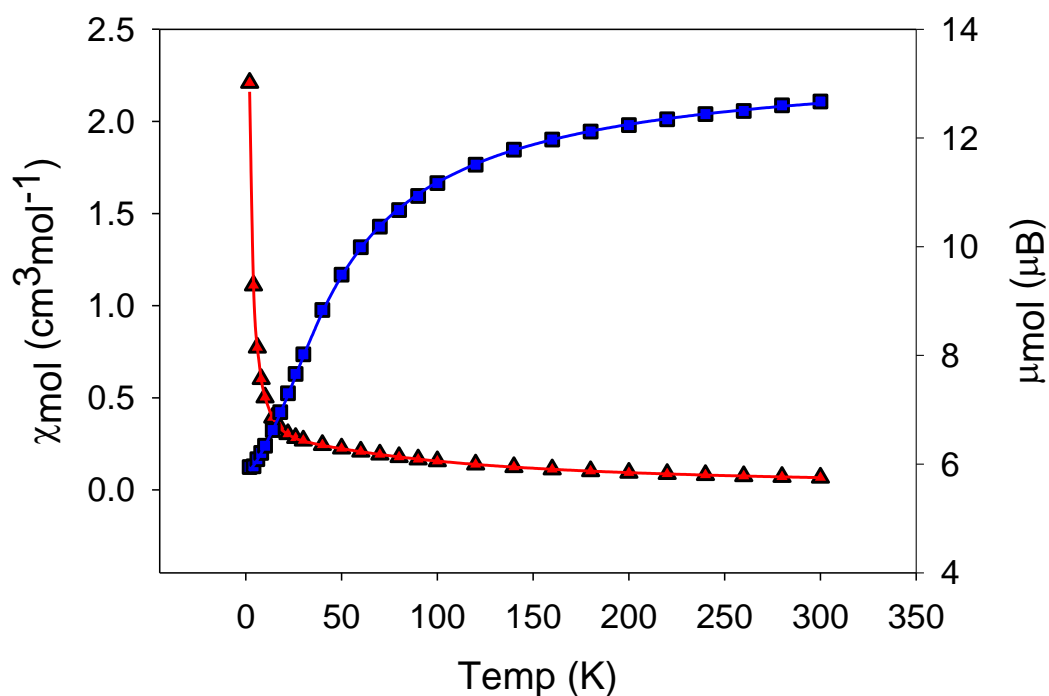


Figure 39: Variable temperature magnetic data (red line for χ and a blue line for μ) for **30**. See text for fitted parameters. See equation (2) for exchange Hamiltonian.

The moment drops from $12.4 \mu\text{B}$ at 300 K to $5.9 \mu\text{B}$ at 2 K. The room temperature value is slightly less than the expected spin only moment for a pentanuclear $\text{Mn}(\text{II})_5$ cluster ($13.2 \mu\text{B}$), and the drop in moment as temperature is lowered signifies the presence of intramolecular antiferromagnetic exchange. The low temperature value (5.9

μ_B) indicates the presence of one uncoupled Mn(II) centre in the ground state ($S = 5/2$), and is associated with the odd number of spin centres in the cluster. The magnetic data were fitted to the exchange Hamiltonian in equation (19) ($S = 5/2$) to give $g = 2.03(6)$, $J = -3.8(3) \text{ cm}^{-1}$, $\text{TIP} = 0 \text{ cm}^3 \text{ mol}^{-1}$, $\rho = 0$, $10^2R = 0.44$. The solid line in Figure 39 was calculated with these parameters, while the experimental data are shown as the triangles and squares. The negative coupling constant confirms the presence of weak intramolecular antiferromagnetic exchange. This compound is similar to the reported complex $[\text{Mn}_5(\text{poap-H})_6](\text{ClO}_4)_4$,¹⁰¹ which has a similar pentanuclear structure and exchange integral.

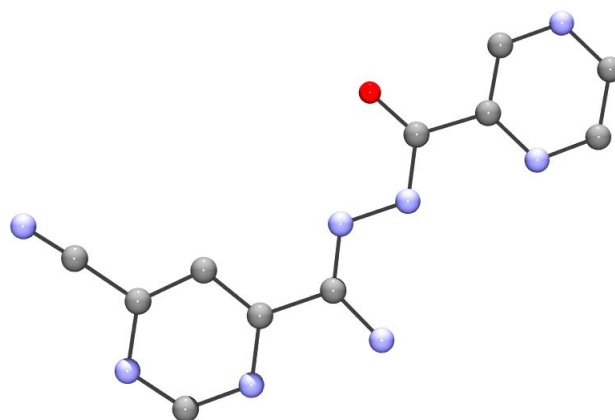


Figure 41: Half substituted ligand synthesized upon reaction of tetratopic ligand L1 with Mn(II) perchlorate. Colour code: Carbon (grey), nitrogen (blue), oxygen (red). Hydrogen atoms are removed for clarity.

The X-ray structure of this organic compound was not completely refined, as the product obtained was not a complex which was targeted. Upon adding the ligand to a solution of Mn(II) perchlorate, the metal cation did not react with the ligand, and possible ligand hydrolysis may have occurred during the reaction to produce the structure in Figure 41. Another possibility may be that the ligand solid may have contained trace amounts of the mono-substituted product (reaction with the iminoester only occurred on one –CN functional group), which crystallized out of the solution upon slow evaporation. This questions the purity of the ligand used in the complexation reactions and illustrates the difficulty to synthesize the precursor tetratopic ligands in a pure state.

A crystalline product was obtained from the reaction of Cu(II) triflate with L1, producing small red crystalline needles, which were too small for a routine structural

determination. This sample was sent to the Advanced Light Source Synchrotron facility in Cincinnati to take advantage of their higher intensity X-ray equipment, but so far limited information has been obtained on the structure (see next page for information obtained on the unit cell).

A major problem encountered with these extended ligands was that upon reactions with metal salts, very soluble products were obtained, making it difficult to obtain crystals by slow evaporation of the solvent. Crystal growth was attempted in the refrigerator as well, but as with slow evaporation at room temperature, any crystals obtained were either too small for X-ray diffraction or did not diffract sufficiently or fell apart on attempting to mount the sample.

3.2.2-Crystallographic Data

The only major crystallographic result to report from this area of the project is the product obtained from the reaction of tetratopic ligand L1 with copper(II) triflate, compound **31** (see experimental section). A sample of red needles of compound **31** was submitted for routine structure determination on a Rigaku Saturn CCD area detector with Mo-K α radiation. The structure of this complex could not be determined due to the small size of the crystals and weak diffraction. The unit cell was however determined; tetragonal unit cell with $a = b = 37.70^\circ$ and $c = 38.95 \text{ \AA}$. The sample was sent for a second attempt using a more powerful synchrotron X-ray source. The results obtained are still under investigation, and the only information obtained thus far corresponds to a large tetragonal unit cell: $a = b = 35.8149(14)^\circ \text{ \AA}$, $c = 38.453(2) \text{ \AA}$, and the slight differences in

the unit cell dimensions obtained from the two sources may be due to the amount of solvent content in the sample.

Orange crystals were also obtained by reaction of Mn(II) perchlorate with L1 as stated previously, but this result was not studied further as it yielded an organic compound, not a complex that could be studied using other methods of characterization.

3.1.4-Magnetic Data

Variable temperature magnetic data were obtained for a sample of compound **31** on the assumption that the large unit cell might indicate the expected grid structure with sixteen Cu(II) centres. Figure 42 shows the magnetic profile of compound **31** as a plot of magnetic susceptibility as a function of temperature.

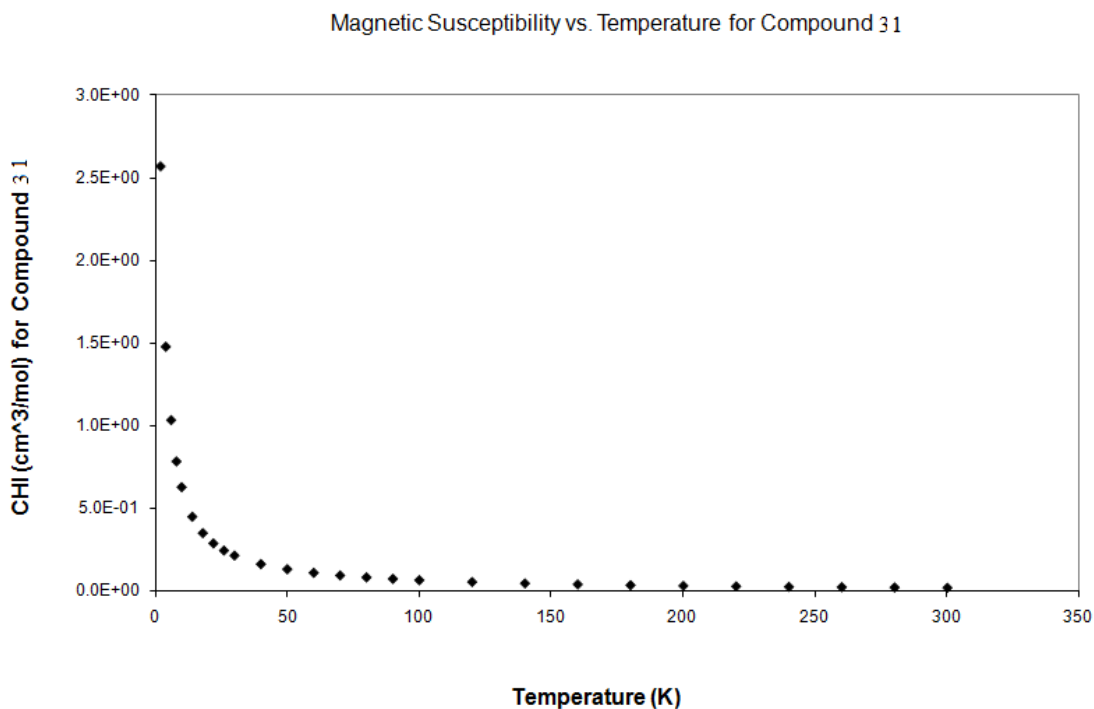


Figure 42: Plot of magnetic susceptibility versus temperature for compound **31**.

Each Cu(II) centre has one unpaired electron ($3d^9$), and therefore if there were 16 Cu(II) centres present in a putative $[4 \times 4]$ grid, a total of 16 unpaired electrons would be available for magnetic exchange. The structure would presumably be similar to a previously reported Ni_{16} square, formed by reaction of Ni(II) nitrate trihydrate with a very similar ligand (Figure 43) to L1 (ligand L2 from the experimental section).¹⁰⁸ Therefore, the anticipated structure of **31** would be a $4 \times [2 \times 2]$ heteroleptic Cu_{16} square. CHN data for this compound were obtained: Anal. (%) Calcd (Found) for $[Cu_{16}(C_{16}H_{15}N_{12}O_2)_8(H_2O)_{16}](CF_3SO_3)_{16}(H_2O)_{17}$ - C, 23.86 (23.73); H, 2.57 (1.84); N, 18.56 (18.19). These data agree quite closely with the percentages of carbon, hydrogen, and nitrogen for this proposed structure.

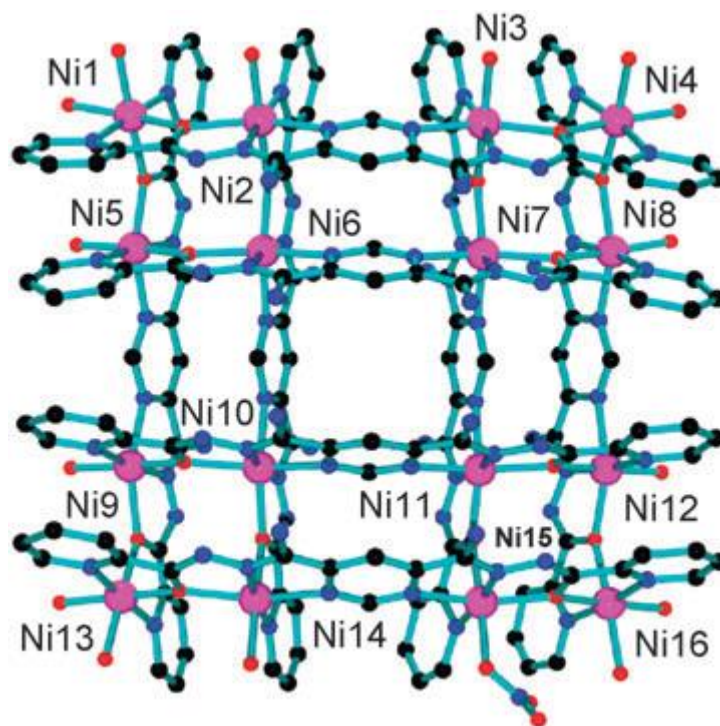


Figure 43: Structure of the cation in $[\text{Ni}_{16}(\text{L}6^{2-})_8(\text{H}_2\text{O})_{15}(\text{NO}_3)](\text{NO}_3)_{15}(\text{H}_2\text{O})_{17}$. Reprinted (adapted) with permission from K. V. Shuvaev, S. S. Tandon, L. N. Dawe, L. K. Thompson, *Chem. Commun.*, **2010**, 46, 4755. Copyright (2010) Royal Society of Chemistry.¹⁰⁸

The structure of compound **31** could therefore mimic the structure in Figure 43, and as a result would contain four μ -O bridged Cu_4 corners, held together by the bridging pyrimidine rings. The molar susceptibility rises on lowering the temperature with a pronounced rise approaching 2 K. This is normal for either a Curie spin system or one where possible ferromagnetic interactions are present.

The putative $[4 \times 4]$ grid would be comprised of four somewhat isolated $[2 \times 2]$ Cu_4 square corners, connected by the pyrimidine bridges (c.f. Figure 43). Typically, such $[2 \times 2]$ Cu_4 grids produced with simpler ligands (e.g. poap) are ferromagnetically coupled,^{102,107} due to strict orthogonality of the copper magnetic ‘d’ orbitals within the μ -

O bridged square structures. The magnetic data for **31** are in agreement with such a model.

In the case of the Ni(II)₁₆ grid the magnetic properties are dominated by intramolecular antiferromagnetic exchange, mostly within each square [2×2] corner.¹⁰⁸ Figure 44 illustrates the variable temperature magnetic data for this grid as plots of magnetic susceptibility and magnetic moment per mole versus temperature:

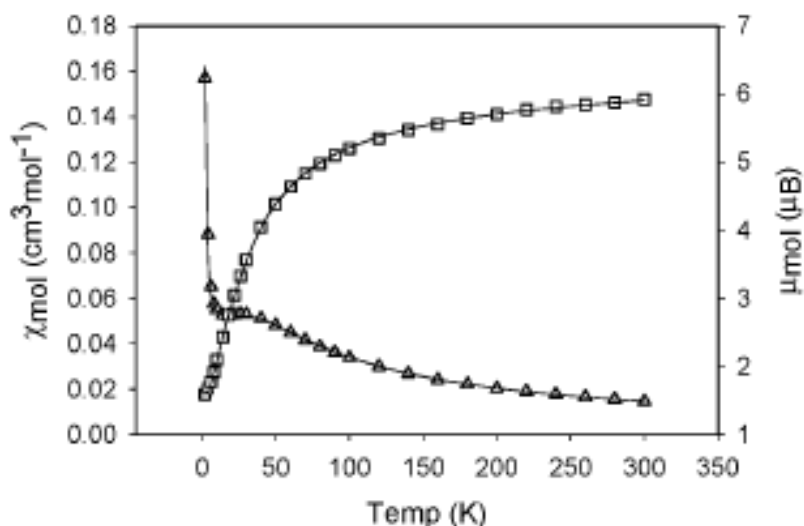


Figure 44: Variable temperature magnetic data for $[\text{Ni}_{16}(\text{L6}^{2-})_8(\text{H}_2\text{O})_{15}(\text{NO}_3)](\text{NO}_3)_{15}(\text{H}_2\text{O})_{17}$, fitted to Ni_4 subunits. Reprinted (adapted) with permission from K. V. Shuvaev, S. S. Tandon, L. N. Dawe, L. K. Thompson, *Chem. Commun.*, **2010**, 46, 4755. Copyright (2010) Royal Society of Chemistry.¹⁰⁸

The magnetic profile shows a distinct rise in the magnetic susceptibility on lowering temperature, with a low temperature shoulder. This is indicative of dominant antiferromagnetic exchange within each [2×2] Ni_4 square ($J = -17.7 \text{ cm}^{-1}$), and the zero value for θ indicates that the pyrimidine bridge does not contribute significantly to the exchange in the cluster.¹⁰⁸

In the current absence of a definitive structure of compound **31**, one can only speculate about its structural properties. However, a general room temperature magnetic moment of $7.2 \mu_B$ is sensible for approximately 16 Cu(II) centres, and the variable temperature magnetic properties are consistent with a Cu(II)₁₆ grid.¹⁰⁷ A full magnetic analysis will be attempted when structural information becomes available.

Chapter 4: Conclusions

Transition metal $[n \times n]$ grid arrays (with $n = 2, 4$) were the primary focus of this project. These metal clusters were synthesized by self-assembly reactions with novel ditopic triazole and benzothiazole hydrazine and tetratopic pyrimidine/ bis(hydrazone) ligands.

In total, four tetratopic ligands (L1, L2, L3, L4) and four ditopic ligands (L5, L6, L7, L8) were successfully synthesized and characterized. Other ligands, including ditopic and tetratopic ligands were synthesized during the project for their potential grid formation. The ligand donor atoms (oxygen and nitrogen) act as hard Lewis bases, and upon reaction with the transition metal Lewis acid, large symmetric chelate rings which are thermodynamically stable can be the resulting product. These ligands were designed to take advantage of supramolecular self-assembly to create new $[n \times n]$ metal grid complexes by reaction with transition metal salts and the ligand. The tetratopic ligands represented significant achievements in ligand synthesis due to many reactions required to produce the pyrimidine centerpieces required to assemble the ligand structures. Their large structure and molecular mass also led to challenges during the characterization process, such as ligand hydrolysis and the potential for a mixture of products. These challenges were overcome by monitoring reaction conditions and reagent amounts to achieve the desired ligands for complexation reactions.

The synthesis of larger tetratopic ligands to produce larger metal arrays has seen some significant progress throughout this project. These ligands have been characterized successfully and there is room for potential expansion of the work done, in particular for

the hexatopic ligands. Setting precedent in ligand synthesis will enable future work in this area, focusing instead on the coordination chemistry of these ligands.

Two [2×2] M₄ Cu(II) grid clusters were formed by self-assembly reactions with the ditopic ligand L5 and were discussed in Chapter 3. These results illustrated the variable nature of the coordination chemistry of transition M(II) cations, and illustrated the thermodynamic stability of the [2×2] grid arrangement in the case of Cu(II). The Cu(II) centres demonstrated square pyramidal geometry around the Cu(II) centres. The crystallographic characterization of these structures was performed, and the results discussed in Chapter 3. The four copper ions in both structures were bridged by deprotonated μ-O hydrazide oxygen atoms in a strictly square arrangement (four-fold symmetry). The copper ions are square pyramidal in geometry, with long axial Cu-O contacts to oxygens, coinciding with the Jahn-Teller axis of each copper centre. The alternating arrangement of axial (long) and basal (short) Cu-O contacts within the Cu₄-(μ-O)₄ square leads to strict orbital orthogonality, suggesting dominant intramolecular ferromagnetic behavior (*vide infra*). The results of the magnetic study were also discussed in Chapter 3.

Two pentanuclear Co(II)₅ clusters (L7 and L8) along with a similar Mn(II)₅ cluster (L8) were also discussed in Chapter 3. Each ligand bridges a pair of M(II) centres via the μ-O hydrazide oxygen atom, and all six ligands coordinate in a similar fashion, with a hydrazide nitrogen, pyridine nitrogen and benzothiazole nitrogen filling the other coordination sites of the octahedral metal centres, resulting in homoleptic clusters. The crystallographic structures of these compounds were discussed in chapter 3, along with

the magnetic profile of each pentanuclear cluster. The presence of antiferromagnetic coupling was observed between the Co(II) and Mn(II) centres in each cluster.

Some interesting and unexpected results were discovered and are worthy of special mention. One Co(III) mononuclear cluster was discussed, along with the crystallographic structure, in Chapter 3. The cluster showed no paramagnetic behavior, but did show significant π - π interactions between the uncoordinated benzothiazole rings. Also, the Mn(II)₅ cluster previously discussed in Chapter 3 demonstrated serendipitous self-assembly to produce a very large novel porous structure with distinct hydrophobic/hydrophilic channels in the expanded lattice. The hydrophobic channels have the aromatic rings pointing into the channel, while the hydrophilic channels have the -NH₂ groups from the ligand pointing in which undergo hydrogen bonding with solvent molecules.

The crystallographic characterization of six complexes was discussed, with an emphasis on coordination geometry and metal connectivity, for the interpretation of magnetic data. The variable temperature magnetic data for each was discussed, along with the magnetic profile for the putative Cu₁₆ grid arrangement.

While there is well-established precedent for designed self-assembly, based on careful ligand construction and metal selection, often other factors, such as solvent conditions, and exposure to atmospheric oxygen and moisture, can result in novel, and unanticipated topologies. Therefore, reaction conditions and metal/ligand combinations both determine the outcome of the reaction. During the research conducted throughout this project and discussed in this thesis, significant progress was made in the area of the

self-assembly of larger $[n \times n]$ clusters. Constructing larger magnetically active metallo-arrays is a strategy for the bottom-up construction of new switchable devices, and the work done during this project continues to expand fundamental knowledge in this area.

References:

- [1] O. Kahn, (1993). *Molecular Magnetism*. New York: VCH Publishers, Inc.
- [2] R. S. Drago, (1992) *Physical Methods for Chemists*. 2nd Ed. Gainesville: Surfside Scientific Publishers.
- [3] A. Earnshaw, (1968). *Introduction to Magnetochemistry*. New York: Academic Press.
- [4] Special Focus on Orbital Physics Issue, *New J. Phys.*, **2004**, 6.
- [5] W. Geertsma, D. Khomskii, *Phys. Rev. B.*, **1996**, 54, 3011.
- [6] T. Moriya, *Phys. Rev.*, **1960**, 120, 91.
- [7] P. W. Anderson, *Phys. Rev.*, **1959**, 115, 2.
- [8] P. W. Anderson, *Phys. Rev.*, **1950**, 79, 350.
- [9] J. B. Goodenough, A. Wold, R. J. Arnett, N. Menyuk, *Phys. Rev.*, **1961**, 124, 373.
- [10] F. E. Mabbs, D. J. Machin. (1973). Chapter 7: The magnetic properties of polynuclear transition metal complexes: Superexchange. In *Magnetism and Transition Metal Complexes*. (pp. 174) New York: Halsted Press.
- [11] R. L. Martin. (1968) Chapter 9: Metal-Metal Interaction in Paramagnetic Clusters. In E. A. V. Ebsworth, A. G. Maddock and A. G. Sharpe (Eds.), *New pathways in inorganic chemistry*. (pp. 175). London: Cambridge United Press.

- [12] L. K. Thompson, Z. Xu, A. E. Goeta, J. A. K. Howard, H. J. Clase, D. O. Miller, *Inorg. Chem.*, **1998**, 37, 3217.
- [13] Z. Xu, L. K. Thompson, D. O. Miller, H. J. Clase, J. A. K. Howard, A. E. Goeta, *Inorg. Chem.*, **1998**, 37, 3620.
- [14] V. H. Crawford, H. W. Richardson, J. R. Wasson, D. J. Hodson, W. E. Hatfield, *Inorg. Chem.*, **1976**, 15, 2107.
- [15] E. Fischer, *Ber. Deutsch. Chem. Gesell.*, **1894**, 27, 2985.
- [16] Nobel Web. (2008) The Nobel Prize in Chemistry 1987. In *The Official Web Site of the Nobel Foundation* from http://nobelprize.org/nobel_prizes/chemistry/laureates/1987/index.html
- [17] J-M. Lehn (Nobel Lecture), *Angew. Chem. Int. Ed.*, **1988**, 27, 89.
- [18] J-M. Lehn, *Science*, **1993**, 260, 1762.
- [19] J. W. Steed, J.L. Atwood, (2000). Chapter 1: Concepts: What is Supramolecular Chemistry. In *Supramolecular Chemistry*. (pp. 2) New York: John Wiley & Sons, Ltd.
- [20] K. B. Mullis was awarded the Nobel Prize in Chemistry in **1993** for his work in surmounting the barrier to synthesize oligonucleotides by the Polymerase Chain Reaction (PCR).
- [21] S. Leininger, B. Olenyuk, P. J. Stang, *Chem. Rev.*, **2000**, 100, 853.
- [22] R. E. P. Winpenny, *Dalton Trans.*, **2002**, 1.

- [23] L. N. Dawe, K. V. Shuvaev, L. K. Thompson, *Inorg. Chem.*, **2009**, 48, 3323.
- [24] J. C. Goodwin, R. Sessoli, D. Gatteschi, W. Wernsdorfer, A. K. Powell, S. L. Heath, *J. Chem. Soc. Dalton Trans.*, **2000**, 1835.
- [25] R. Sessoli, H-L Tsai, A. R. Schake, S. Wang, J. B. Vincent, K. Folting, D. Gatteschi, G. Christou, D.N. Hendrickson, *J. Am. Chem. Soc.*, **1993**, 115, 1804.
- [26] F. K. Larsen, E. S. L. McInnes, H-E Mkami, J. Overgaard, S. Piligkas, G. Rajoromon, E. Rentschlar, A. A. Smith, G. M. Smith, V. Boote, M. Jennings, G. A. Timco, R. E. P. Winpenney, *Angew. Chem. Int. Ed.*, **2003**, 42, 101.
- [27] S. Nayak, M. Evangelisti, A. K. Powell, J. Reedijk, *Chem. Eur. J.*, **2010**, 16, 12865.
- [28] A. Baniodeh, I. J. Hewitt, V. Mereacre, Y. Lan, G. Novitchi, C. E. Anson, A. K. Powell, *Dalton Trans.*, **2011**, 4080.
- [29] M. Ibrahim, Y. Lan, B. S. Bassil, Y. Xiang, A. Suchopar, A. K. Powell, U. Kartz, *Angew. Chem. Int. Ed.*, **2011**, 50, 4708.
- [30] K. V. Shuvaev, L. N. Dawe, L. K. Thompson, *Eur. J. Inorg. Chem.*, **2010**, 4583.
- [31] E. Bruening, G. S. Hanon, F. J. Romero-Salguero, A. M. Garcia, P. N. W. Baxter, J-M Lehn, E. Wegelius, K. Rissonen, H. Nierengarten, A. van Dorsselaer, *Chem. Eur. J.*, **2002**, 8, 3458.
- [32] M. T Youinou, N. Rahmouni, J. Fisher, J. A. Osborn, *Angew. Chem.*, **1992**, 31, 733-.
- [33] P. N. W. Baxter, J-M Lehn, J. Fisher, M. T Youinou, *Angew. Chem.*, **1994**, 33, 2284.

- [34] P. N. W. Baxter, R. G. Khoury, J-M Lehn, G. Boum, D. Fenske, *Chem. Eur. J.*, **2000**, 6, 4140.
- [35] G. S. Hanan, D. Volkmer, U. S. Schubert, J-M Lehn, G. Boum, D. Fenske, *Angew. Chem.*, **1997**, 109, 1929.
- [36] L. N. Dawe, T. S. M. Abedin, L. K. Thompson, *Dalton Trans.*, **2008**, 1661.
- [37] X-Y Cao, J. Harrowfield, J. Nitschke, J. Ramirez, A-M. Stadler, N. Kyritsokos-Gruber, A. Madolen, K. Rissonen, L. Russo, G. Vaughn, J-M Lehn, *Eur. J. Inorg. Chem.*, **2007**, 2944.
- [38] L. Zhao, C. J. Matthews, L. K. Thompson, S. L. Heath, *Chem. Commun.*, **2000**, 265.
- [39] L. N. Dawe, L. K. Thompson, *Angew. Chem. Int. Ed.*, **2007**, 46, 7440.
- [40] A. M. Garcia, F. J. Romero-Salguero, D. M. Bassani, J-M Lehn, G. Boum, D. Fenske, *Chem. Eur. J.*, **1999**, 6, 1803.
- [41] M. Barboui, G. Vaughn, R. Graff, J-M Lehn, *J. Am. Chem. Soc.*, **2003**, 125, 10257.
- [42] M. Ruben, J. Rojo, F. J. Romero-Salguero, L. H. Uppadine, J-M Lehn, *Angew. Chem. Int. Ed.*, **2004**, 43, 3644.
- [43] S. Leininger, O. Bogdan, P. J. Stang, *Chem. Rev.*, **2000**, 100, 853.
- [44] V. A. Milway, V. Niel, T. S. M. Abedin, Z. Xu, L. K. Thompson, H. Grave, D. O. Miller, S. R. Parsons, *Inorg. Chem.*, **2004**, 43, 1874.

- [45] J. Rojo, F.J. Romero-Salguero, J-M Lehn, G. Boum, D. Fenske, *Eur. J. Inorg. Chem.*, **1999**, 1421.
- [46] L. N. Dawe, T. S. M. Abedin, T. L. Kelly, L. K. Thompson, D. O. Miller, L. Zhao, C. Wilson, M. A. Leech, J. A. K. Howard, *J. Mater. Chem.*, **2006**, 16, 2645.
- [47] D. Wu., D. Guo, Y. Sang, W. Huang, C. Duan, Q. Meng, O. Seto, *Inorg. Chem.*, **2008**, 48, 854.
- [48] C. J. Matthews, K. Avery, Z. Xu, L. K. Thompson, L. Zhao, D. O. Miller, K. Biradha, K. Poirier, M. J. Zaworotka, C. Wilson, A. E. Goeta, J. A. K. Howard, *Inorg. Chem.*, **1999**, 38, 5266.
- [49] S. K. Dey, T. S. M. Abedin, L. N. Dawe, S. S. Tandon, J. L. Collins, L. K. Thompson, A. V. Postnikov, M. S. Alam, *Inorg. Chem.*, **2007**, 46, 7767.
- [50] V. A. Milway, V. Niel, T. S. M. Abedin, Z. Xu, L. K. Thompson, H. Grove, D. O. Miller, S. R. Parsons, *Inorg. Chem.*, **2004**, 43, 1874.
- [51] V. A. Milway, T. S. M. Abedin, V. Niel, T. L. Kelly, L. N. Dawe, S. K. Dey, D. W. Thompson, D. O. Miller, M. S. Alam, P. Muller, L. K. Thompson, *Dalton Trans.*, **2006**, 2835.
- [52] L. K. Thompson, T. L. Kelly, L. N. Dawe, H. Grove, M. T. Lemaire, J. A. K. Howard, E. C. Spencer, C. J. Matthews, S. T. Onions, S. J. Coles, P. N. Horton, M. B. Hursthouse, M. E. Light, *Inorg. Chem.*, **2004**, 43, 7605.

- [53] L. Zhao, Z. Xu, L. K. Thompson, D. O. Miller, *Polyhedron*, **2001**, 20, 1359.
- [54] S. K. Dey, L. K. Thompson, L. N. Dawe, *Chem. Commun.*, **2006**, 4967.
- [55] N. M. Randell, M. U. Anwar, M. W. Drover, L. N. Dawe, L. K. Thompson, *Inorg. Chem*, **2013**, 11, 6731.
- [56] M. U. Anwar, L. K. Thompson, L. N. Dawe, F. Habib, M. Murugesu, *Chem. Commun.*, **2012**, 48, 4576.
- [57] M. U. Anwar, L. N. Dawe, S. S. Tandon, S. D. Bunge, L. K. Thompson, *Dalton Trans.*, **2013**, 42, 7781.
- [58] L. K. Thompson, L. N. Dawe, *Coord. Chem. Rev.*, **2015**, 289, 13.
- [59] P. Zhang, Y-N. Guo, J. Tang, *Coord. Chem. Rev.*, **2013**, 11, 1728.
- [60] P. Zhang, L. Zhang, J. Tang, *Dalton Trans.*, **2015**, 44, 3923.
- [61] H. Tian, L. Zhao, Y-N. Guo, Y. Guo, J. Tang, Z. Liu, *Chem. Commun.*, **2012**, 48, 708.
- [62] X. Feng, W. Zhou, Y. Li, H. Ke, J. Tang, R. Clerac, Y. Wang, Z. Su, E. Wang, *Inorg. Chem.*, **2012**, 51, 2722.
- [63] H. Grove, T. L. Kelly, L. K. Thompson, L. Zhao, Z. Xu, T. S. M. Abedin, D. O. Miller, A. E. Goeta, C. Wilson, J. A. K. Howard, *Inorg. Chem.*, **2004**, 43, 4278.

- [64] T. L. Kelly, V. A. Milway, H. Grove, V. Niel, T. S. M. Abedin, L. K. Thompson, L. Zhao, R. G. Harvey, D. O. Miller, M. Leech, A. E. Goeta, J. A. K. Howard, *Polyhedron*, **2005**, 24, 807.
- [65] L. K. Thompson, Z. Xu, A. E. Goeta, J. A. K. Howard, H. J. Chase, D. O. Miller, *Inorg. Chem.*, **1998**, 37, 3217.
- [66] L. Zhao, V. Niel, L. K. Thompson, Z. Xu, V. A. Milway, R. G. Harvey, D. O. Miller, C. Wilson, M. Leech, J. A. K. Howard, S. L. Heath, *Dalton Trans.* **2004**, 1446.
- [67] S. S. Tandon, , L. K. Thompson, J. N. Bridson, V. Mckee, A. J. Downard, *Inorg. Chem.*, **1992**, 31, 4635.
- [68] C. J. Matthews, L. K. Thompson, S. R. Parsons, Z. Xu, D. O. Miller, S. L. Heath, *Inorg. Chem.*, **2001**, 40, 4448.
- [69] L. K. Thompson, C. J. Matthews, L. Zhao, Z. Xu, D. O. Miller, C. Wilson, M. A. Leech, J. A. K. Howard, S. L. Heath, A. G. Whittaker, R. E. P. Winpenny, *J. Sol. State Chem.*, **2001**, 159, 308.
- [70] S. S. Tandon, L. K. Thompson, J. N. Bridson, C. Benelli, *Inorg. Chem.*, **1995**, 34, 5507.
- [71] V. Niel, V. A. Milway, L. N. Dawe, H. Grove, S. S. Tandon, T. S. M. Abedin, T. L. Kelly, E. C. Spencer, J. A. K. Howard, J. L. Collins, D. O. Miller, L. K. Thompson, *Inorg. Chem.*, **2008**, 47, 176.

- [72] Z. Xu, , L. K. Thompson, D. O. Miller, *Chem. Commun.*, **2001**, 1170.
- [73] B. Kwak, H. Rhee, S. Park, M. S. Lah, *Inorg. Chem.*, **1998**, 37, 3599.
- [74] L. K. Thompson, C. J. Matthews, L. Zhao, C. Wilson, M. A. Leech, J. A. K. Howard, *Dalton Trans.*, **2001**, 2258.
- [75] C. J. Matthews, S. T. Onions, G. Marata, L. J. Davis, S. L. Heath, D. J. Price, *Angew. Chem. Int. Ed.*, **2003**, 42, 3166.
- [76] K. V. Shuvaev, S. S. Tandon, L. N. Dawe, L. K. Thompson, *Chem. Commun.*, **2010**, 46, 4755.
- [77] M. U. Anwar, A. S. Elliott, L. K. Thompson, L. N. Dawe, *Dalton Trans.*, **2011**, 40, 4623.
- [78] K. Kambe, *J. Phys. Soc. Jpn.*, **1950**, 5, 48.
- [79] K. S. Murray, *Adv. Inorg. Chem.*, **1995**, 43, 261.
- [80] MAGMUN4.11/OW01.exe is available as a combined package free of charge from the authors (<http://www.ucs.mun.ca/~lthomp/magmun>). MAGMUN was developed by Dr. Zhiquiang Xu (Memorial University), and OW01.exe was developed by Dr. O. Waldmann. We do not distribute the source codes. The programs may be used only for scientific purposes, and economic utilization is not allowed. If either routine is used to obtain scientific results, which are published, the origin of the programs should be quoted.

- [81] C. J. Matthews, K. Avery, Z. Xu, L. K. Thompson, L. Zhao, D. O. Miller, K. Biradha, K. Poirier, M. J. Zaworotko, C. Wilson, A. E. Goeta, J. A. K. Howard, *Inorg. Chem.*, **1999**, 38, 5266.
- [82] G. H. Spencer, P. C. Cross, K. B. Wilberg, *J. Chem. Phys.*, **1961**, 35, 1939.
- [83] S. Sueur, M. Lagrence, F. Abraham, C. Bremard, *J. Heterocycl. Chem.*, **1987**, 24, 1285.
- [84] I. Odriozola, N. Kyritsakas, J-M. Lehn, *Chem. Commun.*, **2004**, 62.
- [85] C. A. C. Haley, P. Maitland, *J. Chem. Soc.*, **1951**, 3155.
- [86] V. N. Kozhevnikov, D. N. Kozhevnikov, T. V. Nikitina, V. L. Rusinov, O. N. Chupakhin, M. Zabel, B. Konig, *J. Org. Chem.*, **2003**, 68, 2882.
- [87] R. R. Hunt, J. F. W. McOmie, E. R. Sayer, *J. Chem. Soc.*, **1959**, 525.
- [88] O. I. Gorbyleva, M. I. Evstratova, L. N. Yakhontov, *Chem. Heterocycl. Com.*, **1983**, 10, 1419.
- [89] H. L. Yale, K. Losee, J. Martins, M. Holsing, F. M. Perry, J. Bernstein, *J. Am. Chem. Soc.*, **1953**, 75, 1933.
- [90] C. J. Matthews, Z. Xu, S. K. Mandal, L. K. Thompson, K. Biradha, K. Poirier, M.J. Zaworotko, *Chem. Commun.*, **1999**, 347

- [91] CrystalClear: Rigaku Corporation, 1999. CrystalClear Software User's Guide, Molecular Structure Corporation, © 2000. J.W. Pflugrath (1999) Acta Cryst. D55, 1718-1725.
- [92] SIR92: A. Altomare, G. Cascarano, C. Giacovazzo, A. Guagliardi, M. Burla, G. Polidori, M. Camalli, (1994) *J. Appl. Cryst.*, 27, 435.
- [93] DIRDIF99: Beurskens, P. T., Admiraal, G., Buerskens, G., Bosman, W. P., de Gelder, R., Israel, R. and Smits, J. M. M. (1999). The DIRDIF-99 program system, Technical report of the Crystallography Laboratory, University of Nijmegen, The Netherlands.
- [94] Cromer, D. T. & Waber, J. T.; "The International Tables for X-Ray Crystallography", Vol. IV, The Kynoch Press, Birmingham, England, Table 2.2 A (1974).
- [95] Creagh, D. C. & McAuley, W. J.; "International Tables for Crystallography", Vol C, (A.J.C. Wilson, ed.), Kluwer Academic Publishers, Boston, Table 4.2.6.8, pages 219-222 (1992).
- [96] Creagh, D. C. & Hubbell, J. H.; "International Tables for Crystallography", Vol C, (A.J.C. Wilson, ed.), Kluwer Academic Publishers, Boston, Table 4.2.4.3, pages 200-206 (1992).
- [97] CrystalStructure 3.7.0: Crystal Structure Analysis Package. Rigaku and Rigaku/MSC (2000-2005). 9009 New Trails Dr. The Woodlands TX 77381 USA.

- [98] CRYSTALS Issue 10: Watkin, D. J., Prout, C. K. Carruthers, J. R. & Betteridge, P. W. Chemical Crystallography Laboratory, Oxford, UK. (**1996**)
- [99] SHELX97: Sheldrick, G.M. (1997)
- [100] A. L. Spek, **2015**. *Acta Cryst.* C71, 9.
- [101] L. N. Dawe, T. S. M. Abedin, T. L. Kelly, L. K. Thompson, D. O. Miller, L. Zhao, C. Wilson, M. A. Leech, J. A. K. Howard, **2006**. *J. Mater. Chem.*, 16, 2645. [46]
- [102] L. N. Dawe, K. V. Shuvaev, L. K. Thompson, **2009**, *Inorg. Chem.*, 48, 3323.
- [103] S. Radosavljevic, V. Scepanovic, S. Stevic, D. Milojkovic, *J. Fluorine Chem.*, **1979**, 13, 465.
- [104] S. S. Tandon, L. K. Thompson, J. N. Bridson, J. C. Dewan, *Can. J. Chem.*, **1992**, 11, 2771.
- [105] S. K. Ghosh, J. Ribas, M. Salah El Fallah, Bharadwaj., *Inorg. Chem.*, **2005**, 11, 3856.
- [106] D. Sun, S. Ma, Y. Ke, T. M. Peterson, H-C. Zhou, *Chem. Commun.*, **2005**, 2663.
- [107] L. N. Dawe, L. K. Thompson, *Angew. Chem.*, **2007**, 39, 7440.
- [108] K. V. Shuvaev, S. S. Tandon, L. N. Dawe, L. K. Thompson, *Chem. Commun.*, **2010**, 46, 4755.